NOVA SCHOOL OF SCIENCE & TECHNOLOGY

DEPARTMENT OF PHYSICS

CAROLINA ROLO MARTINS SANTOS SILVA

Bachelor of Science in Biomedical Engineering

EFFECTS OF MODEL PERSONALISATION ON THE STUDY OF CROUCH GAIT BIOMECHANICS

A MUSCULOSKELETAL MODELLING APPROACH

MASTER IN BIOMEDICAL ENGINEERING

NOVA University Lisbon
April, 2025

NOVA SCHOOL OF SCIENCE & TECHNOLOGY

DEPARTMENT OF PHYSICS

EFFECTS OF MODEL PERSONALISATION ON THE STUDY OF CROUCH GAIT BIOMECHANICS

A MUSCULOSKELETAL MODELLING APPROACH

CAROLINA ROLO MARTINS SANTOS SILVA

Bachelor of Science in Biomedical Engineering

Adviser: Prof. António Prieto Veloso
Full Professor, University of Lisbon

Co-adviser: Prof. Cláudia Regina Quaresma
Assistant Professor, NOVA University Lisbon

MASTER IN BIOMEDICAL ENGINEERING

NOVA University Lisbon
April, 2025

Effects of model personalisation on the study of crouch gait biomechanics
A musculoskeletal modelling approach

This dissertation was carried out as part of:
Project: Development of a simulation platform based in musculoskeletal models to predict recovery of gait following orthopaedic interventions in cerebral palsy children.
https://doi.org/10.54499/PTDC/EMD-EMD/5804/2020 - PTDC/EMD-EMD/5804/2020

This document was created with the (pdf/Xe/Lua)LaTeX processor and the NOVAthesis template (v6.10.10) [1].

Acknowledgements

Em primeiro lugar, gostaria de expressar o meu profundo agradecimento ao Professor Doutor António Veloso pela oportunidade de realizar esta tese sob a sua orientação. Agradeço também à Professora Cláudia Quaresma pela disponibilidade, atenção e carinho que me demonstrou ao longo do curso. Dirijo ainda um agradecimento especial ao Doutor Basílio Gonçalves e ao Engenheiro Rodrigo Mateus pelo acompanhamento e apoio prestado ao longo desta etapa.

Não percebo para onde o tempo foi, mas chegando ao final da faculdade e, consequentemente, ao início da vida que vou sempre tentar adiar, tenho de agradecer às minhas pessoas, que dão sentido a tudo e fizeram, e fazem, tudo valer a pena:

“Be curious, not judgemental.” (Ted Lasso)

Abstract

Cerebral Palsy (CP) is the most prevalent cause of physical disability in childhood. Children with CP often exhibit crouch gait, a severe pathological gait pattern. Musculoskeletal (MSK) modelling is used to study crouch gait, with the ultimate goal of enhancing treatment, rehabilitation, and forecasting surgical outcomes, typically relying on generic models based on healthy adults. Femoral and tibial torsion are often pathological in children with CP and therefore generic MSK models are not specific to this population. Recent software developments allow for easy and quick personalisation of torsion parameters prior to MSK simulations, hopefully improving outcomes.

This dissertation investigated a single case of a patient with CP who underwent Single-Event Multilevel Surgery. Using different levels of personalisation, lower limb muscle forces during self-paced walking were analysed pre-, one-year post-, and ten-year post-surgical intervention. The aim of this dissertation was to compare the outcomes of different models with increased level of personalisation.

Muscle forces and muscle contributions to centre of mass acceleration were calculated using 1) Generic Scaled and 2) Torsion Personalised MSK models in OpenSim. Personalised models were created accounting for the variability in the anatomical geometry used for personalisation. Comparisons were made between the models at each time point, as well as between pre- and post-surgery data for both models.

This dissertation contributes an overview of theoretical concepts related to pathological gait and modelling in CP, alongside a literature review of subject-specific modelling approaches. Results showed that generic models result in muscle forces beyond measurement variability. Specifically, generic models underestimated *Gluteus Medius*, Vasti, *Iliopsoas*, and *Soleus*, while overestimating *Gluteus Maximus* and ankle plantarflexor muscle forces. However, both models captured surgical outcomes similarly, suggesting that personalisation needs may depend on the application. Therefore, this dissertation highlights the potential of personalisation to improve muscle force predictions, address generic models limitations, and enhance the role of MSK modelling in real-world clinical contexts.

Keywords: Crouch Gait, Musculoskeletal Modelling, Subject-Specific, Lower limb torsion deformities, Muscle Forces

Resumo

A Paralisia Cerebral (PC) constitui a principal causa de deficiência motora na infância, frequentemente associada à marcha em agachamento (*crouch gait*), um padrão de marcha patológica grave. Para estudar este tipo de marcha, recorre-se à modelação musculoesquelética, cujo objetivo é aprimorar estratégias terapêuticas e de prognóstico cirúrgico. Contudo, os modelos existentes baseiam-se tipicamente em adultos saudáveis, não contemplando particularidades geométricas como a torção femoral e tibial frequentemente observadas nesta população. Avanços recentes permitem personalizar parâmetros de torção óssea antes da execução de simulações, com a perspetiva de melhoria dos resultados.

Esta dissertação analisou um caso clínico de um paciente com PC submetido a Cirurgia Multinível de Evento Único, utilizando modelos musculoesqueléticos com diferentes níveis de personalização para avaliar as forças musculares do membro inferior durante a marcha autónoma em três momentos: pré-cirurgia, um ano e dez anos pós-cirurgia, com enfoque na influência da personalização de parâmetros de torção óssea nos resultados.

Para tal, utilizaram-se dois modelos no *software* OpenSim: 1) Modelo genérico escalonado e 2) Modelo personalizado, ajustado às torções individuais do paciente. Os modelos personalizados foram desenvolvidos tendo em consideração a variabilidade na medição das torções utilizadas para a sua criação. Os resultados obtidos foram comparados nos três momentos, seguida de uma comparação direta entre os dados pré e pós-operatórios.

Esta dissertação contribui com uma visão geral da marcha em agachamento e modelação em PC, além de uma revisão da literatura referente a abordagens de modelação específicas. Os resultados revelaram que o modelo genérico subestimou as forças do *Gluteus Medius*, Vasti, *Iliopsoas* e *Soleus*, enquanto superestimou o *Gluteus Maximus* e os plantarflexores do tornozelo. Apesar destas diferenças, ambos os modelos capturaram tendências pós-cirúrgicas semelhantes, sugerindo que a necessidade de personalização depende do contexto. Assim, esta dissertação destaca o potencial da personalização geométrica para melhorar a quantificação de forças musculares, colmatar as limitações dos modelos genéricos e aprimorar o papel da modelação musculoesquelética em contextos clínicos reais.

Palavras-chave: Marcha em Agachamento, Modelação Musculoesquelética, Personalização, Deformidades de torção do membro inferior, Forças Musculares

Contents

List of Figures

List of Tables

Glossary

clonus Involuntary and rhythmic muscle contractions [2]. *(p. 3)*

hyperreflexia Overactive or overresponsive reflexes [2]. *(p. 3)*

iatrogenic Consequences of medical action [2]. *(p. 15)*

kinematics The study of motion without considering the forces and moments that produce that motion [3]. *(pp. xi, 6, 11, 13, 14, 21–23, 26, 56, 57)*

kinetics The study of forces and moments that cause or result from motion [3]. *(pp. 6, 11, 13, 14, 26)*

osteotomy A surgical operation in which a bone is divided or a piece of bone is excised to correct a deformity [2]. *(pp. 5, 7, 17, 30)*

spasticity Increased, involuntary, velocity-dependent muscle tone that causes resistance to movement [2]. *(pp. 3, 6, 7, 16)*

Abbreviations

3D Three-dimensional *(pp. 4, 8, 16, 17)*
3DGA Three-Dimensional Gait Analysis *(p. 11)*

AVA Anteversion Angle *(pp. 4, 5, 9, 10, 14, 16, 17, 19, 20, 26, 28, 49, 53)*

BW Body Weight *(pp. 12, 27–32, 34, 69, 71, 72, 74–77, 79–81)*

CGA Clinical Gait Analysis *(pp. vii, xi, 1, 3, 6, 11, 15–17, 22, 24, 25, 52, 55, 82, 83)*
CMC Computed Muscle Control *(pp. viii, xii, xiv, 19, 23, 24, 27, 64, 65, 82, 83)*
COM Centre of Mass *(pp. viii, x, xiii, 2, 13, 23, 24, 35–37, 87–92)*
CP Cerebral Palsy *(pp. vii, x, 1–7, 11–13, 15, 16, 24, 28, 29, 32, 34, 38, 40, 48, 69, 71, 74, 76, 77, 79, 80)*
CT Computerised Tomography *(pp. 4, 5, 13, 19, 40)*

DoF Degrees of Freedom *(pp. 8, 9, 22, 24, 26, 27, 64, 65)*

EMG Electromyography *(pp. vii, viii, xii, 3, 6, 8, 10, 14, 16–18, 24, 35, 40, 50, 82, 83)*

GMFCS Gross Motor Function Classification System *(pp. x, 4, 7, 15, 48)*
GRF Ground Reaction Force *(pp. 11, 16–19, 22–24, 35, 86, 87)*

IAA Induced Acceleration Analysis *(pp. viii, ix, xiii, 19, 24, 35, 37, 84–87)*
ID Inverse Dynamics *(pp. viii, 19, 21–23, 26, 27, 59–63)*
IK Inverse Kinematics *(pp. viii, xi, 19, 21–23, 26, 56, 57)*

JCF Joint Contact Forces *(p. 14)*
JRF Joint Reaction Forces *(p. 14)*

LoA Limits of Agreement *(pp. x, xii, xiii, 5, 19, 20, 32–34, 53, 56–60, 74, 76, 77, 79, 80, 82, 85, 86)*

MRI Magnetic Resonance Imaging *(pp. 4, 14, 20, 40)*

MSK Musculoskeletal *(pp. vii, x, 1–3, 6–14, 16, 17, 19–21, 33, 38–40, 49)*

NSA Neck-Shaft Angle *(pp. 4, 5, 9, 10, 14, 16, 17, 19, 20, 26, 49, 53)*

QTM Qualisys Track Manager *(pp. 16, 17)*

RMS Root Mean Square *(pp. 22, 27, 61–65)*

ROM Range of Motion *(pp. xiv, 6, 7, 9, 16, 19, 20)*

RRA Residual Reduction Algorithm *(pp. viii, xi, xiv, 19, 22, 23, 26, 27, 58–63)*

SEMLS Single-Event Multilevel Surgery *(pp. 6, 7, 15, 17, 28–30, 32, 34, 37, 69, 71, 74, 76, 77, 79, 80)*

TD Typically Developing *(pp. 1, 4, 8, 13, 18, 24, 40)*

TFA Thigh-Foot Angle *(pp. 5, 16, 49)*

TMA Transmalleolar Axis *(pp. 5, 16, 49)*

TPAT Trochanteric Prominence Angle Test *(pp. 4, 16)*

TT Tibial Torsion *(pp. 4, 5, 7, 9, 10, 12, 16, 17, 19, 20, 26, 28, 30, 31, 36, 37, 49, 53)*

1 Introduction

1.1 Context and Motivation

Gait, as the primary mode of human locomotion, plays a vital role in the daily life of individuals, preserving independence, mental well-being, and overall quality of life [4]. While a Typically Developing (TD) gait pattern is important for individuals of all ages, it is particularly crucial for children due to their ongoing development and growth.

Cerebral Palsy (CP), a neurodevelopmental non-progressive disorder caused by injury to the developing brain, is the most prevalent cause of physical disability in childhood, responsible for 2–3 in every 1000 live births worldwide [5]. CP often leads to a large range of pathological gait patterns, with crouch gait being the most common and severe [6]. A crouched posture places increased demands on muscles, making walking less effective, and leads to bone deformities and joint pain.

To address these issues, bony procedures, involving the manipulation, reshaping or repositioning of bones to improve alignment and reduce abnormal forces on the joints, have shown promise [7]. Moreover, the integration of Clinical Gait Analysis (CGA) enhances understanding of gait deviations, including crouch gait biomechanics, and contributes to a deeper comprehension of treatment effects on these deviations [8].

To gain a deeper understanding of abnormal gait, with the ultimate goal of enhancing treatment and rehabilitation as well as forecasting surgical outcomes, Musculoskeletal (MSK) modelling is employed. However, in most cases, this method relies on a generic model based on a healthy adult, overlooking the importance of subject-specificity, which has a significant impact in clinical populations like CP [9].

In recent years, there has been a noticeable increase in the development of subject-specific MSK models, showing considerable variations in the level of detail. Nevertheless, these methods tend to be time- and cost-intensive and may require a high level of technical expertise. In comparison, a faster and simpler approach for integrating subject-specificity into MSK models involves exclusively implementing personalised femoral and tibial geometries [9]. This modelling process has the potential to enhance the practicality and accuracy of MSK simulations while being straightforward in its application.

1.2 Objectives

The main objective of this dissertation is to investigate the impact, sensitivity, and potential application of a personalised model, incorporating an individual's specific geometries, on crouch gait biomechanics in children with CP, as opposed to a generic model. The outlined approach is based on a new automated tool, the Torsion Tool [9], for personalising femoral and tibial geometries in OpenSim models. The prospective benefits of considering the specificities of each subject include improvements in clinical understanding and diagnostic accuracy, as well as the potential for tailored treatments and improved surgical decision-making.

Within this scope, the objective can be segmented into the following distinct purposes:

1. **Pre-Surgical Analysis:**
    - **Generic Model Simulations:** Estimate muscle forces and the muscles' contributions to the Centre of Mass (COM) accelerations using the generic Gait2392 model for the pre-surgery time point, and compare the results with the expectations from the literature.
    - **Subject-specific Simulations:** The second goal resembles the preceding one, this time implementing a subject-specific MSK model considering lower limb anatomical variations, using the Torsion Tool within OpenSim. Additionally, compare the generic and subject-specific models' results, considering the margin of measurement variability in the differences between them.
2. **Post-Surgical Analysis:** Repeat the simulations using the generic and subject-specific models to evaluate muscle forces and contributions one-year and ten-year post-surgery. Compare these findings and the pre-surgery results to understand surgical outcomes, their long-term evolution, and the impact of the two models in studying these effects.

1.3 Document Structure

This document is divided into six chapters. The first and present chapter introduced the dissertation's motivation and objectives. The following chapter outlines the main theoretical notions guiding the dissertation. The third chapter reviews research on MSK modelling, focusing on subject-specific techniques. The fourth chapter examines the methodology adopted to achieve the main aims of this dissertation, from subject details, gait analysis, and the pipeline followed. The fifth chapter presents and critically interprets the findings. The sixth and final chapter concludes the dissertation by highlighting the main insights, challenges, opportunities for improvement, and proposals for future exploration.

2

Theoretical Concepts

This chapter is structured into six main sections, each presenting fundamental concepts crucial for the research. The initial section centres on CP, its classification, and associated anatomic abnormalities. The second delves into gait, the gait cycle, CGA, and pathological gait. Moreover, the third section discusses crouch gait, along with treatment approaches. The fourth section addresses MSK modelling, followed by an overview of OpenSim software in the fifth section. The final section explores Electromyography (EMG).

2.1 Cerebral Palsy

CP describes a group of permanent neuromotor disorders that affect muscle tone, posture and movement, resulting in compromised functional skills. These conditions are primarily attributed to non-progressive damage or malformations to the developing fetal or infant brain, with manifestations occurring before, during, or shortly after birth. CP impacts both the MSK system, leading to symptoms such as muscle spasticity and bony deformities [10], and the neurological system, manifesting as sensory disturbances and cognitive impairments, for example [11]. The prognosis of CP is described in terms of survival, motor function and quality of life. Even though most people with CP live to adulthood, life expectancy is generally lower and depends on how severe the impairment is.

Considering the patterns and nature of motor impairment, spastic CP (80%) is the most prevalent form, followed by dyskinetic (15%), and ataxic (5%) forms [11]. A visual summary presented in Figure A.1 (Appendix A) illustrates the affected body parts and characteristic postures across the various subtypes of CP, namely hemiplegia, diplegia, quadriplegia, athetoid, dystonic, and ataxic presentations. Spastic-predominating CP is characterised by muscle spasticity, hyperreflexia, clonus, and extensor plantar response. This leads to muscle stiffness, reduced voluntary control, and slow and effortful voluntary movements. There are three subtypes based on the distribution of abnormal tone: hemiplegia, which predominates on one side of the body; diplegia, where the lower limbs are more severely affected than the upper limbs; and quadriplegia, which uniformly impacts the muscles of all four limbs and is accompanied by severe comorbidities due to extensive central nervous system involvement.

Considering the extent of functional impairment, the most standardised and widely

used system is the Gross Motor Function Classification System (GMFCS), which categorises motor function based on an individual's age and usual performance in home, school, and community settings. The GMFCS comprises five levels, with higher levels indicating reduced function and limited rehabilitative potential. Each level is accompanied by separate descriptions for various age ranges, covering until the 18th birthday [12]. In Figure A.2 (Appendix A), a concise overview of this system is presented.

2.1.1 Femoral and Tibial Rotations: Implications for Children with Cerebral Palsy

In a CP children, the muscles become tight causing the bones to develop in a twisted position. Excess variations in femoral version and Tibial Torsion (TT) have been shown to impact gait mechanics and lead to discomfort in children with an underlying neuromuscular disease, such as CP. Understanding these rotations is essential for this study, with measurement illustrations provided in Figure A.3 (Appendix A).

2.1.1.1 Femoral Anteversion Angle

Femoral anteversion corresponds to the angle between the axis of the femoral neck and head and the axis of the distal femoral condyles at the most posterior points in the transverse plane, indicating the degree of internal femur torsion. In typically developing (TD) children, Anteversion Angle (AVA) decreases from 30-40 degrees at birth to 10-15 degrees in adolescence [13]. An increased anteversion alters lower limb alignment, leading to internal rotation of the hip joint, patellar malalignment, and in-toeing [14], [15].

AVA can be measured using imaging techniques (Computerised Tomography (CT), Magnetic Resonance Imaging (MRI), radiography) or physical examination (Trochanteric Prominence Angle Test (TPAT)). While CT is the gold standard for precise axial plane analysis [13], physical examination is frequently used due to its safety, cost-effectiveness, and absence of radiation exposure. The TPAT (Figure A.3(a)) is commonly used, where AVA is measured as the leg's angle when the greater trochanter reaches its most lateral prominence in the prone position. Although CP-related factors, such as stiffness, abnormal femur positioning, and bony deformities may reduce measurement accuracy, the TPAT has demonstrated excellent validity and reliability in measuring femoral AVA [16].

2.1.1.2 Femoral Neck-Shaft Angle

The femoral Neck-Shaft Angle (NSA), formed between the femoral shaft and head-neck axes, is crucial for diagnosing and therapeutic planning hip pathologies and CP. In TD children, it decreases from approximately 140° at birth to 125-135 degrees in adulthood, with a global mean of 126.4 degrees. Deviations can result in coxa valga (>140 degrees) or coxa vara (<120 degrees) [15], [17]. Unlike AVA, NSA cannot be measured through clinical examination and relies on imaging techniques such as CT, MRI, and radiography. While Three-dimensional (3D) imaging offers greater accuracy for surgical planning [18], conventional radiography

remains widely used due to its accessibility and cost-effectiveness. NSA measurements from anteroposterior hip internal rotation radiographs have demonstrated good validity and reliability [16]. An illustration of the NSA measured on an anteroposterior radiograph of the hips is shown in Figure A.3(b).

2.1.1.3 Tibial Torsion

TT refers to the rotation of the tibia, defined by the angle between the femoral transcondylar axis and the Transmalleolar Axis (TMA). Internal TT leads to in-toeing, while external TT, common in CP, causes out-toeing and may require surgical intervention, such as tibial osteotomy. Physiological TT angles vary depending on imaging methods and reference axes, but the literature reports a range starting near 0 degrees at birth, increasing to an average of 20 degrees in adulthood, with a reported range of 0-47 degrees [13]. Rotational asymmetries exceeding 15 degrees are considered abnormal [19].

TT is measured through physical examination using a goniometer with the Thigh-Foot Angle (TFA) and TMA techniques. TFA (Figure A.3(c)) measures the angle between the longitudinal axes of the thigh and foot, with negative angles indicating internal rotation and positive values indicating external rotation. TMA (Figure A.3(d)) measures the angle between the longitudinal axis of the thigh and a line perpendicular to the axis connecting the most prominent portions of the malleoli. Both methods are performed in a prone position with the knee flexed at 90 degrees. The TFA can be affected by foot deformities and joint instability, while the TMA is considered more reliable [20]. Since femoral torsion influences tibial alignment, femoral rotation is assessed first during the examination.

It is important to note that each of these measurements come with a margin of error. For this reason, in this thesis, the difference between the measurement techniques used for the NSA, AVA, and TT and the gold standard method, the CT scan, were considered. According to the Bland-Altman analysis, the Limits of Agreement (LoA) are used for method comparison and indicate the range within which 95% of the differences between two measurement methods are expected to fall. The LoA are defined as the mean difference between the methods, plus and minus 1.96 times the standard deviation of the differences. By considering the LoA, the potential range of variability in the measurements is accounted for.

2.2 Gait

Gait is defined as a particular way of walking or moving on foot. Human gait has been a key focus of many researchers for the past century. To investigate pathological gait patterns effectively, it is crucial to completely understand the gait cycle, a fundamental unit of gait [21].

Each gait cycle begins with one foot contacting the ground and ends with the same foot striking again. Within one gait cycle, each foot makes one ground contact, which corresponds to the stance phase, that lasts for approximately 60% of the entire cycle. The following period, where the foot is lifted off the ground, named the swing phase, accounts for the remaining

40%. During the stance phase, there exist two types of support periods, double support and single support. The double support periods occur at the first and last 10% of the phase, being known as early stance and pre-swing, while the single support, characterised by only one foot contacting the floor, and further divided into mid-stance and terminal stance, covers the remaining 40% of the phase [21], [22]. Figure A.4 (Appendix A) depicts a representation of one full gait cycle.

2.2.1 Clinical Gait Analysis

Since pathological gait patterns are not always visually detectable, a quantitative analysis is often required. CGA is a specialised evaluation which purpose is to identify the underlying cause of a patient's walking pattern, whether it is MSK, neurological, or biomechanical problems. It provides a large amount of detailed data, essentially spatiotemporal, kinematics, kinetics and EMG data. In addition, the session is recorded, and a physical examination of the lower limbs is performed with the goal of measuring anthropometry, passive Range of Motion (ROM), muscle force and spasticity [8].

Currently, due to the complex nature of gait, particularly pathological gait, CGA is commonly used to detect, measure, and comprehend the impairments of a patient and has become an integral part of the clinical decision-making process for patients with complex gait disorders [8]. CGA can be particularly helpful in understanding gait disturbances in children with CP and analysing treatment efficacy, by providing a scientific evaluation of the way that orthopaedic surgical interventions modify gait. Therefore, it complements clinical data and is an auxiliary means in surgical planning and outcomes. In fact, Single-Event Multilevel Surgery (SEMLS) based on CGA is increasingly performed to correct lower-limb skeletal abnormalities [23].

2.2.2 Gait Patterns in Cerebral Palsy

As it was mentioned in Section 2.1, CP children have complex and heterogeneous motor disorders that result in a large variety of gait deviations. Gait deviations in CP are not well delineated groups; in fact, they tend to be a continuum of deviations. However, to enhance communication, they can be categorised into the gait patterns of unilateral spastic CP and bilateral spastic CP, by observing the kinematics in the sagittal plane [8], [24]. This thesis explores the gait patterns associated with bilateral spastic CP, specifically crouch gait biomechanics, which is considered the ultimate stage in the progression of gait disorders.

2.3 Crouch Gait

Crouch gait is a pattern of gait disorder characterised by excessive hip and knee flexion, and excessive dorsiflexion during stance phase [10], which distinguishes it from the other flexed knee gait patterns, such as jump gait and apparent equinus. It affects children with severe diplegia and most children with spastic quadriplegia. This degradation is eased by the progressively high displacement of the patella, known as patella alta, which is almost

universal in those with crouch, and torsional deformities of the limb segments, for example, excessive anteversion of the femur and TT, which cause dysfunction of the levers and reduce the force generated by muscle contraction [24]. This form of walking is physically demanding and is frequently connected with patellofemoral pain. Due to the excessive joint loading and significantly higher energy expenditure needed when compared to unimpaired gait, this gait pattern is highly inefficient and unsustainable in the long term, so if left untreated, it may lead to a loss of independent ambulation ability. Crouch gait may stem from a range of factors, highly dependent on each patient, including ankle plantarflexors weakness, knee extensors weakness, contracture of hip and knee flexors, lever arm dysfunction, or combinations of the mentioned [24], [25].

2.3.1 Treatment Approaches

The main purpose of treatment approaches, which should initiate at the time of diagnosis, is to manage and improve gait efficiency, with the ultimate goal of increasing the child's independence in daily functional tasks and minimising the extent of disability. The efficacy of treatments can be classified according to the patient's functional status, mainly from the GMFCS, to monitor impairment over time [26].

Approaches range from physical and occupational therapy to orthopaedic interventions. Physical therapy is considered the first approach, and its main goal is to improve ROM, stamina, and coordination, enhancing mobility and transfers. Instead, occupational therapy focuses on fine motor skills and self-care or caregiver support in activities of daily living. There is a variety of other treatments that aim to reduce the severity of symptoms, such as oral medications, injections, and spasticity reduction procedures [25], [26].

Severe crouch gait requires orthopaedic procedures to address secondary MSK deviations by preventing or correcting joint abnormalities, maximising function, improving gait, and reducing pain. Treatment planning is based on clinical assessment, severity of symptoms, and patient and caregiver objectives. These interventions mainly include soft tissue or bone surgeries, often combined in a SEMLS [26]. Soft tissue procedures involve the lengthening, release, or transfer of muscle-tendon units and are performed when abnormal muscle action or contractures interfere with function; however, they result in minor improvements in gait function. In contrast, bone surgeries, such as osteotomy, permanently correct abnormalities by limiting changes to the growth plate (regions of new bone development in children), improving alignment, or fusing joints. SEMLS is widely used among children with CP, allowing multiple corrections in a single procedure under one anaesthesia, reducing the number of surgeries and recovery time [26].

2.4 Musculoskeletal Modelling

MSK modelling is a computational simulation technique used to study, in a non-invasive way, the function and mechanics of the human MSK system. These models are built upon dynamic analyses of linked rigid-segment models, which represent the body as a series of

solid body segments connected by mechanical joints. In addition, MSK models also include detailed models of individual muscles and neurological control. The body moves in a virtual space defined by a global Cartesian coordinate system, and models can include as few or as many body segments as necessary to answer the question of interest [27]. They involve mathematical models that simulate the complex interaction between bones, joints, muscles, and tendons to analyse a range of MSK variables that are not directly observable: linear and angular displacements, velocities, and accelerations for body segments; muscle length, moment arm, forces, and activation (regardless of having EMG data); and joint contact and reaction forces.

MSK models have a wide range of applications, from studying healthy and pathological human movements, allowing for a better understanding of human performance in daily living or physical activities, to developing strategies to prevent or rehabilitate MSK injuries and to predict surgery outcomes, thereby functioning as a clinical intervention or decision-making tool [28].

2.5 OpenSim

Delp and colleagues [3] created OpenSim in 2007, an open-source platform for modelling, simulating, and evaluating the neuromusculoskeletal system. OpenSim allows researchers to create models of the human MSK system, consisting of rigid body segments connected by joints and articulated by actuators that simulate muscles and generate force and motion. This enables the investigation of biomechanical features and execution of dynamic simulations for a wide variety of studies, such as athletic performance, neuromuscular coordination, and TD or pathological gait. OpenSim encourages multidisciplinary research by offering a shared repository for the biomechanics community to share, test, evaluate, and improve simulations through multi-institutional collaboration.

2.5.1 Generic Musculoskeletal Model: 'Gait2392'

The Gait2392 MSK model [3], [29], displayed in Figures 2.1(b) and 2.1(c), is a 3D computer model of the human MSK system widely used in biomechanical research for dynamic simulations. It was developed by Darryl Thelen (University of Wisconsin-Madison) and Ajay Seth, Frank C. Anderson, and Scott L. Delp (Stanford University), and includes lower extremity joint definitions adopted from Delp *et al.* [29], low back joint and anthropometry adopted from Anderson and Pandy [30], and a planar knee model adopted from Yamaguchi and Zajac [31].

The Gait2392 is a lower extremity MSK model with two legs and a torso segment. The lower limbs are modelled as 11 different segments, one pelvis, two femurs, two tibias, two taluses, two feet, and two toe bodies, described in Table A.1 (Appendix A). All these segments have a fixed reference frame, which is represented in Figure 2.1(a). Additionally, it features 23 Degrees of Freedom (DoF) and 92 musculotendon actuators, representing 76 muscles in the lower extremities and torso. In terms of muscle geometry, the paths of the muscle-tendon

actuators are represented by a series of line segments (shown in red in Figures 2.1(b) and 2.1(c)) and are defined by anatomical landmarks. For most muscles, the origin and insertion points are sufficient for an accurate description of the muscle path. However, for muscles that wrap around other muscles or bones during their ROM, intermediate via points or wrapping points are needed within the muscle's path to depict their path more precisely. It features the Thelen model, a Hill-type muscle model that is adjusted for each muscle included in the model.

The model's default configuration represents a subject who is 1.80 metres tall and weighs 75.16 kilograms. The mass and inertial properties of most segments are based on the average anthropometric data collected from five subjects. However, for the toes and hindfoot, the inertial properties are determined by modelling the volumes of the segments as sets of connected vertices. Based on Veerkamp *et al.* [9], the model presents a NSA of 123 degrees, AVA of 17 degrees, and TT angle of 0 degrees. Although it does not present upper limbs, Gait2392 can still be used as a full-body model when focusing on lower limb movements [32], [33].

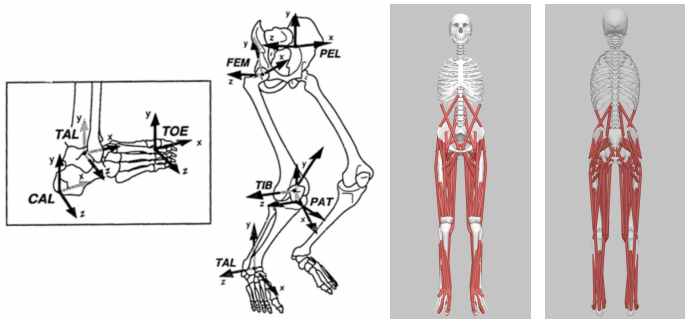

(a) (b) (c)

Figure 2.1: Gait2392 MSK model: (a) Body-segmental reference frames for the pelvis (PEL), femur (FEM), patella (PAT), tibia (TIB), talus (TAL), calcaneus (CAL), and toes (TOE). The patella was later removed by Ajay Seth to avoid kinematic constrains, (b) and (c) Gait2392 simbody model in OpenSim, viewed from the positive and negative X-axis (antero-posterior direction), respectively. Retrieved from [34] and OpenSim 4.4 [3].

In summary, Gait2392 offers a detailed representation of the MSK system, however, as a generic model, it uses bony geometry derived from non-pathological adult cadavers. Although the model may be scaled to match the anthropometrics of individuals, it may not be fully adequate to investigate children or populations with pathological conditions. Furthermore, while the model has 23 DoF, only one is assigned to the knee joint, limited to flexion-extension, potentially restricting its applicability in studies where a detailed knee is preferable or required.

2.5.2 Subject-Specific Musculoskeletal Model: Torsion Tool

Subject-specific MSK modelling covers a broad category of approaches with different levels of detail that personalise geometric features, internal muscle parameters, and neural control

parameters to better represent individual anatomy and function. Personalisation is expected to be particularly relevant in pathological populations. The Torsion Tool is a MATLAB-based tool for personalising femoral and tibial geometries in OpenSim MSK models, thus emerging as a fast and simple way to include personalised geometry [9]. It requires as input an individual's AVA, NSA, and TT, using that input to rotate the corresponding bones and associated muscle points, creating a new MSK model, that can be directly used for simulations.

For the femur, the subject-specific rotations are implemented using Arnold and Delp [35] and Arnold *et al.* [36], and extended to include NSA. The generic Gait2392 femur has AVA and NSA and of 17 and 123 degrees [9], respectively, from which are subtracted the input angles to obtain the required rotations. Assuming torsions are primarily in the proximal femur, three transformations are performed: (1) rotating the vertices of the femoral head, neck, and greater trochanter (AVA around the shaft, and NSA around an axis perpendicular to the neck and shaft axis); (2) rotating the lesser trochanter and proximal shaft with a linearly decreasing AVA along the shaft; and (3) translating the femoral head, neck, trochanters, and shaft to restore the femoral head's original position. The distal shaft is then gradually adjusted to align with the fixed femoral epicondyles. Since the femoral head and epicondyles do not change, hip and knee joint centers are not affected. Finally, femoral muscle attachments are adjusted by mirroring the transformations applied to the bone geometry [9].

For TT, the Torsion Tool applies Hicks *et al.* [37] techniques. The generic tibia's angle is 0 degrees [9]. To rotate it, the tibia is divided into three segments along its long axis. The distal third and foot (talus, calcaneus, and toes) are rotated by the full torsional angle, including the ankle, subtalar, and metatarsophalangeal joint centers and rotational axes. The middle third is rotated with a linearly increasing tibial angle, while the proximal third remains constant.

2.6 Electromyography

EMG is a technique for measuring muscle response or electrical activity in response to a nerve's stimulation of the muscle. There are primarily two types of EMG commonly used: surface EMG, a non-medical procedure where electrodes are placed on the skin's surface, and intramuscular EMG, performed with a needle electrode or a needle containing two fine-wire electrodes inserted directly into a muscle. When a muscle contracts, it generates an electrical current known as action potentials, which propagate through the muscle tissue and is detected by the electrodes. Muscle contraction is, therefore, measured by detecting the potential difference between two electrodes. The current is generally proportional to the level of muscle activity, so the amplitude, measured in microvolts, and frequency of these electrical signals provide information about the degree and timing of muscle activation. The most used technique for gait analysis is surface EMG. The frequencies of surface EMG signals typically range between 6 and 500 Hz, with the majority of frequency power concentrated between 20 and 150 Hz [38].

3

Literature Review

This chapter provides a review of literature studies on MSK modelling and is subdivided into three sections. In the first section, the MSK modelling domain is explored and discussed. The second section offers a comprehensive review of studies focusing on crouch gait. Lastly, the third focuses on state-of-the-art techniques for subject-specific modelling and personalisation.

3.1 Musculoskeletal Modelling in Gait Analysis

The study of human motion, especially gait abnormalities caused by neurological disorders, has become increasingly important in clinical diagnosis. Gait analysis plays a crucial role in identifying pathological gait patterns that may not be evident through visual observation, aiding clinical diagnosis, treatment planning, and rehabilitation in neuromuscular and MSK diseases [39].

Gait analysis dates to the late 19th century, but it wasn't until the development of video camera systems that it gained widespread application in biomedical engineering. The standard method of gait analysis involves using a multi-camera motion capture system and force platforms to measure Ground Reaction Force (GRF)s. However, this method requires specialised laboratories, expensive equipment, and extensive setup and post-processing [40].

Nowadays, Three-Dimensional Gait Analysis (3DGA) techniques are used to estimate joint kinematics and kinetics to help clinical decision-making in individuals with CP, although they often do not give direct objective MSK information. Therefore, to establish a surgical strategy based on 3DGA data, surgeons need to extrapolate its results to infer MSK impairments.

Recent advancements in computer modelling and simulation have enhanced the study of movement by not only providing a comprehensive view of the kinematics and kinetics, but also an understanding of how the nervous system and muscles cooperate to generate synchronised movement of the body parts, thus bridging that gap in gait analysis. This approach, known as neuromusculoskeletal modelling has been increasingly used in sports performance research and CGA over the last two decades [10], which is justified, taking into account the recognised need for individualised therapy [41].

In recent years, OpenSim, a widely used open-source MSK modelling software [3], has

facilitated the estimation of kinematic, muscle-related and joint forces outputs. It addresses limitations of a previous modelling environment developed by Delp and Loan [29], named SIMM (Software for Interactive Musculoskeletal Modelling), which was the first software aimed at developing and evaluating anatomical models. Ultimately, OpenSim enhances clinical decision-making by providing additional biomechanical insights into MSK disorders [42].

Despite its potential, MSK modelling has not yet been widely incorporated in clinical protocols, and a well-established framework for reliably predicting the neuromusculoskeletal dynamics of healthy and pathologic subjects is still lacking. This is thought to be due to the lack of gold standard validation methods, making it difficult to assess the benefits and drawbacks of available approaches [41]. In addition, most MSK models are based on cadaveric data from adults, which are then scaled to match the anthropometry of a subject. This method poorly represents paediatric populations, particularly those with CP, who exhibit altered muscle composition, morphology, and bony structures [43].

Many clinical gait laboratories still rely on the generic gait models that do not take into account subject-specific anatomical variations. However, personalisation is expected to be extremely relevant in pathological populations, where, for example, individual femoral geometry plays a crucial role in muscle forces and joint loading. Understanding these variations could help clinicians improve treatment strategies for patients with femoral abnormalities. Kainz *et al.* [15] stated that neglecting an individual's femoral geometry can result in inaccuracies exceeding five times the Body Weight (BW) in joint contact force estimations. Nevertheless, most modelling in the literature relies on generic models due to their simplicity and accessibility.

3.2 Understanding Crouch Gait Biomechanics

Crouch gait is one of the most prevalent and severe gait patterns in children with CP. Various studies have used MSK modelling and experimental gait analysis to investigate the biomechanical factors that contribute to crouch gait, comparing it with unimpaired gait to develop effective interventions.

Hicks *et al.* (2008) [44] investigated the impact of crouch posture on the ability of muscles to extend the hip and knee joints and the joint flexions induced by gravity during single-limb stance gait phase. Their findings showed that all crouch severity levels reduced the ability to extend the joints, with major reductions observed in the joints' accelerations for important stance-phase muscles while increasing joints' accelerations induced by gravity. The study concluded that crouch gait is biomechanically unsustainable, and the negative impacts increase with worsening severity. The authors also explored how variations in TT influence crouch gait biomechanics, demonstrating that increasing the angle of deformity resulted in a reduction in hip and knee extension accelerations. These results demonstrated that correcting a patient's tibial alignment may lead to significant improvement in gait efficiency.

Building on this, Steele *et al.* (2012) [10] examined how muscle forces and compressive tibiofemoral loads change with the increasing knee flexion associated with crouch. Using a

scaled MSK model to compare TD children with CP children with different levels of crouch severity, the researchers concluded that moderate-to-severe crouch leads to significantly higher tibiofemoral compressive forces, caused by an elevated quadriceps force required to support for the body.

Further exploring muscle strength requirements, Steele *et al.* [45] directed another study in the same year simulating muscle weakness (by reducing the force-generating capacity of certain muscle groups) to assess its impact on crouch gait. Their findings confirmed that walking in a crouched posture demands higher quadriceps strength than typical walking, and that increased crouch severity further exacerbates this demand. While, the impact of strength training on children with CP remains uncertain, this study suggests that targeting the muscle groups that contribute the most to an individual's abnormal gait may optimise rehabilitation strategies.

Expanding on these insights, Steele *et al.* (2010) [46] investigated how muscles contribute to COM and joint angular accelerations during single limb period in crouch gait. This was the first study based on muscle-driven simulations to examine muscle contributions in individuals with crouch, revealing that crouch gait demands greater muscle forces than unimpaired gait for both support and propulsion. Interestingly, although similar muscles are used for body support in both gait patterns, the propulsion strategy differs, with crouch gait requiring prolonged activation of support muscles throughout single-limb stance. These findings suggest that some children with CP may adopt a crouched posture as a functional strategy due to their neurological limitations.

3.3 Subject-Specific Musculoskeletal Modelling

Subject-specific models are appealing as they consider individual anatomical variations, allowing for a more reliable estimation of a subject's biomechanics. Various approaches exist, differing in their level of personalisation and complexity. However, most studies focus on kinematics and kinetics, with limited research assessing their impact on muscle force estimations.

The work of Akhundov *et al.* [47] explored the impact of personalising MSK model geometry, such as body segment mass, inertia, joint centre, and maximum isometric muscle force, on kinematics, kinetics, and muscle-tendon unit dynamics. Its findings revealed the greater physiological precision of subject-specific models, presenting more plausible fibre lengths, higher fibre velocities, and lower muscle forces, highlighting their potential, particularly in populations with substantial anatomical variability.

Another strategy using peronalisation was presented by Song *et al.* [48], who investigated the role of geometric specificity in modelling dysplastic hips. They compared three models with increasing degrees of specificity in pelvis geometry: a low specificity model, Gait2392 generic model isotropically scaled based on marker measurements; a moderate specificity model, an anisotropically scaled model based on CT pelvis reconstructions; and a fully subject-specific model, created by replacing OpenSim's pelvis segment with the exact CT pelvis geometry at the corresponding location and orientation in the model. The authors

concluded that high geometric specificity significantly impacted hip Joint Reaction Forces (JRF)s and muscle forces, whereas moderate specificity did not estimate hip biomechanics differently than generic models. This suggests that while precise geometry is valuable, certain levels of personalisation may not yield substantial improvements in biomechanical estimates.

In order to study the combined effects of geometric and motor control personalisation, Kainz *et al.* [49] compared generic, generic EMG-informed, and MRI-based models with and without EMG data. Their results showed minimal differences in joint kinematics and kinetics but pointed out the influence of personalisation on muscle forces and Joint Contact Forces (JCF)s. Specifically, subject-specific hip geometry significantly impacted JCFs, whereas motor control personalisation had a greater impact on ankle biomechanics. Kainz drew the conclusion that despite their advantages, subject-specific MSK models are time-consuming and introduce additional uncertainties.

3.3.1 Torsion Tool

In 2021, Veerkamp *et al.* [9] developed the Torsion Tool, as a less time- and cost-intensive personalisation approach that does not require a high level of technical expertise.

Additionally, they investigated the Torsion Tool's femoral performance by comparing the personalised femur bones and generic femurs against measurements from MRI segmentations. The results showed that the Torsion Tool produced femur geometries that were significantly closer to the segmented femur geometries compared to generic femurs. Furthermore, the tool showed larger improvements for femurs with higher NSA and AVA deviations from the generic values.

The initial version of the Torsion Tool had a few limitations, as it was only implemented for a single model, the Gait2392 [29], one of the most used models in the literature. Additionally, mass and inertial properties are not adjusted by the tool, however, these changes are expected to be minimal, given that only a relatively small portion of the femur is being rotated. Despite these limitations, the authors stated that the use of the Torsion Tool is expected to improve the accuracy of MSK simulations, particularly in cases with substantial torsional deformities [9]. An updated version expanded the tool's compability to additional generic models, including 'Rajagopal' [50], 'Lernagopal' [50], [51], 'Lenhart' [52] and 'Hamner' [53].

4

Methodology

The research work described in this dissertation was carried out in accordance with the norms established in the ethics code of Universidade Nova de Lisboa. The work described and the material presented in this dissertation, with the exceptions clearly indicated, constitute original work carried out by the author.

This dissertation consists of a retrospective analysis of biomechanical data previously collected in the Biomechanics and Functional Morphology Laboratory of FMH-UL, following an acquisition protocol approved by the Faculty of Human Kinetics Ethics Committee (see Annex II). This research is part of the project 'Development of a simulation platform based in musculoskeletal models to predict recovery of gait following orthopaedic interventions in cerebral palsy children' (https://doi.org/10.54499/PTDC/EMD-EMD/5804/2020). For this thesis, the analysis centred on a specific subject with CP, severe crouch gait pattern, multiple CGA sessions, and who underwent SEMLS surgery.

This chapter starts with a clinical description of the subject, followed by data acquisition and processing methods, and an explanation of the OpenSim pipeline followed to achieve the thesis objectives, organised into six subsections.

4.1 Subject

In the presented case, the subject is a child diagnosed with spastic diplegia CP and iatrogenic crouch gait, classified with GMFCS Level III (see Figure A.2). Gait data was collected across four distinct sessions. The initial session took place approximately one month before SEMLS for gait diagnostic purposes and surgical planning. The subsequent two sessions occurred one and two years after surgery as follow-ups. The last session took place ten years after the first. For this thesis, the pre-, one-year post-, and ten-year post-surgery were selected and labeled as sessions one, two, and three, respectively. The subject's physical characteristics throughout these sessions can be found in Table 4.1.

Table 4.1: Anthropometric data for the subject's three clinical sessions: pre-surgery, one-year post- and ten-year post-surgery, respectively.

	Anthropometric Data				
	Age (years)	**Weight (kg)**	**Height (cm)**	**GMFCS**	**Walking Speed (m/s)**
CP session 1	13	60.60	169.70	III	0.593
CP session 2	14	62.80	170.80	III	0.760
CP session 3	23	76.35	-	III	-

4.2 Data acquisition

4.2.1 Gait Data Acquisition

All sessions followed the same protocol. The acquisition started with a clinical examination to measure anthropometric features, muscle strength, lower limb ROM, and spasticity. The AVA and TT were measured in the clinical examination using the TPAT (see Section 2.1.1.1) and TFA (see Section 2.1.1.3) methods. However, the TFA measurements were not considered realistic, and TT was obtained using the Visual3D software (C-motion Inc., Kingston, Canada) as the angular difference between the shank segment defined by the transcondylar axis and the segment defined by the TMA. The NSA was assessed through X-ray imaging.

Following physical examination, gait analysis took place using 3D marker-based motion capture with Qualisys Track Manager (QTM) software (Qualisys Inc., Gothenburg, Sweden) and 14 infrared Qualisys Oqus cameras at 100 Hz. The cameras recorded the position of 53 reflective markers for sessions one and two, and 36 markers for session three. The markers were placed on the participants' lower limbs, pelvis, and trunk, placed on specific bony prominences, based on the CAST (Calibrated Anatomical Systems Technique) marker set [54], with an adapted Oxford Foot Model [55] marker set for the feet. GRFs were collected on three ground embedded force platforms, represented in Figure A.5 (Appendix A), at 1000 Hz.

The gait analysis included static trials for scaling the MSK model, followed by dynamic trials where the participant walked at natural speed over the force plates. Additional data were collected for plantar pressure and EMG of lower limb muscles.

4.2.1.1 Pre-Surgery Data

Concerning the pre-surgery data, the CGA showed that the child revealed specific impairments contributing to the crouch gait pattern and signs of spasticity. The lower limb torsional angles before surgery are presented in Table 4.2, referred to as ROM for CP session one. The AVA and TT were obtained using the TPAT and the Visual3D software (C-motion Inc., Kingston, Canada), respectively, as aforementioned. The NSA was measured in a radiograph.

Gait analysis showed both knees persistently flexed, with excessive right hip flexion and internal rotation. Although both feet generated a plantarflexor moment and power during push-off, the ankle exhibited excessive supination and a toe-out moment.

4.2.1.2 Post-Surgery Data

The surgical intervention consisted of a SEMLS with five major courses of action around the three lower limb joints: at the hip joint, a bilateral *rectus femoris* proximal tenotomy was performed; at the knee joint, a *semitendinosus* tendon transfer to the adductor tubercle and suturing about itself bilaterally were performed, along with a femur extension osteotomy (percutaneous on the right and open on the left); at the ankle joint, a bilateral internal derotation osteotomy of the tibia with osteosynthesis was performed, as well as a left peroneal distal oblique osteotomy.

The post-surgery data were divided into session two (one-year post-surgery) and session three (ten-year post-surgery).

In the second session, the CGA showed notable improvements in the patient's gait and lower limb biomechanics. The right AVA and TT showed the greatest improvements, with nearly 40 degrees of external TT reduction, bringing it closer to the generic model, while the left TT exhibited just a slight decrease. These angles are presented in Table 4.2. The NSA was considered the same as in the previous session since no new radiographs were taken, and the proximal femur, which affects the NSA, was not involved in the surgery. Overall, an improved posture and gait were observed.

The third session, performed ten-year post-surgery, showed some values worsened over time, as observed in Table 4.2. Specifically, both AVA increased, with the right limb being closer to the first CGA values than the second. The TT angles were similar to the one-year post-surgery time point. The NSA values, measured from the latest radiography, were similar to those in previous sessions, as expected, since the NSA was not affected by the SEMLS and tends to stabilise once skeletal maturity is reached.

4.2.2 Electromyography Data Acquisition

EMG signal acquisition was performed using the Trigno Wireless Biofeedback System from Delsys [56], with a sampling rate of 1000 Hz. Electromyographic data were recorded for the *gluteus medius*, *rectus femoris*, *adductor longus*, *semitendinosus*, *tibialis anterior*, and *gastrocnemius medialis* during sessions one and two. However, EMG data were not collected for session three.

4.3 Data Processing

4.3.1 Gait Data Processing

The data was processed after each CGA using QTM and Visual3D software (C-motion Inc., Kingston, Canada). The QTM programme was used for marker identification/digitalisation. The marker trajectories, GRFs, and EMG data were then exported to the Coordinate 3D (.c3d) format using Visual3D (C-motion Inc., Kingston, Canada). These .c3d files served as the starting point for MSK modelling in this thesis.

Gait trial selection, identification of gait events, and visualisation of GRFs and EMG signals were performed using Mokka (MOtion Kinematic & Kinetic Analyser) software, provided by The Biomechanical ToolKit (BTK) [57]. The analysis focused on the single support phase, as double support could not be explored due to a lack of force plate data. Nevertheless, examining the single-limb phase is clinically significant since the inability to support the mass centre during this period may contribute to crouch gait [46]. Children with a crouch gait pattern show extended double support periods, resulting in shorter single support phases compared to TD children.

For the first session, two trials were selected, while for the other two sessions, three trials for both lower limbs. The choice of trials was based on the following criteria: both feet not being in contact with the same force platform during the stance phase (because the output from the force platforms is the total resulting GRF vector), feet being entirely inside the platform, good centres of pressure, expected force platform graphs, and good EMG graphs, i.e., with clear muscle activation patterns, a high signal-to-noise ratio, absence of artefacts, and adequate magnitude. The single support phase was identified from the contralateral foot off and foot strike events based on GRFs and marker position data.

4.3.2 Electromyography Data Processing

The EMG data were pre-processed with a high-pass filter at 30 Hz to remove low-frequency noise and artefacts. To assess muscle activation patterns during the single support phase, the EMG data were further processed in Python to extract activation profiles. This process involved three stages: noise reduction, signal rectification, and envelope extraction.

Noise reduction was performed using the NeuroKit2 library [58] in two steps: a fourth-order 100 Hz high-pass Butterworth filter (carried out using SciPy library [59]), followed by a constant baseline detrending to centre the signal around 0 and remove gradual shifts in the baseline level. The 100 Hz cutoff frequency was chosen based on the assumption that the muscle activation in EMG is typically contained in higher frequencies, while noise and artefacts occur at lower frequencies.

Following noise reduction, rectification was applied to obtain absolute values of the cleaned signals. Subsequently, EMG envelopes were extracted by applying a fourth-order Butterworth low-pass filter of 8 Hz, implemented using the SciPy library [59] and expressed as a fraction of the Nyquist frequency. The filter was applied using a dual-pass zero-phase filtering method. The combination of rectification and low-pass filtering results in the signal's linear envelope, which is a widely accepted measure of muscle activation in research and clinical practice.

For this study, the normalisation of the EMG signals was achieved based on the peak value of each muscle in the trial under examination, i.e., the maximum of the EMG linear envelopes. The peak value method cannot distinguish different levels of muscle activation, disregarding valuable information about innervation levels. However, for this study, which focuses on comparing only the same muscles and EMG patterns within the gait cycle, this method is suitable [38].

4.4 OpenSim Implementation

The MSK simulations were implemented in OpenSim 4.4 [3] following the pipeline illustrated in Figure A.6 (Appendix A). From the models available in the platform, the Gait2392 (see Section 2.5.1) was selected as the baseline model for the simulations. The input static and dynamic marker trajectory files, along with .mot files, which were used to create GRF files for OpenSim, were generated using a MATLAB script by loading the .c3d files.

The workflow includes the scaling, Inverse Kinematics (IK), Inverse Dynamics (ID), Residual Reduction Algorithm (RRA), Computed Muscle Control (CMC), and Induced Acceleration Analysis (IAA) tools, and was applied to every trial for the following models: linearly scaled Gait2392 model and personalised torsion model created using the Torsion Tool to incorporate the subject's femoral and tibial deformities. The values of these deformities are presented in Table 4.2 as ROM.

Since bone deformities were assessed using clinical analysis and radiography, both prone to measurement variability, two additional models were developed to account for the maximum estimated measurement variability (see Section 2.1.1). For femoral AVA, the LoA range was calculated based on the data from Sangeaux *et al.* [60], using the mean difference CT minus physical examination and the associated variability. As for NSA, LoA were determined between the CT and the radiograph measurements stated by Chung *et al.* [16]. Finally, for TT, LoA were calculated from Hawi *et al.* [61] as CT minus clinical examination. The input values used for personalised models, along with LoA, are detailed in Table 4.2. 'ROM-LoA' accounts for the lower-bound extreme limits, while 'ROM+LoA' for the upper-bound LoA. Including models that account for the LoA between different measurement techniques ensures the analysis captures the realistic variability introduced by the measurement methods used.

4.4.1 Model Preparation

The Gait2392 was linearly scaled for each session, and three additional models were created using the Torsion Tool per session. In total, nine Torsion Tool models were generated and studied: Personalised, 'Personalised-LoA', and 'Personalised+LoA' for each session.

Prior to initiating the workflow, it was necessary to run the Torsion Tool to generate the subject-specific MSK models mentioned above [9]. This process involved executing a MATLAB script to create an OpenSim model with personalised geometries and an adjusted marker set, using as inputs the AVA, NSA, and TT (see Table 4.2), and the virtual marker file. Additionally, default angles of the generic Gait2392 model geometry were also specified. The default angles were the ones mentioned in Section 2.5.2, and are also presented in Table 4.2.

The Torsion Tool computes the rotations as explained in Section 2.5.2 and creates a new model with the corresponding adjusted torsions. An example of the outputs computed by the Torsion Tool when rotating the femur and tibia to create the personalised model is shown in Figure A.7 (Appendix A) for the pre-surgery data (session one), following the values in

Table 4.2: Lower limb rotations, shown in degrees, for the Gait2392 model and the subject's three clinical sessions: pre-surgery (session one), one-year post-surgery (session two), and ten-year post-surgery (session three). For each session, the ROM (see Section 4.2.1.1) is presented alongside the lower and upper bounds of the LoA, sourced from [16], [60], [61]. The default AVA, NSA and TT values from the Gait2392 model are referenced from [9] (see Section 2.5.1). The 'Personalised' model uses ROM, while 'Personalised-LoA' and 'Personalised+LoA' models incorporate the lower and upper LoA bounds, respectively.

		Lower Limb Rotations (degrees)					
		AVA		NSA		TT	
		Left	Right	Left	Right	Left	Right
Linear Scaling Gait2392		17		123		0	
LoA	Lower Bound (-LoA)	-25.44		-10.66		-9.35	
	Upper Bound (+LoA)	29.44		2.66		8.45	
CP session 1	ROM	44	50	140	140	31	44
	ROM-LoA	18.56	24.56	129.34	129.34	21.65	34.65
	ROM+LoA	73.44	79.44	142.66	142.66	39.45	52.45
CP session 2	ROM	30	28	140	140	27	7
	ROM-LoA	4.56	2.56	129.34	129.34	17.65	-2.35
	ROM+LoA	59.44	57.44	142.66	142.66	35.45	15.45
CP session 3	ROM	34	40	144	142	25	6
	ROM-LoA	8.56	14.56	133.34	131.34	15.65	-3.35
	ROM+LoA	63.44	69.44	146.66	134	33.45	14.45

Table 4.2. The four models generated for the pre-surgery time point are illustrated in Figure A.8 (Appendix A), allowing the visualisation of the differences between the generic model and the Torsion Tool-generated models.

4.4.2 Scaling

The first step in the OpenSim pipeline for the four models was scaling [3] to adjust the anthropometry of the models to match the subject's characteristics as closely as possible. This was achieved by applying the distances between the experimental markers from the static trial to the corresponding virtual markers on the model. Ideally, MRI data would be used to scale the geometry of bodies and accurately place model markers, but such data was not available.

The scaling tool required two inputs: the model and the experimental marker trajectories from the static trial; and two setting files: the marker set with the virtual markers, and the scale setup file, containing the mass of the subject, scale factors, and static pose weights. The resulting output was a linearly scaled OpenSim MSK model scaled to the dimensions of the subject.

The adjusted anthropometry was achieved by computing scale factors for each body segment, determined from the relative distances between experimental and virtual markers.Uniform scaling was applied to most segments and non-uniform scaling used for the pelvis and torso, meaning that the x-y-z axes were treated independently. These scale factors were then applied to joint locations, mass properties, muscle attachment points, and

length-dependent parameters, while targeting the individual's mass.

Marker registration was performed to align tracking markers, such as marker clusters and other markers placed on non-specific body landmarks, which are not used for the scaling itself, with the experimental data. In contrast, anatomical markers placed on bony landmarks, were fixed to track body segments. Additionally, marker weights were assigned based on confidence in their placement, prioritising reliable anatomical markers to determine how strongly the virtual markers should track the experimental marker positions. Once this was assigned, a static pose was computed. Regarding foot markers, a simplification of the Oxford Foot Model [55] was applied for sessions one and two, using a reduced set of markers, which remained consistent with those used in session three. The metatarsophalangeal joint was locked in a neutral position, while the subtalar joint was locked after scaling to maintain realistic foot kinematics. This was necessary because the ankle's role in muscle force estimation is particularly sensitive to errors due to its lower mass compared to other segments.

To determine the accuracy of scaling it is important to recognise that simulations, particularly scaling a model, are subjective processes. However, one approach to evaluate the scaling was to ensure that the static pose seemed realistic and resembled the subject's pose in the static trial. The anatomical virtual markers were also confirmed to remain in place during marker registration and close to the corresponding experimental markers.

4.4.3 Inverse Kinematics

The second step was IK, which was used to determine joint angles needed to best match the virtual markers (and associated body) to the experimental markers over a specific interval. This corresponds to the pose that minimises the sum of weighted squared errors between the experimental marker data and the virtual markers from the scaled model.

IK, as the name suggests, is an inverse method, just like ID, meaning it uses the desired data or motion to estimate the values required to generate that data or motion. The primary inputs were: the scaled model, dynamic marker data, time range of interest (single support phase), and a setup file with marker weights. Similar to scaling, marker weights are relative and determine how well the virtual markers should track experimental markers. However, in IK, since there is movement, the markers more likely to fall off or move, such as the medial knee and medial ankle markers, were attributed lower weights. On the contrary, stable markers, for example clusters, were given higher weights to improve tracking accuracy and reduce kinematic errors. Having redundant tracking markers in IK is useful because it allows for a better distribution of weights over multiple markers. The output was a motion file containing the generalised coordinate trajectories, i.e., joint angles and body positions.

The drawback of this approach is that it is a global optimisation method that optimises all joint angles simultaneously, meaning that marker errors in one segment can influence the joint angles in others. It is used in MSK modelling because it ensures consistent segment lengths across the trial and prevents bone penetrations [62].

For evaluating IK results, good kinematics rely on accurate data and a well-scaled model.

Therefore, if the results were considered unsatisfying, the scaling process was repeated. The first step in the evaluation was to assess the results visually by comparing virtual and experimental markers across motion frames, identifying errors exceeding acceptable thresholds. OpenSim documentation [3] accepts Root Mean Square (RMS) marker errors under 2 cm and maximum errors within 2–4 cm, as segment lengths and joints remain fixed and unchanged. Moreover, kinematic plots for joint angles were verified against expected patterns from the gait analysis reports obtained from Visual3D (C-motion Inc., Kingston, Canada).

4.4.4 Inverse Dynamics

After determining joint angles and positions, the next stage was to calculate joint moments. The ID tool uses output from IK, together with GRFs, to calculate generalised forces, i.e., net forces and torques, around each joint responsible for a given movement, while applying a 6 Hz filter to kinematic data. Therefore, the required inputs for this analysis were the scaled OpenSim model, the motion file from the IK, containing the time histories of generalised coordinates, and a GRFs file [3]. The resulting output was a time history of net torques around the joints and residual forces acting on the ground-linked body (i.e., the pelvis).

The ID tool uses the model's known motion derived from IK, defined by generalised positions, velocities, and accelerations, to calculate the unknown internal generalised forces required to maintain the motion. These joint moments were compared with the CGA reports. Results reflect the internal joint moments generated by the body to counterbalance the moments produced by external forces (i.e., GRF and inertial properties of the different bodies), enabling the observed kinematics to occur while constrained to external loads.

Handling *in vivo* kinematic data often comes along with unwanted experimental errors, usually related to inaccurate mass distribution, noise, and modelling assumptions. These errors result in dynamic inconsistencies between the measured kinematic data and the GRFs. As a result, non-physical external compensatory forces and moments arise to account for these discrepancies, the residuals.

4.4.5 Residual Reduction Algorithm

The RRA tool uses the ID result, calculated from joint kinematics and experimentally measured GRFs, and reduces the magnitude of pelvis residuals while making as few adjustments to the joint kinematics and model mass properties. This is significant because large residuals can distort the kinematic data.

The RRA needed as inputs the scaled model, kinematics from IK tool, the GRFs file, a tracking tasks file, specifying which coordinates to track and their weights from the IK data, and an actuators file, defining the ideal residual and reserve joint actuators. The reserve actuators are the DoF that connect rigid body segments and assist joint torques where muscle forces are insufficient (replace the muscles in the model). The residual actuators correspond to the six DoF between the pelvis and the ground, which include three translational DoFs (residual forces F_x, F_y, F_z) and three rotational DoFs (residual moments M_x, M_y, M_z). Similar

to ID, a 6 Hz filter was applied. The algorithm generates several outputs, including adjusted kinematics and a new model with adjusted mass properties.

The RRA is a form of forward dynamics simulation in which a tracking controller follows the kinematics obtained from IK. The tool iteratively computes actuator forces necessary to move the model to the desired configuration at the end of each step, adjusts the model's COM , specified for the torso, and suggests modifying segment masses to reduce residuals. The process was repeated until recommended adjustments were no longer relevant and residual forces and moments were below the recommended threshold given by OpenSim [3]. At each repetition, a new model file with the adjusted torso COM was created and used for the next repetition. This step was crucial for generating a realistic simulation for the next step, CMC, by reducing residual forces, ensuring the kinematics remain accurate.

4.4.6 Computed Muscle Control

The new model generated from the RRA is used by the CMC tool to calculate the individual muscle excitations that guide the model to track the adjusted kinematics from the RRA in the presence of external forces (GRF).

Several data files are required as input to run the CMC, including the model with the adjusted COM from the RRA, the adjusted kinematic data from RRA (filtered at 6 Hz as previously), GRFs file, and three setup files: tasks and actuators files (similar to those used in RRA and explained previously), and an additional control constraints file. This new file defines the limits of excitation for all actuators (muscles, residuals, and reserves). Residual actuators control the model's global position by acting directly between the model and the ground, with small control values applied since residuals were expected to be small given their reduction in the previous step. Reserve actuators, used only when necessary to compensate for muscle strength deficits, were specified with low optimal forces and large constraint values, so they require very high excitation values to apply significant forces and are penalised if used. The tool generates three main outputs: a forces file, with muscle forces, reserves and residuals (forces and moments); a states file, containing model and muscle states (joint angles and velocities, muscle fibre lengths, and activations); and a controls file, with muscle excitations and controls for residual and reserve actuators.

The CMC algorithm computes the muscle excitations necessary to produce the desired kinematics. Before starting, the model's initial states are calculated, including joint angles, velocities, and muscle states (i.e., muscle-tendon unit length and velocities). The algorithm's first step is to determine the desired accelerations to propel the model coordinates towards the experimental kinematic data. Then, the required actuator controls (generalised forces) to achieve these desired accelerations are computed. These controls are distributed synergistically across the actuators, meaning that the algorithm considers the interactions and dependencies between muscles to ensure efficient coordination. In cases where muscle forces alone are unable to achieve the necessary accelerations, reserve torques (actuators) are activated to compensate. Finally, muscle excitations are calculated and used as input for a forward dynamic simulation that progresses in time. These steps are repeated at each time

step, ensuring the model accurately tracks the kinematic data.

The muscle groups analysed were the *gluteus medius*, *gluteus maximus*, vasti, hamstrings, *gastrocnemius*, ankle dorsiflexors, *iliopsoas*, *soleus*, and *rectus femoris* (see Table A.2 in Appendix A). These were selected as a combination of the primary muscles used in TD gait and those impacted by neuromuscular deviations in spastic CP [63]. Muscle forces were compared across models and years, and simulated muscle activations compared to experimental EMG data from CGA, as described in Sections 4.2.2 and 4.3.2. The reserve actuator outputs were analysed as a validation method for the CMC simulations.

4.4.7 Induced Acceleration Analysis

After computing muscle forces, the IAA was performed to estimate how individual muscle forces contribute to the acceleration of the COM during the single-limb period in the antero-posterior, vertical, and mediolateral directions. IAA provides insights into how muscle forces influence not only the segments they directly act upon but also other body segments through dynamic coupling, allowing for a more comprehensive understanding of muscle contributions to the acceleration of the whole body [64].

The analysis uses the same model and external loads as the CMC step, along with the controls and states files generated by CMC. The primary output is the induced accelerations for each force contributor (muscles, reserves, residuals, gravity, and forces due to velocity effects) for each coordinate (DoF) and the COM.

The COM acceleration is driven by the contact between the body and the ground, captured as GRFs, since when the foot pushes against the ground, it generates a force that propels the body forward or upward. Although internal forces, such as muscle forces, play a crucial role in generating movement, they do not directly accelerate the body's COM. Instead, muscle forces contribute to the accelerations of body segments through dynamic coupling, indirectly influencing the COM. To understand how each muscle force contributes to the external GRFs and the COM's acceleration, the IAA decomposes the external GRFs into the contributions of each internal force (muscles, reserves, residuals, etc.) to show how much of the GRFs come from each of the internal forces. Induced accelerations are the accelerations produced by the forces within the body.

The IAA tool computes these induced contributions by solving the equations of motion while simulating foot-ground contact with appropriate kinematic constraints [53] that allow the tool to treat the interaction as a system of equations rather than directly applying forces. The 'RollingOnSurface' constraint was chosen for its accuracy, including non-penetrating, antero-posterior and mediolateral no-slip, and no-twist constraints.

As part of the IAA validation, the accuracy of the rolling constraint in representing contact conditions was assessed by comparing total induced reaction forces with measured GRFs. Additionally, to ensure the consistency of results, the total acceleration was compared to the sum of the accelerations induced by each muscle and gravity.

5

Results and Discussion

The primary aim of this study was to compare the generic linearly scaled model with a linearly scaled model incorporating personalised tibial and femoral torsion, while accounting for measurement variability in the creation of the personalised models. This chapter compares these models across the workflow described in Chapter 4 and represented in Figure A.6, with a particular focus on muscle force estimation at different time points, both individually and in comparison between them. For details on the subject's data, see Section 4.1.

5.1 Scaling Results

The static poses obtained using the scale tool for both the linearly scaled generic and personalised models are shown in Figure 5.1 for all time points. Additional perspectives, along with a comparison to the CGA static trial are provided in Appendix B.

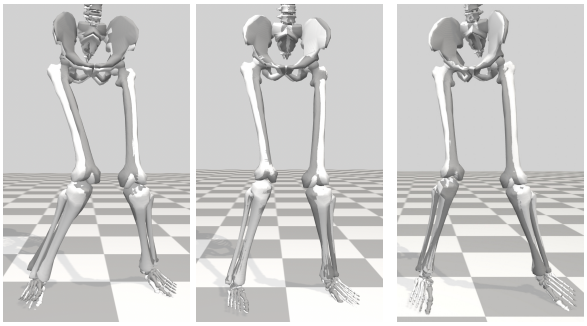

(a) (b) (c)

Figure 5.1: Pre- and post-surgery static poses obtained for both the linearly scaled generic and personalised models, computed using the OpenSim's scaling tool: (a) pre-surgery, (b) one-year post-surgery, and (c) ten-year post-surgery. The generic scaled model is shown in white, and the personalised scaled model in grey.

In both Figures 5.1(a) and 5.1(b), the two models show a good representation of the crouch posture, with flexed hips, flexed knees and turned inward, and heel elevation. In the first session, the personalised model correctly reflects the anterior rotation of the femoral head and its increased verticality relative to the diaphysis. It also shows less hip flexion

compared to Gait2392 model and a more realistic foot eversion, correcting the excessive eversion observed in the generic model. In the second session, one-year post-surgery, hip and knee flexion are reduced, the knees no longer meet at the centre, and the feet show improved stability. For Figure 5.1(c), the static pose closely resembles the one in 5.1(b). The subject required assistance to maintain a static posture, causing some hip rotation due to difficulties in standing unsupported.

5.2 Joint Kinematics and Moments

Figures C.1 and C.2 present the joint angles during walking for the sagittal plane at the hip, knee, and ankle during the single support period for the left and right legs, respectively. The DoF in the sagittal plane represent hip and knee flexion/extension, and ankle plantarflexion/dorsiflexion. These results correspond to the pre-surgery, one-year post-surgery, and ten-year post-surgery time points across all models (see Section 4.4.1). The hip, knee, and ankle were selected given their significance in crouch gait biomechanics.

Pre-surgery, all models show excessive hip and knee flexion and ankle dorsiflexion, characteristic of crouch gait [65]. Concerning differences between models, there was little variation in hip and knee flexion curves, while ankle angles showed more variability, particularly in the right lower limb at the pre-surgery time point. The linearly scaled generic model exhibits less dorsiflexion, while the Torsion Tool-generated models show higher dorsiflexion, likely due to increased TT, which was highest in the right ankle pre-surgery (see Table 4.2). This suggests that TT had a higher impact on joint kinematics compared to femoral AVA and NSA, contributing to the noticeable differences between models in the ankle joint, as corroborated by [66].

Focusing on the effects of surgery, one-year post-surgery results showed a marked decrease in knee flexion (more than 20 degrees), near zero dorsiflexion at the ankle, and no notable change in hip flexion. These results align with existing literature on multilevel orthopedic interventions, which typically improve sagittal plane kinematics by increasing extension at the hip and knee and reducing dorsiflexion at the ankle [65]. At the ten-year time point, both hip flexion and ankle plantarflexion increased by 20 degrees, which contrasts with findings from long-term studies [67], where the differences observed one-year post-surgery were reported to be maintained in the long term.

In line with the IK results, joint moment curves for the hip, knee and ankle joints computed using the RRA tool are presented in Figures D.1 and D.2 (Appendix D) for the left and right lower limbs, respectively. All curves are normalised by the subject's mass. In general, the results show a strong similarity between models, with the curves closely resembling each other. Any small differences observed are likely due to trial variations rather than model differences. Appendix D also illustrates comparisons between net joint moments obtained using the ID and RRA tools.

The overall similarities observed between models in both kinematics and kinetics are in line with [49] and suggest that modelling choices have a minor impact on joint kinematics and kinetics.

5.3 Residuals Reduction

In most trials, RRA was iterated at least twice until the mass adjustments were minimal and the residuals reached a stable value within the acceptable limits, ensuring consistent kinematics while preserving physiologically realistic joint moments.

Tables E.1-E.3 (Appendix E) illustrate the range of residual forces and moments for ID and RRA to evaluate the effectiveness of RRA. Mean reductions are detailed in Table 5.1, showing that residual forces decreased notably across all models and sessions, with mean reductions exceeding 70% in all directions. Residual moments were more challenging to reduce, especially in the mediolateral direction (MZ) for sessions one and three. However, all peak and RMS values remained within or close to acceptable limits defined by OpenSim [3].

Table 5.1: Mean percentage reductions between ID and RRA in residual forces (F) and moments (M) across sessions and models. The numbers refer to the trial numbers, while the letters '*l*' and '*r*' specify the lower limb, left and right, respectively, associated with each single support period.

		Mean Reduction (%)					
		FX	FY	FZ	MX	MY	MZ
CGA Sessions	Session 1	90.980	74.502	94.505	63.158	65.237	51.642
	Session 2	88.227	80.694	87.924	49.268	80.527	77.892
	Session 3	86.815	75.207	88.484	78.484	66.720	32.550
Models	Generic	87.166	76.213	89.825	63.752	70.775	56.160
	Personalised	87.922	78.226	89.911	64.016	71.979	58.453
	Personalised - LoA	91.001	78.555	89.234	62.764	71.334	55.033
	Personalised + LoA	87.448	75.358	90.149	64.253	72.020	47.658

5.4 Muscle Forces

To validate the CMC tool, each joint's DoF was analysed to verify whether the reserve actuator outputs were in accordance with the established acceptable thresholds. Tables F.1-F.3 (Appendix F.1) present the range values for the reserve actuators and RMS values for each DoF across the three time points. According to the OpenSim documentation [3], all values follow the recommended criteria, peak reserve limits of 25 Nm and RMS limits of 10 Nm, suggesting that the simulations were successfully executed.

The analysis of muscle forces is divided into three parts: comparison of generic vs. personalised models, pre- vs. post-surgery analysis, and measurement variability analysis.

5.4.1 Generic vs. Personalised Muscle Force Patterns

5.4.1.1 Pre-Surgery: Generic vs. Personalised

For the pre-surgery time point, Figure 5.2 shows the variations in BW-normalised muscle forces for both lower limbs in the generic and personalised models during the single support period for the selected muscle groups (see Table A.2 in Appendix A).

The vasti and the left *soleus* produce the highest muscle forces, aligning with the demands of crouch gait to counteract knee flexion and ankle dorsiflexion. Additionally, the *rectus*

femoris shows the second-highest average muscle force for the right leg. These results are consistent with literature [10], [45]. However, the right *soleus* shows lower-than-expected forces. This asymmetry between left and right lower limbs is evident in Figure F.2 (Appendix F.2.1), where the plantarflexors show the highest forces for the left leg, whereas the right limb relies more on knee extensors and hip flexors. This aligns with the high level of asymmetry frequently present in pathological gait patterns [68].

The right limb exhibits the largest discrepancies between models. In terms of patterns, Figure 5.2 highlights three muscle groups with notable differences throughout the single support period: the *gluteus medius*, hamstrings, and *iliopsoas*. Regarding force magnitudes, the personalised model consistently produces higher forces across muscle group functions, and these discrepancies are more pronounced in muscles that are highly active during the task. This is corroborated by [49], who stated that geometrical differences between models alter moment arms of specific muscles, but these changes primarily influence muscle estimates when the muscles are major contributors to the individual's gait.

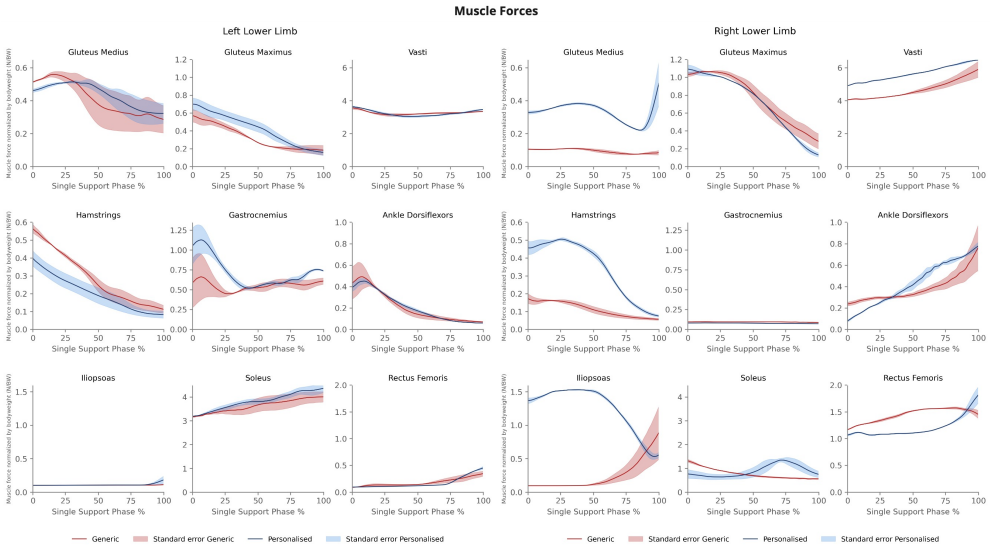

Figure 5.2: Pre-surgery muscle forces during the single support phase of walking in a child with CP scheduled for SEMLS. Data are presented as mean (lines) and standard errors (shaded) for generic (red) and torsion personalised (blue) models. Muscle forces are normalised to the child's BW.

These force discrepancies are further illustrated in Figure F.1 (Appendix F.2.1), which reinforce the higher forces observed in the personalised model, with noticeable differences of approximately 1 BW in the right vasti and right *iliopsoas*. On the left leg, both models exhibit similar patterns and magnitudes. These differences between legs might be explained by the greater AVA and TT observed on the right limb in session one (see Table 4.2), suggesting that greater torsions result in higher simulated muscle forces compared to the generic. The right *rectus femoris* contradicts this trend, with the generic model showing slightly higher forces. Notably, despite much lower forces compared to the vasti, the right *rectus femoris* requires strength at 80% of its maximum isometric force, which is comparable to the vasti (see Figure F.3 in Appendix F.2.1). A similar high demand on the *rectus femoris* in crouch gait was also

reported in [69], further supporting this observation.

5.4.1.2 Post-Surgery: Generic vs. Personalised

The post-surgery muscle force patterns are shown for the one-year time point, following the same logic as the pre-surgery analysis. Figure 5.3 displays the force patterns, while Figure F.5 presents the average muscle forces categorised by muscle function during single support. The corresponding ten-year time point results can be found in Appendix F.2.2.2 (Figures F.7 and F.9).

At both time points, Figures 5.3 and F.7 show that the vasti and *soleus* muscles exhibit the greatest forces, consistent with their primary roles in knee extension and ankle plantarflexion [10], [45]. These trends are further demonstrated in Appendix F.2.2, where the average muscle forces are presented in bar graphs. In the one-year post-surgery analysis, the force patterns between the generic and personalised models are quite similar, except for the *iliopsoas* and right *rectus femoris*. This is expected, as the child had less torsion in the short term postoperatively compared to pre-surgery, resulting in muscle forces that more closely resemble those of the generic model. Similarly, prior studies have reported that moderately personalised models do not always estimate biomechanics differently compared to generic models [48].

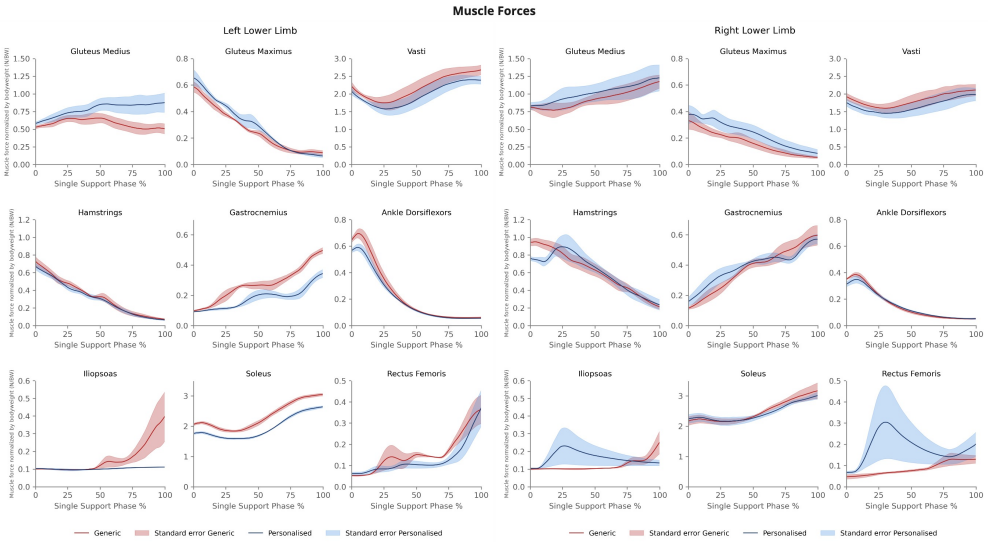

Figure 5.3: One-year post-surgery muscle forces during the single support phase of walking in a child with CP who underwent SEMLS. Data are presented as mean (lines) and standard errors (shaded) for generic (red) and torsion personalised (blue) models. Muscle forces are normalised to the child's BW.

The average muscle forces by muscle function, presented in Figure F.5 for session two, and Figure F.5 for session three, highlight a consistent trend across both time points and across models. The only difference worth referring to is in the left ankle plantarflexors, where the personalised model produces lower forces compared to the generic. These discrepancies between models are solely observed on the left, probably because of the greater deformity

on that side, particularly the higher TT input angles (Table 4.2). This suggest that a higher TT in the Torsion Tool may lead to a decrease in muscle force production.

The required muscle strengths post-surgery are shown in Figures F.6 and F.10 in Appendix F.2.2.

5.4.2 Pre- vs. Post-Surgery Muscle Force Patterns

Entering the second stage of the muscle force analysis, this chapter shifts focus from comparing the generic and torsion personalised models individually to comparing the changes in the generic model against the personalised model across sessions. The aim is to evaluate whether the additional effort required to create a personalised model is justified when comparing pre- and post-surgery outcomes, or if both models provide similar insights in longitudinal comparisons.

Figure 5.4 presents the average muscle force values, normalised to BW, for both models during the single support phase at three time points. The following section will examine the outcomes of the SEMLS on muscle forces, comparing pre- and post-operative muscle force differences between the generic and torsion personalised models. Additional figures can be found in Appendix F.3.

As previously explained in Section 4.2.1.2, the *rectus femoris* underwent a proximal tenotomy on both limbs, which resulted in a reduction of its muscle force post-surgery, as expected [70], particularly evident in the right limb, observed in both models. However, the personalised model shows a smaller reduction, decreasing by 50% in maximum isometric force used, compared to the linear scaled generic model, which showed a 70% decrease (see Figure F.13). This highlights how individual variability in the personalised model may influence the extent of improvement.

The right *iliopsoas* also displays a noteworthy difference, with the personalised model showing a greater force reduction (around 1 BW) between pre- and one-year post-surgery, while the generic model maintains similar muscle forces at these time points. This is further evident in Figure F.13, where the required muscle strength in the personalised model presents a decrease of almost 30%, while the generic shows a decrease of less than 5%. Overactive hip flexors are characteristic of crouch gait, leading to a flexed position at the hip [6]. Given that the *iliopsoas* is the primary hip flexor, and the *rectus femoris* also showed overactivity that decreased post-surgery, the personalised model, which captures a similar trend for the *iliopsoas*, may offer a more realistic representation of post-surgical muscle behavior.

Similarly, both models show reduced overactivity in the vasti muscles and the right *rectus femoris* following the femoral extension osteotomy, which allowed the knee to straighten [65]. However, the personalised model exhibits a larger decrease in right vasti force (approximately 4 BW compared to 3 BW in the generic model). This difference suggests that the personalised model may better capture individual variations in muscle behaviour, leading to a more significant reduction in muscle force.

Regarding the ankle joint, a tibial internal derotation osteotomy was performed to correct excessive external torsion, which improved function of the right *soleus* post-surgery, as

expected from literature [71]. Even though both models show similar trends for the *soleus* in both legs, divergences are observed in the right ankle plantarflexors group (see Figure F.12), where the generic model shows an increase of 1.5 BW from pre- to post-surgery, whereas the personalised model shows a decrease of about 1/4 BW.

Focusing on long-term changes, both models exhibit similar trends in muscle force patterns over the ten-year follow-up, supporting the stability of the surgical interventions, as found in literature [72], for both models.

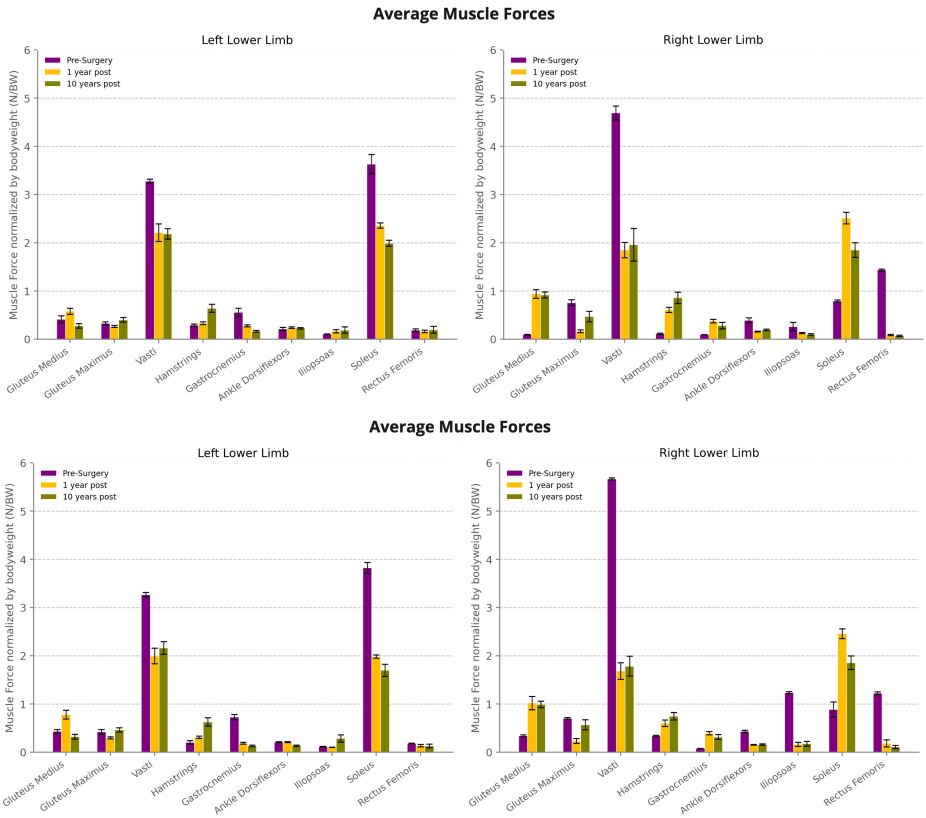

Figure 5.4: Pre- vs. post-surgery average muscle forces for generic (top), and torsion personalised (bottom) models, categorised by muscle group (see Table A.2). Muscle forces are normalised to the child's BW. Error bars are ±1 standard error.

5.4.3 Impact of Measurement Variability on Muscle Forces

To account for variability in measuring femoral and TT angles, the following results present muscle forces for four model types: the previously studied generic and personalised models, along with two additional models representing the lower and upper bounds of measurement variability (see Section 4.4.1 and Table 4.2).

The primary objective is to observe where the linear scaled generic model falls relative to the range defined by the variability models. The personalised model, being based on measured anatomical inputs, is expected to reflect a central value within this range. By comparing the generic model's placement, we can assess whether the differences between the generic and personalised models are within the expected variability or if they extend

beyond it. It is important to note that the variability models represent a plausible range of expected variation rather than definitive anatomical limits.

5.4.3.1 Pre-Surgery Muscle Force Variability

For the first session, Figure 5.5 illustrates variations in muscle force, normalised to BW, during the single support period for the generic model, with the shaded region representing the variability interval between the lower and upper bound models. This highlights how the generic model aligns with the expected range of variability. Additionally, Figure 5.6 presents a comparison of required muscle strength, expressed as a percentage of maximum isometric force, between the generic and personalised models, with error bars representing the variability across both LoA models. Here, the 'personalised' result is the average of the two LoA models ('Personalised-LoA' and 'Personalised+LoA'). Additional plots for all models, including curves with standard errors, average muscle forces categorised by group and function, and required muscle strength, can be found in Appendix F.4.1.

The generic model frequently falls outside the variability range, for example for the right *gluteus medius*, vasti, and *iliopsoas*, indicating that the differences between the generic and personalised models go beyond what can be attributed to measurement variability. In contrast, for the left hamstrings and left *gastrocnemius*, the model remains within the variability range, suggesting that for these muscles the differences between models might be explained by measurement errors in the input angles. However, in these cases it tends to be close to the limit. This results highlight that, even though the generic model does not incorporate individual geometry, it provides a reasonable approximation in muscle forces for some muscle groups. However, it may not fully account for the biomechanical consequences of individual anatomical variations.

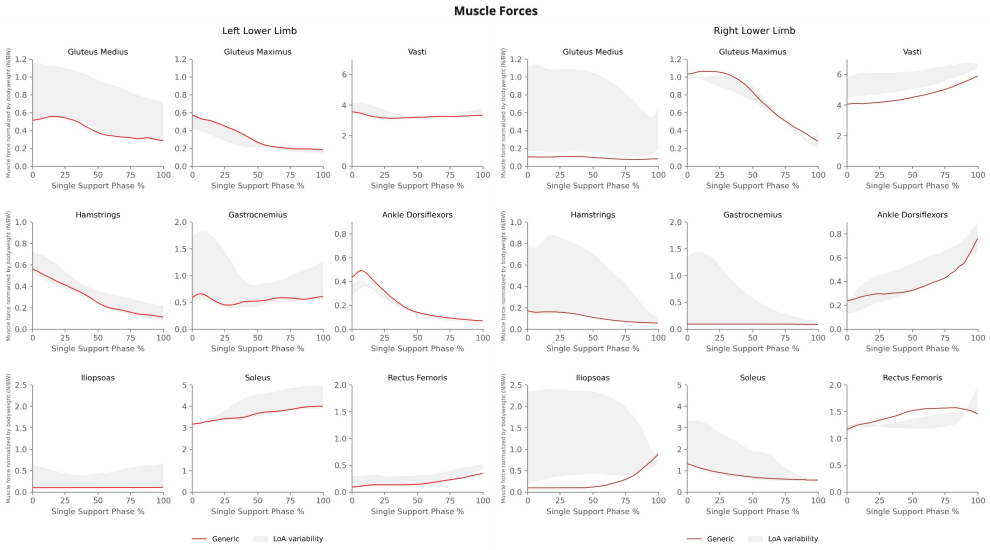

Figure 5.5: Pre-surgery muscle forces during the single support phase of walking in a child with CP scheduled for SEMLS. Data are presented as mean (lines) for the generic model (red) and the shaded region represents the variability interval between the two LoA models. Muscle forces are normalised to the child's BW.

From Figure 5.6, the large error bars in muscles such as the *gluteus medius*, *gastrocnemius*, *iliopsoas* and *soleus* indicate that these muscles are particularly sensitive to changes in torsional parameters. On the other hand, the *gluteus maximus* and left vasti show that torsional parameters have less impact on force predictions for some muscle groups, as the variability is smaller.

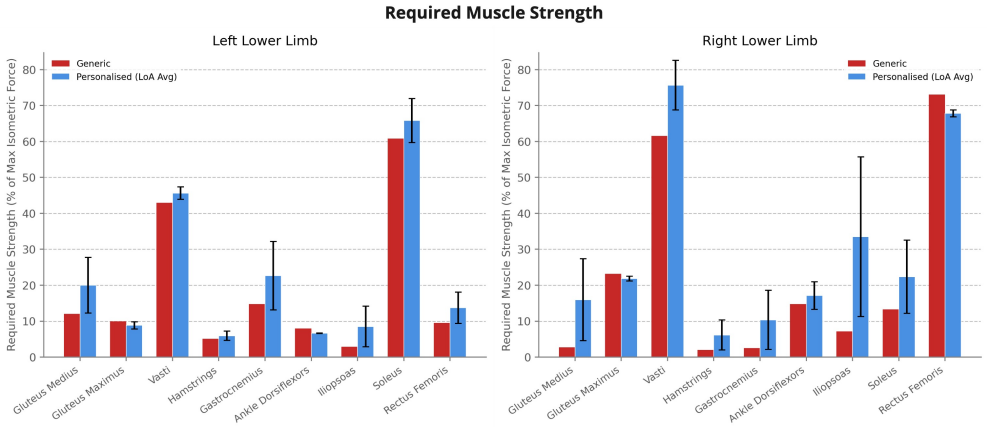

Figure 5.6: Pre-surgery comparison of required muscle strength as a percentage of maximum isometric force between generic and personalised models (average of 'Personalised-LoA' and 'Personalised+LoA'). Error bars represent the variability across both LoA models.

Similar to how anatomical variability in musculotendon point locations affects muscle force predictions in MSK models [73], the variability in anatomical angles in this study also impacts muscle force outcomes, emphasising the importance of accounting for anatomical variability in model personalisation. Additionally, the *iliacus* and *psoas* were identified as the muscles most sensitive to perturbations in the anatomical variability in their study. Similarly, in this study, the *ilopsoas* (right leg) shows the highest sensitivity in the pre-surgery data, with the greatest differences observed between the variability models. In summary, the findings suggest that personalisation could be important for improving the accuracy of MSK modelling in certain cases.

5.4.3.2 Post-Surgery Muscle Force Variability

For the post-surgery analysis, Figure 5.7 presents the average muscle force variations for the generic model with the shaded interval representing the variability range between the LoA models. Figure 5.8 illustrates the required muscle strength for the generic and average personalised models accounting once again for the variability across LoA models. Further details on all models, along with corresponding ten-year post-surgery results, are provided in Appendix F.4.2.

Compared to pre-surgery, both post-surgery time points show reduced variability and greater agreement between the LoA models. This suggests that post-surgery, with improved mechanical efficiency, the influence of measurement variability on muscle force estimates diminishes.

At one-year post-surgery, the generic model mostly remains within the variability range for the right limb, but shows greater discrepancies for the left, although still less pronounced than those observed pre-surgery. This is likely due to the torsion values used as inputs for the post-surgery being much lower than those pre-surgery (see Table 4.2), particularly for the right leg, which showed the greatest angular reduction. This suggests that the smaller the torsion angles, the closer to the personalised the generic model's estimate is, indicating that the personalised model will likely have a more significant impact in cases of major deformities.

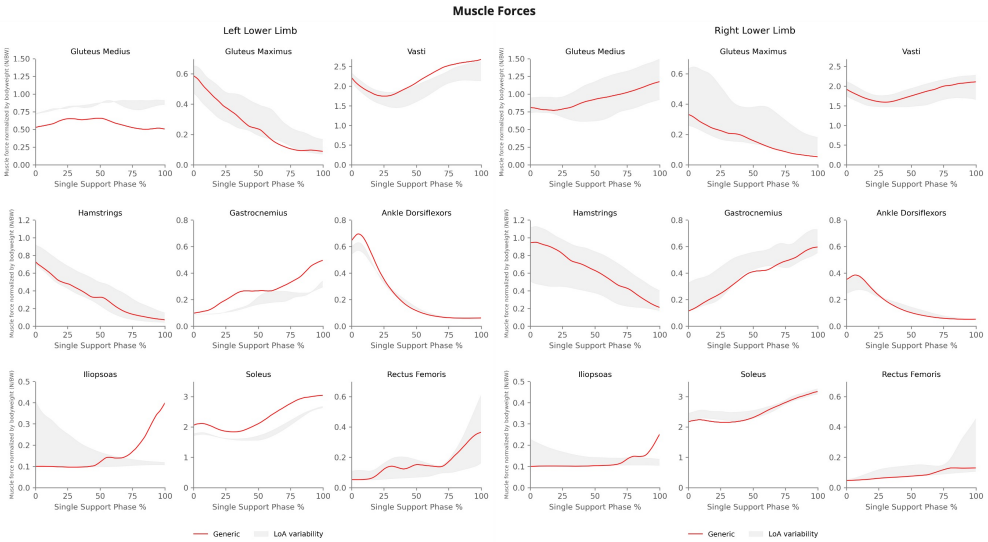

Figure 5.7: One-year post-surgery muscle forces during the single support phase of walking in a child with CP who underwent SEMLS. Data are presented as mean (lines) for the generic model (red) and the shaded region represents the variability interval between the two LoA models. Muscle forces are normalised to the child's BW.

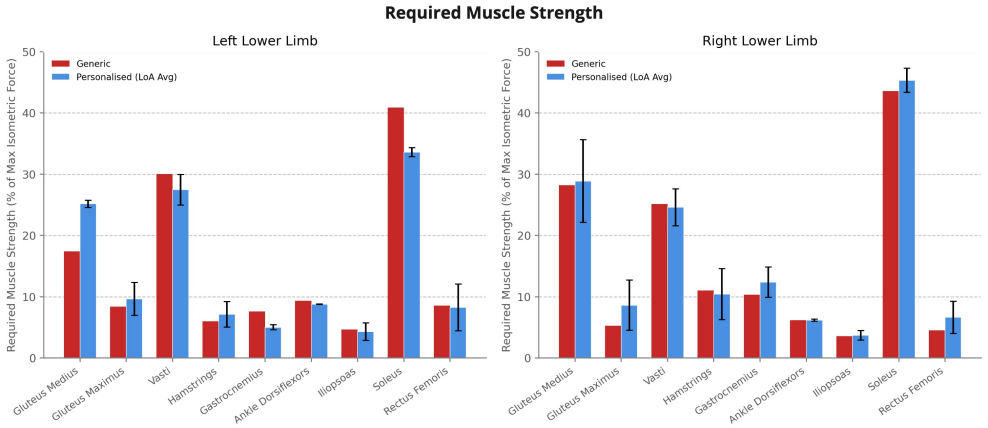

Figure 5.8: One-year post-surgery comparison of required muscle strength as a percentage of maximum isometric force between generic and personalised models (average of 'Personalised-LoA' and 'Personalised+LoA'). Error bars represent the variability across both LoA models.

At ten-year post-surgery, the small variability regions reflect continued stability, with

force patterns closely resembling the one-year results, indicating long-term consistency in muscle force estimates [72].

5.4.4 Muscle Activation Validation

The EMG activation plots from the first two sessions, processed as described in Section 4.3.2, alongside the muscle activations from the generic and personalised models, are presented in Appendix F.5 (Figures F.31 and F.32). The focus is on activation timing and curve shape, as amplitude is not directly comparable due to normalisation methods. Overall, the simulated activations align with the EMG patterns, though some discrepancies are observed. In the first session, the *adductor longus*, *rectus femoris*, and left *tibialis anterior* show mismatched shapes, and in the second session, the left *semitendinosus* and *tibialis anterior* also show poor alignment. The right leg shows better agreement overall. Some unreliable EMG data were excluded. The generic and personalised models show similar activation patterns, with minor exceptions.

These EMG representations serve only as a visual reference, as the scales are not comparable and electromechanical delay was not taken into consideration. Therefore, using this EMG data as a penalisation would be inappropriate.

5.5 Muscle Contributions to Centre of Mass Acceleration

Although the primary focus of this dissertation is on muscle force estimation, the IAA results are included to provide insight into muscle contributions to movement, which help contextualise the muscle force findings and confirm the consistency of the modelled gait patterns over time.

To validate the IAA tool, the total acceleration results were compared to the sum of accelerations from each muscle and gravity, as shown in Appendix G.1. The total and muscle+gravity accelerations align well, especially in the vertical direction, with some amplitude deviations in the mediolateral direction.

Additionally, Appendix G.1 illustrates the comparison between total induced reaction forces and measured GRFs to assess the accuracy of the constraint in representing contact conditions. The curves overall align well, particularly in the antero-posterior and vertical directions, indicating successful constraint implementation.

This section is organised similarly to Chapter 5.4 on Muscle Forces, starting with a comparison of all models at different time points, followed by an analysis of the contributions across the years for the generic and personalised models.

5.5.1 Generic vs. Torsion Tool Centre of Mass Acceleration Analysis

This section presents muscle contributions in the antero-posterior direction, while vertical and mediolateral contributions are provided in Appendix G.2.

Figure 5.9 illustrates the antero-posterior muscle contributions for all models pre-surgery. Model differences are particularly pronounced in the right leg, where the generic and

personalised models exhibit differences beyond measurement variability. Notably, the right *soleus* demonstrates that higher torsion input parameters reduce its propulsion ability, with the generic model indicating much higher contribution than the models incorporating lower limb rotations. These results align with [74], which studied the effect of TT on the ability of the *soleus* to support and propel the body during gait, stating that excess TT diminishes its body COM support and propulsion. In this study, in fact, the higher the TT used as input, the lower the estimation of its propulsive contribution. This suggests that, in this case, personalisation is necessary for more realistic results. By one-year and ten-year post-surgery (see Appendix G.2.1), these differences become less pronounced, suggesting the influence of measurement variability decreases with reduced torsion.

In the vertical direction contributions (Appendix G.2.2), which provide main support and resistance to gravity, pre-surgery the *soleus* showed the highest differences between models. Specifically, higher values of TT diminished its body COM support, aligning with [74]. Post-surgery, the contributions were consistent across different models. The mediolateral muscle contributions (Appendix G.2.3), which help stabilise the body during gait, present similar results between models, with more pronounced pre-surgery, while post-surgery, the contributions became more comparable. This further suggests that the greater the torsional deformities, the more visible the impact of the Torsion Tool compared to the generic model.

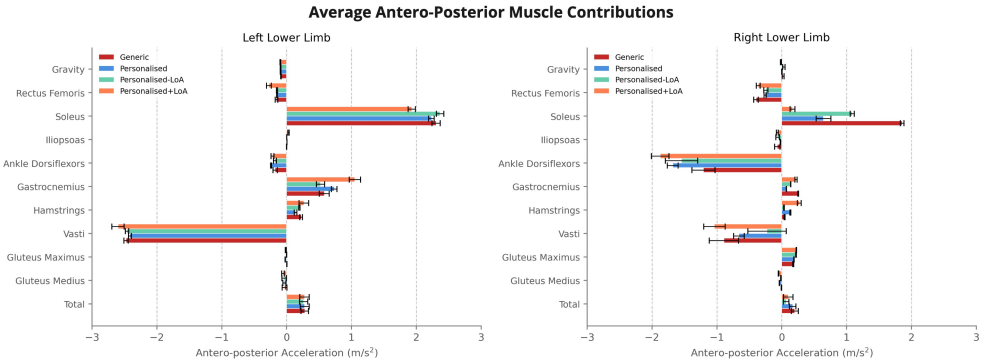

Figure 5.9: Pre-surgery average muscle contributions to antero-posterior COM acceleration for all four models during the single support phase. The total acceleration and contributions from gravity are also shown. Error bars are ±1 standard error. Positive values indicate anterior acceleration, while negative values indicate posterior acceleration.

5.5.2 Pre- vs. Post-Surgery Centre of Mass Acceleration Analysis

This section compares pre- vs. post-surgery muscle contributions for the generic and personalised models to evaluate if they show similar trends over time. The focus is on the antero-posterior direction, with the vertical and mediolateral contributions included in Appendix G.3.

Figure 5.10 illustrates muscle contributions before and after surgery in the antero-posterior direction for the generic and personalised models, both showing comparable trends. The main exception is the right *soleus*, where the generic model shows a decrease

in propulsion from pre- to post-surgery, while the personalised model shows an increase. This discrepancy is due to different estimations pre-surgery, as observed in Section 5.5.1, because the results for one-year and ten-year post-surgery are identical between models. Since TT affects the propulsive contribution of the *soleus*, as corroborated by [74], the torsion personalised model is considered more realistic. Therefore, the increase in contribution from pre- to post-surgery observed with this model likely reflects a more accurate representation of the effect of SEMLS on the muscle's propulsive role. Additionally, the left vasti and right ankle dorsiflexors show slightly greater decreases in the torsion personalised model after the SEMLS compared to the generic. Long-term results are identical between models.

Vertical muscle contributions (Figure G.15) show similar trends between models, indicating consistent behaviour when assessing vertical contributions with the IAA tool. In the mediolateral direction (Figure G.16), even though total accelerations remain consistent across models, the torsion personalised shows a greater reduction in right ankle dorsiflexors and a more pronounced increase in the right *soleus*. For full results on these directions, see Appendix G.3.

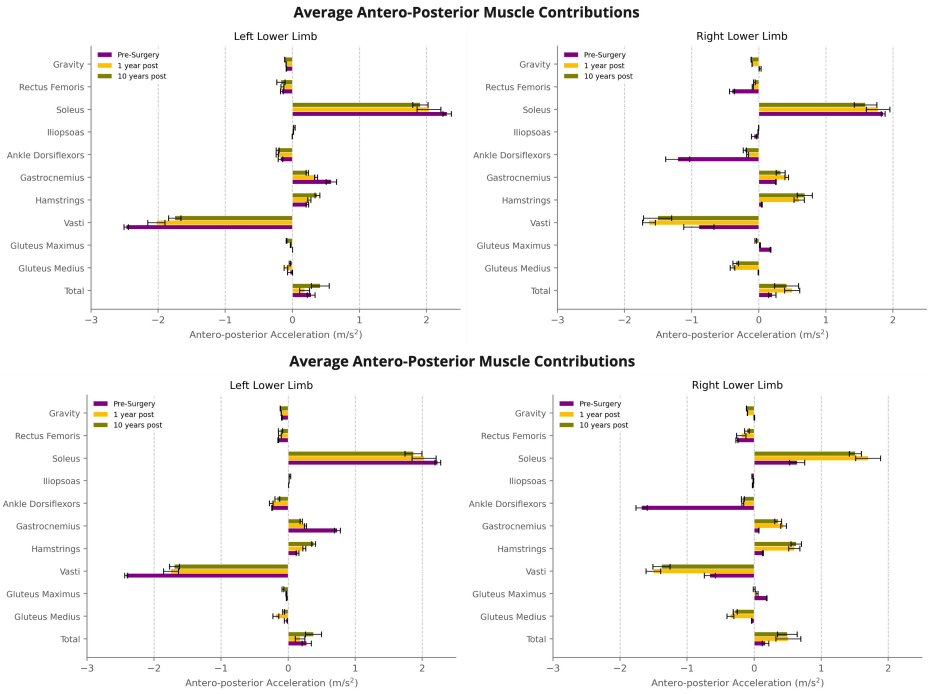

Figure 5.10: Pre- vs. post-surgery average muscle contributions to antero-posterior COM acceleration for generic (top), and torsion personalised (bottom) models, during the single support phase. The total acceleration and contributions from gravity are also shown. Error bars are ±1 standard error. Positive values indicate anterior acceleration, while negative values indicate posterior acceleration.

6

Conclusions and Future Work

This chapter concludes the dissertation by summarising its key findings and contributions to biomedical research. Additionally, it discusses the study's limitations and explores potential future approaches to enhance model personalisation.

6.1 Conclusions

MSK modelling is a crucial tool in biomechanics, providing insights into the causes for human movement and serving as a clinical intervention or decision-making aid. There is growing interest in subject-specific modelling approaches to address the challenges of representing clinical populations with models based on healthy adults.

Despite advancements in personalisation, subject-specific techniques remain time consuming, complex, and often require specialised expertise, limiting their widespread application. Recent developments, such as the Torsion Tool, allow for easy and quick personalisation of torsion deformities common in children with CP. While these tools have been validated for its torsional adjustments, its impact on simulations had not yet been explored.

This dissertation investigated different levels of personalisation by using the Torsion Tool to adjust the Gait2392 generic model to a patient with CP presenting significant femoral and tibial deformities. The adopted approach aimed to evaluate whether lower limb muscle forces and muscle contributions obtained with the tool differed from those of the linear scaled generic model, ultimately evaluating its potential as a more accurate alternative without the extensive effort typically required for subject-specific modelling.

Hence, the first stage of this work involved a comprehensive analysis of the relationships between different models and muscle force predictions, considering both the generic and torsion personalised models. Instead of focusing solely on the comparison between muscle forces predicted by the two models, this study also accounted for variability in measuring the input required for the creation of personalised models, examined their behavior in studying surgical outcomes, and simulated muscle contributions. The decision to analyse these relationships stemmed from the fact that each model personalisation method interacts with anatomical data in a unique way, making it important to observe how personalising femoral and tibial geometries influences muscle force estimates and overall model performance.

Regarding model comparison, linear scaled torsion personalised models generated different muscle force estimates from the linear scaled Gait2392 models, indicating that torsion personalisation influenced muscle force predictions. These discrepancies were more pronounced when higher femoral and tibial torsion values were used as input, which corresponded to greater differences from the default Gait2392 torsional parameters. In these cases, the generic model typically underestimated muscle forces relative to the personalised model.

Although some differences could be attributed to measurement error or variability, in most cases, even when accounting for variability in torsional angles used to create the personalised models, differences were still observed. This suggests that torsional personalisation influences muscle force predictions beyond just measurement variability. Additionally, the impact of measurement variability decreased with improved anatomical alignment and mechanical efficiency.

In terms of pre- and post-surgery analysis, both linear scaled generic and torsion personalised models showed similar trends in muscle forces. The main differences were observed in magnitude rather than in the overall patterns, suggesting that when the focus relies on this comparison, both models provide valuable insights, and the additional effort of personalisation may not result in notably different outcomes in both the short and long term.

These findings raise the question of whether the current approach to model personalisation is truly beneficial for accurately predicting muscle forces in real-world situations. Two key aspects are the contribution to the field of biomechanics and MSK modeling, as well as the implications for clinical practice. Regarding the contribution to the field, despite the lack of studies exploring the use of the Torsion Tool in this context, this work provides valuable insights into its potential for subject-specific modelling in MSK research. It enables a moderate level of personalisation, greater than simply linearly scaling the generic model, without being overly time-consuming, particularly when pronounced anatomical variations are present. For clinical practice, these findings may contribute to the development of more effective treatment plans by offering a more realistic representation of the individual and more realistic simulations of muscle forces. In summary, this dissertation identified patterns in the impact of the Torsion Tool, highlighting its promise in improving muscle force predictions through personalised modelling.

6.2 Limitations and Future Work

While the previous section highlighted the main contributions of this dissertation, particularly the applicability of the Torsion Tool for subject-specific modelling, the findings should be interpreted in the context of modelling assumptions. Further refinements could enhance its reliability and broaden its usability in MSK research.

One inherent limitation of the Torsion Tool, mentioned in Section 3.3.1, is that it currently adjusts only the rotation angles of the bones, without accounting for mass and inertial properties. Additionally, although the tool enables the personalisation of both femoral and tibial angles, it has not yet been evaluated for the tibial component.

Another fragility is the lack of studies regarding the Torsion Tool, which makes it challenging to make comparisons and contextualise the results within the broader context of the literature.

The inherent limitations of the Gait2392 model should also be considered. Even though this model is widely used and has been adapted for lower limb deformities, it does not perfectly represent children, particularly those with CP. Future work could explore alternative base models for the Torsion Tool, for example the Lernagopal model [51], which offers a more detailed representation of the knee and may better capture the anatomical and biomechanical features of walking in crouch. Additionally, all MSK simulations are approximations of real-world behaviour, which should be considered when interpreting the results.

Moreover, this dissertation only studied one subject, and increasing the number of participants could improve the generalisability of the findings. Furthermore, because only one subject was considered, this work consisted of a descriptive and qualitative analysis rather than a statistical one. While this approach provided insights into model differences, it is worth incorporating larger samples and statistical analyses.

Additionally, since this work focused on comparing generic and personalised models, including four different Torsion Tool-generated models, a comparison with TD children, serving as healthy controls, was not conducted. However, such a comparison could provide valuable context to further understand the specific impacts of CP on gait.

Lastly, regarding the Torsion Tool, there are many alternative approaches to explore as future work. For instance, integrating imaging-based angle measurements, especially from CT scans, could be considered. In addition, instead of solely comparing the performance of the Torsion Tool to a generic model, future work could also compare it with other personalisation approaches, such as EMG-, CT-, or MRI-based models, to better evaluate its impact on functional and clinical outcomes.

Bibliography

[1] J. M. Lourenço, *The NOVAthesis LaTeX Template User's Manual*, NOVA University Lisbon, 2021. [Online]. Available: https://github.com/joaomlourenco/novathesis/raw/master/template.pdf (cit. on p. ii).

[2] Medscape. "Medscape". (2025), [Online]. Available: https://www.medscape.com (visited on 2025-02-12) (cit. on p. xv).

[3] S. L. Delp, F. C. Anderson, A. S. Arnold, *et al.*, "Opensim: Open-source software to create and analyze dynamic simulations of movement", *IEEE Transactions on Biomedical Engineering*, vol. 54, pp. 1940–1950, 11 2007. DOI: 10.1109/TBME.2007.901024 (cit. on pp. xv, 8, 9, 11, 19, 20, 22, 23, 27, 53).

[4] K. Mikkelsen, L. Stojanovska, M. Polenakovic, M. Bosevski, and V. Apostolopoulos, "Exercise and mental health", *Maturitas*, vol. 106, pp. 48–56, 2017. DOI: 10.1016/J.MATURITAS.2017.09.003 (cit. on p. 1).

[5] E. M. Chin, H. E. Gwynn, S. Robinson, and A. H. Hoon, "Principles of medical and surgical treatment of cerebral palsy", *Neurologic Clinics*, vol. 38, p. 397, 2 2020. DOI: 10.1016/J.NCL.2020.01.009 (cit. on p. 1).

[6] R. A. Pandey, A. N. Johari, and T. Shetty, "Crouch gait in cerebral palsy: Current concepts review", *Indian Journal of Orthopaedics*, vol. 57, pp. 1913–1926, 12 2023. DOI: 10.1007/s43465-023-01002-5 (cit. on pp. 1, 30).

[7] S. A. Galey, Z. F. Lerner, T. C. Bulea, S. Zimbler, and D. L. Damiano, "Effectiveness of surgical and non-surgical management of crouch gait in cerebral palsy: A systematic review", *Gait and Posture*, vol. 54, pp. 93–105, 2017. DOI: 10.1016/j.gaitpost.2017.02.024 (cit. on p. 1).

[8] S. Armand, G. Decoulon, and A. Bonnefoy-Mazure, "Gait analysis in children with cerebral palsy", *EFORT Open Reviews*, vol. 1, pp. 448–460, 12 2016. DOI: 10.1302/2058-5241.1.000052 (cit. on pp. 1, 6).

[9] K. Veerkamp, H. Kainz, B. A. Killen, H. Jónasdóttir, and M. M. van der Krogt, "Torsion tool: An automated tool for personalising femoral and tibial geometries in opensim musculoskeletal models", *Journal of Biomechanics*, vol. 125, p. 110 589, 2021. DOI: 10.1016/j.jbiomech.2021.110589 (cit. on pp. 1, 2, 9, 10, 14, 19, 20, 53).

[10] K. M. Steele, M. S. DeMers, M. H. Schwartz, and S. L. Delp, "Compressive tibiofemoral force during crouch gait", *Gait and Posture*, vol. 35, pp. 556–560, 4 2012. DOI: 10.1016/j.gaitpost.2011.11.023 (cit. on pp. 3, 6, 11, 12, 28, 29).

[11] S. Paul, A. Nahar, M. Bhagawati, and A. J. Kunwar, "A review on recent advances of cerebral palsy", *Oxidative Medicine and Cellular Longevity*, vol. 2022, pp. 1–20, 4 2022. DOI: 10.1155/2022/2622310 (cit. on p. 3).

[12] R. Palisano, P. Rosenbaum, D. Bartlett, *et al.*, "Gmfcs – e & r", *Dev Med Child Neurol*, vol. 39, pp. 214–223, 1997 (cit. on pp. 4, 48).

[13] M. Albersheim, B. Noonan, M. Chau, T. Cooper, and M. Tompkins, "Rotational osteotomy for femoral version/tibial torsion", *Current Reviews in Musculoskeletal Medicine*, vol. 15, pp. 667–672, 6 2022. DOI: 10.1007/s12178-022-09807-x (cit. on pp. 4, 5).

[14] J. M. G. Jr., "Femoral anteversion", in *Smith's Recognizable Patterns of Human Deformation (Third Edition)*. Elsevier Inc., 2007, ch. 9, pp. 61–63 (cit. on p. 4).

[15] H. Kainz, G. T. Mindler, and A. Kranzl, "How do the femoral anteversion angle and neck-shaft angle influence muscle forces and joint loading during walking?", 2022. DOI: 10.21203/rs.3.rs-2293229/v1 (cit. on pp. 4, 12).

[16] C. Y. Chung, K. M. Lee, M. S. Park, S. H. Lee, I. H. Choi, and T. J. Cho, "Validity and reliability of measuring femoral anteversion and neck-shaft angle in patients with cerebral palsy", *Journal of Bone and Joint Surgery*, vol. 92, pp. 1195–1205, 5 2010. DOI: 10.2106/JBJS.I.00688 (cit. on pp. 4, 5, 19, 20, 49).

[17] J. Feger. "Femoral neck-shaft angle". (2021), [Online]. Available: https://radiopaedia.org/articles/femoral-neck-shaft-angle (visited on 2024-02-06) (cit. on p. 4).

[18] Á. T. Schlégl, V. Nyakas, D. Kovács, P. Maróti, G. Józsa, and P. Than, "Neck-shaft angle measurement in children: Accuracy of the conventional radiography-based (2d) methods compared to 3d reconstructions", *Scientific Reports*, vol. 12, 1 2022. DOI: 10.1038/s41598-022-20832-1 (cit. on p. 4).

[19] J. Feger, C. Hacking, and D. Bell. "Femoral neck-shaft angle". (2025), [Online]. Available: https://radiopaedia.org/articles/tibial-torsion (visited on 2024-02-22) (cit. on p. 5).

[20] S. H. Lee, C. Y. Chung, M. S. Park, I. H. Choi, and T. J. Cho, "Tibial torsion in cerebral palsy: Validity and reliability of measurement", *Clinical Orthopaedics and Related Research*, vol. 467, pp. 2098–2104, 8 2009. DOI: 10.1007/s11999-009-0705-1 (cit. on pp. 5, 49).

[21] T. Schmeltzpfenning and T. Brauner, "Foot biomechanics and gait", in *Handbook of Footwear Design and Manufacture*. Elsevier Inc., 2013, pp. 27–48 (cit. on pp. 5, 6).

[22] G. Cicirelli, D. Impedovo, V. Dentamaro, R. Marani, G. Pirlo, and T. R. D'Orazio, "Human gait analysis in neurodegenerative diseases: A review", *IEEE Journal of Biomedical and Health Informatics*, vol. 26, pp. 229–242, 1 2022. DOI: 10.1109/JBHI.2021.3092875 (cit. on pp. 6, 49).

[23] N. Khouri and E. Desailly, "Contribution of clinical gait analysis to single-event multilevel surgery in children with cerebral palsy", *Orthopaedics and Traumatology: Surgery and Research*, vol. 103, S105–S111, 1S 2017. DOI: 10.1016/J.OTSR.2016.11.004 (cit. on p. 6).

[24] J. Rodda and H. K. Graham, "Classification of gait patterns in spastic hemiplegia and spastic diplegia: A basis for a management algorithm", *European Journal of Neurology*, vol. 8, pp. 98–108, Suppl 5 2001. DOI: 10.1046/j.1468-1331.2001.00042.x (cit. on pp. 6, 7).

[25] P. Kedem and D. M. Scher, "Evaluation and management of crouch gait", *Current Opinion in Pediatrics*, vol. 28, pp. 55–59, 1 2016. DOI: 10.1097/MOP.0000000000000316 (cit. on p. 7).

[26] B. E and W. A, "Cerebral palsy: Treatment of spasticity, dystonia, andassociated orthopedic issues", in Wolters Kluwer, 2023. [Online]. Available: https://www.uptodate.com/contents/cerebral-palsy-treatment-of-spasticity-dystonia-and-associated-orthopedic-issues (cit. on p. 7).

[27] A. D. Sylvester, S. G. Lautzenheiser, and P. A. Kramer, "A review of musculoskeletal modelling of human locomotion", *Interface Focus*, vol. 11, 5 2021. DOI: 10.1098/rsfs.2020.0060 (cit. on p. 8).

[28] S. H. Smith, R. J. Coppack, A. J. van den Bogert, A. N. Bennett, and A. M. Bull, "Review of musculoskeletal modelling in a clinical setting: Current use in rehabilitation design, surgical decision making and healthcare interventions", *Clinical Biomechanics*, vol. 83, 2021. DOI: 10.1016/j.clinbiomech.2021.105292 (cit. on p. 8).

[29] S. L. D. E. W., J. P. Loan, M. G. Hoy, F. E. Zajac, E. L. Topp, and J. M. Rosen, "An interactive graphics-based model of the lower extremity to study orthopaedic surgical procedures", *IEEE Transactions on Biomedical Engineering*, vol. 37, pp. 757–767, 8 1990. DOI: 10.1109/10.102791 (cit. on pp. 8, 12, 14).

[30] F. C. Anderson and M. G. Pandy, "A dynamic optimization solution for vertical jumping in three dimensions", *Computer Methods in Biomechanics and Biomedical Engineering*, vol. 2, pp. 201–231, 3 1999. DOI: 10.1080/10255849908907988 (cit. on p. 8).

[31] G. T. Yamaguchi and F. E. Zajac, "A planar model of the knee joint to characterize the knee extensor mechanism", *Journal of Biomechanics*, vol. 22, pp. 1–10, 1 1989. DOI: 10.1016/0021-9290(89)90179-6 (cit. on p. 8).

[32] O. Documentation. "Gait 2392 and 2354 models". (2024), [Online]. Available: https://simtk-confluence.stanford.edu:8443/display/OpenSim/Gait+2392+and+2354+Models (visited on 2024-02-02) (cit. on p. 9).

[33] Z. Jing, J. Han, and J. Zhang, "Comparison of biomechanical analysis results using different musculoskeletal models for children with cerebral palsy", *Frontiers in Bioengineering and Biotechnology*, vol. 26, 11 2023. DOI: 10.3389/fbioe.2023.1217918 (cit. on p. 9).

[34] S. L. Delp, "Surgery simulation: A computer graphics system to analyze and design musculoskeletal reconstructions of the lower limb.", M.S. thesis, Stanford University, 1990 (cit. on p. 9).

[35] A. S. Arnold and S. L. Delp, "Rotational moment arms of the medial hamstrings and adductors vary with femoral geometry and limb position: Implications for the treatment of internally rotated gait", *Journal of Biomechanics*, vol. 34, pp. 437–447, 4 2001. DOI: 10.1016/S0021-9290(00)00232-3 (cit. on p. 10).

[36] A. S. Arnold, S. S. Blemker, and S. L. Delp, "Evaluation of a deformable musculoskeletal model for estimating muscle-tendon lengths during crouch gait", *Annals of Biomedical Engineering*, vol. 29, pp. 263–274, 3 2001. DOI: 10.1114/1.1355277 (cit. on p. 10).

[37] J. Hicks, A. Arnold, F. Anderson, M. Schwartz, and S. Delp, "The effect of excessive tibial torsion on the capacity of muscles to extend the hip and knee during single-limb stance", *Gait and Posture*, vol. 26, pp. 546–552, 4 2007. DOI: 10.1016/j.gaitpost.2006.12.003 (cit. on p. 10).

[38] P. Konrad, *The ABC of EMG – A Practical Introduction to Kinesiological Electromyography*. Noraxon Inc., 2005 (cit. on pp. 10, 18).

[39] J. Nonnekes, R. J. Goselink, E. Růzicka, A. Fasano, J. G. Nutt, and B. R. Bloem, "Neurological disorders of gait, balance and posture: A sign-based approach", *Nature Reviews Neurology*, vol. 14, pp. 183–189, 3 2018. DOI: 10.1038/nrneurol.2017.178 (cit. on p. 11).

[40] W. Tao, T. Liu, R. Zheng, and H. Feng, "Gait analysis using wearable sensors", *Sensors*, vol. 12, pp. 2255–2283, 2 2012. DOI: 10.3390/s120202255 (cit. on p. 11).

[41] M. Conconi, E. Montefiori, N. Sancisi, and C. Mazzà, "Modeling musculoskeletal dynamics during gait: Evaluating the best personalization strategy through model anatomical consistency", *Applied Sciences (Switzerland)*, vol. 11, 18 2021. DOI: 10.3390/app11188348 (cit. on pp. 11, 12).

[42] H. Kainz, D. Graham, J. Edwards, *et al.*, "Reliability of four models for clinical gait analysis", *Gait and Posture*, vol. 54, pp. 325–331, 5 2017. DOI: 10.1016/j.gaitpost.2017.04.001 (cit. on p. 12).

[43] G. Davico, C. Pizzolato, D. G. Lloyd, S. J. Obst, H. P. Walsh, and C. P. Carty, "Increasing level of neuromusculoskeletal model personalisation to investigate joint contact forces in cerebral palsy: A twin case study", *Clinical Biomechanics*, vol. 72, pp. 141–149, 2020. DOI: 10.1016/j.clinbiomech.2019.12.011 (cit. on p. 12).

[44] J. L. Hicks, M. H. Schwartz, A. S. Arnold, and S. L. Delp, "Crouched postures reduce the capacity of muscles to extend the hip and knee during the single-limb stance phase of gait", *Journal of Biomechanics*, vol. 41, pp. 960–967, 5 2008. DOI: 10.1016/j.jbiomech.2008.01.002 (cit. on p. 12).

[45] K. M. Steele, M. M. V. D. Krogt, M. H. Schwartz, and S. L. Delp, "How much muscle strength is required to walk in a crouch gait?", *J Biomech*, vol. 45, pp. 2564–2569, 15 2012. DOI: 10.1016/j.jbiomech.2012.07.028 (cit. on pp. 13, 28, 29).

[46] K. M. Steele, A. Seth, J. L. Hicks, M. S. Schwartz, and S. L. Delp, "Muscle contributions to support and progression during single-limb stance in crouch gait", *Journal of Biomechanics*, vol. 43, pp. 2099–2105, 11 2010. DOI: 10.1016/j.jbiomech.2010.04.003 (cit. on pp. 13, 18).

[47] R. Akhundov, D. J. Saxby, L. E. Diamond, *et al.*, "Is subject-specific musculoskeletal modelling worth the extra effort or is generic modelling worth the shortcut?", *PLoS ONE*, vol. 17, 1 2022. DOI: 10.1371/journal.pone.0262936 (cit. on p. 13).

[48] K. Song, A. E. Anderson, J. A. Weiss, and M. D. Harris, "Musculoskeletal models with generic and subject-specific geometry estimate different joint biomechanics in dysplastic hips", *Computer Methods in Biomechanics and Biomedical Engineering*, vol. 22, pp. 259–270, 3 2019. DOI: 10.1080/10255842.2018.1550577 (cit. on pp. 13, 29).

[49] H. Kainz, M. Wesseling, and I. Jonkers, "Generic scaled versus subject-specific models for the calculation of musculoskeletal loading in cerebral palsy gait: Effect of personalized musculoskeletal geometry outweighs the effect of personalized neural control", *Clinical Biomechanics*, vol. 87, 2021. DOI: 10.1016/j.clinbiomech.2021.105402 (cit. on pp. 14, 26, 28).

[50] A. Rajagopal, C. L. Dembia, M. S. DeMers, D. D. Delp, J. L. Hicks, and S. L. Delp, "Full-body musculoskeletal model for muscle-driven simulation of human gait", *IEEE Transactions on Biomedical Engineering*, vol. 63, pp. 2068–2079, 10 2016. DOI: 10.1109/TBME.2016.2586891 (cit. on p. 14).

[51] Z. F. Lerner, M. S. DeMers, S. L. Delp, and R. C. Browning, "How tibiofemoral alignment and contact locations affect predictions of medial and lateral tibiofemoral contact forces", *Journal of Biomechanics*, vol. 48, pp. 644–650, 4 2015. DOI: 10.1016/j.jbiomech.2014.12.049 (cit. on pp. 14, 40).

[52] R. L. Lenhart, J. Kaiser, C. R. Smith, and D. G. Thelen, "Prediction and validation of load-dependent behavior of the tibiofemoral and patellofemoral joints during movement", *Annals of Biomedical Engineering*, vol. 43, pp. 2675–2685, 11 2015. DOI: 10.1007/s10439-015-1326-3 (cit. on p. 14).

[53] S. R. Hamner, A. Seth, and S. L. Delp, "Muscle contributions to propulsion and support during running", *Journal of Biomechanics*, vol. 43, pp. 2709–2716, 14 2010. DOI: 10.1016/j.jbiomech.2010.06.025 (cit. on pp. 14, 24).

[54] J. Richards and D. Thewlis, "Chapter 9: Anatomical models and marker sets", in *Biomechanics in Clinic and Research*. Churchill Livingstone, 2008, pp. 117–128 (cit. on p. 16).

[55] O. G. Laboratory. "Oxford foot model". (2025), [Online]. Available: https://www.ouh.nhs.uk/gait-lab/ (visited on 2024-02-24) (cit. on pp. 16, 21).

[56] Delsys, "Trigno ® wireless biofeedback system user's guide", Delsys Incorporated, Tech. Rep., 2021 (cit. on p. 17).

[57] A. Barre and S. Armand, "Biomechanical toolkit: Open-source framework to visualize and process biomechanical data", *Elsevier*, vol. 114, pp. 80–7, 1 2014. DOI: 10.1016/j.cmpb.2014.01.012 (cit. on pp. 18, 52).

[58] D. Makowski, T. Pham, Z. J. Lau, *et al.*, "NeuroKit2: A python toolbox for neurophysiological signal processing", *Behavior Research Methods*, vol. 53, pp. 1689–1696, 4 2021. DOI: 10.3758/s13428-020-01516-y (cit. on p. 18).

[59] P. Virtanen, R. Gommers, T. E. Oliphant, *et al.*, "Scipy 1.0: Fundamental algorithms for scientific computing in python", *Nature Methods*, vol. 17, pp. 261–272, 2020. DOI: 10.1038/s41592-019-0686-2 (cit. on p. 18).

[60] M. Sangeux, J. Mahy, and H. K. Graham, "Do physical examination and ct-scan measures of femoral neck anteversion and tibial torsion relate to each other?", *Gait and Posture*, vol. 39, pp. 12–16, 1 2014. DOI: 10.1016/j.gaitpost.2013.05.020 (cit. on pp. 19, 20).

[61] H. Hawi, T. F. Kaireit, C. Krettek, and E. Liodakis, "Clinical assessment of tibial torsion differences. do we always need a computed tomography?", *European Journal of Trauma and Emergency Surgery*, vol. 48, pp. 3229–3235, 4 2022. DOI: 10.1007/s00068-022-01884-4 (cit. on pp. 19, 20).

[62] G. Mantovani and M. Lamontagne, "How different marker sets affect joint angles in inverse kinematics framework", *Journal of Biomechanical Engineering*, vol. 139, 4 2017. DOI: https://doi.org/10.1115/1.4034708 (cit. on p. 21).

[63] J. Zhou, E. E. Butler, and J. Rose, "Neurologic correlates of gait abnormalities in cerebral palsy: Implications for treatment", *Frontiers in Human Neuroscience*, vol. 11, p. 103, 2017. DOI: 10.3389/fnhum.2017.00103 (cit. on p. 24).

[64] Y. C. Lin, H. J. Kim, and M. G. Pandy, "A computationally efficient method for assessing muscle function during human locomotion", *International Journal for Numerical Methods in Biomedical Engineering*, vol. 27, pp. 436–449, 3 2011. DOI: 10.1002/cnm.1396 (cit. on p. 24).

[65] J. M. Rodda, H. K. Graham, G. R. Nattrass, M. P. Galea, R. Baker, and R. Wolfe, "Correction of severe crouch gait in patients with spastic diplegia with use of multilevel orthopaedic surgery", *Journal of Bone and Joint Surgery*, vol. 88, pp. 2653–2664, 12 2006. DOI: 10.2106/JBJS.E.00993 (cit. on pp. 26, 30).

[66] H. Jónasdóttir, "The effect of femoral anteversion and tibial torsion on simulation of cerebral palsy gait", M.S. thesis, Delft University of Technology, 2016 (cit. on p. 26).

[67] S. Õunpuu, M. Solomito, K. Bell, P. DeLuca, and K. Pierz, "Long-term outcomes after multilevel surgery including rectus femoris, hamstring and gastrocnemius procedures in children with cerebral palsy", *Gait and Posture*, vol. 42, pp. 365–372, 3 2015. DOI: 10.1016/j.gaitpost.2015.07.003 (cit. on p. 26).

[68] H. Böhm and L. Döderlein, "Gait asymmetries in children with cerebral palsy: Do they deteriorate with running?", *Gait and Posture*, vol. 35, pp. 322–327, 2 2012. DOI: 10.1016/j.gaitpost.2011.10.003 (cit. on p. 28).

[69] C. G. Cardadeiro, "Model-based comparative biomechanics and muscle function analysis of simulated crouch gait by healthy children and crouch gait in cp children", M.S. thesis, NOVA School of Science and Technology, 2020 (cit. on p. 29).

[70] S. D. Asakawa, S. S. Blemker, E. G. Gold, and L. S. Delp, "In vivo motion of the rectus femoris muscle after tendon transfer surgery", *Journal of Biomechanics*, vol. 35, pp. 1029–1037, 8 2002. DOI: 10.1016/s0021-9290(02)00048-9 (cit. on p. 30).

[71] M. S. Er, O. Abousamra, K. J. Rogers, *et al.*, "Long-term outcome of internal tibial derotation osteotomies in children with cerebral palsy", *Journal of Pediatric Orthopaedics*, vol. 37, pp. 454–459, 7 2015. DOI: 10.1097/BPO.0000000000000671 (cit. on p. 31).

[72] T. Dreher, P. Thomason, M. Švehlík, *et al.*, "Long-term development of gait after multilevel surgery in children with cerebral palsy: A multicentre cohort study", *Developmental Medicine and Child Neurology*, vol. 60, pp. 88–93, 1 2018. DOI: 10.1111/dmcn.13618 (cit. on pp. 31, 35).

[73] L. Bosmans, G. Valente, M. Wesseling, *et al.*, "Sensitivity of predicted muscle forces during gait to anatomical variability in musculotendon geometry", *Journal of Biomechanics*, vol. 48, pp. 2116–2123, 10 2015. DOI: 10.1016/j.jbiomech.2015.02.052 (cit. on p. 33).

[74] M. Schwartz and G. Lakin, "The effect of tibial torsion on the dynamic function of the soleus during gait", *Gait and Posture*, vol. 17, pp. 113–118, 2 2003. DOI: 10.1016/s0966-6362(02)00058-9 (cit. on pp. 36, 37).

[75] J. Upadhyay, N. Tiwari, and M. N. Ansari, "Cerebral palsy: Aetiology, pathophysiology and therapeutic interventions", *Clinical and Experimental Pharmacology and Physiology*, vol. 47, pp. 1891–1901, 12 2020. DOI: 10.1111/1440-1681.13379 (cit. on p. 48).

A

Additional Content

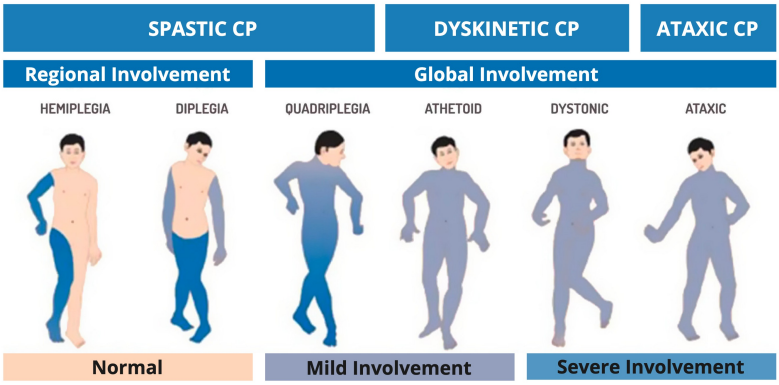

Figure A.1: Topographical classification of CP. Adapted from [75].

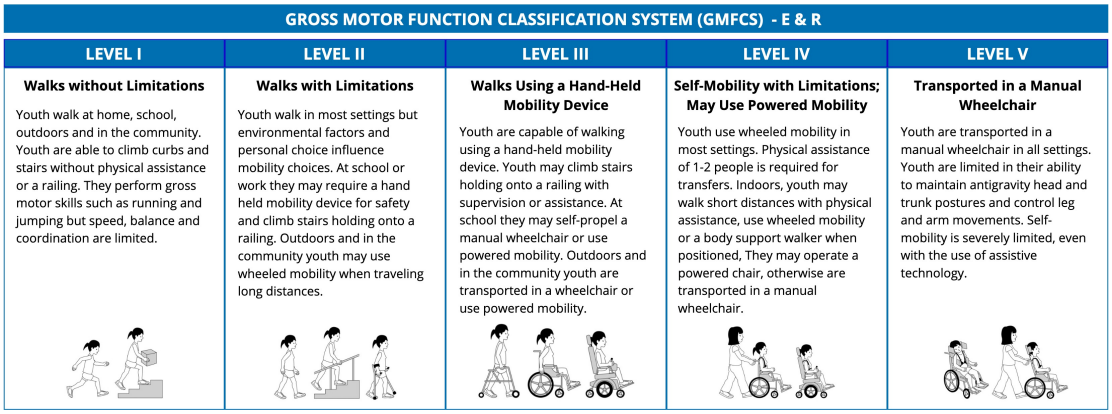

Figure A.2: GMFCS - E&R (Expanded and Revised) between 12^{th} and 18^{th} birthday: Descriptors and illustrations. Adapted from [12].

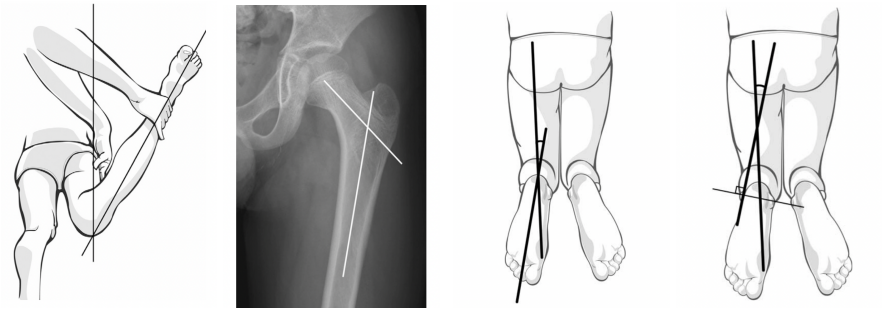

(a) (b) (c) (d)

Figure A.3: Measurement of femoral and tibial rotations: (a) Femoral AVA, (b) Femoral NSA, (c) TT angle using the TFA method, (d) TT angle using the TMA method. Adapted from [16], [20].

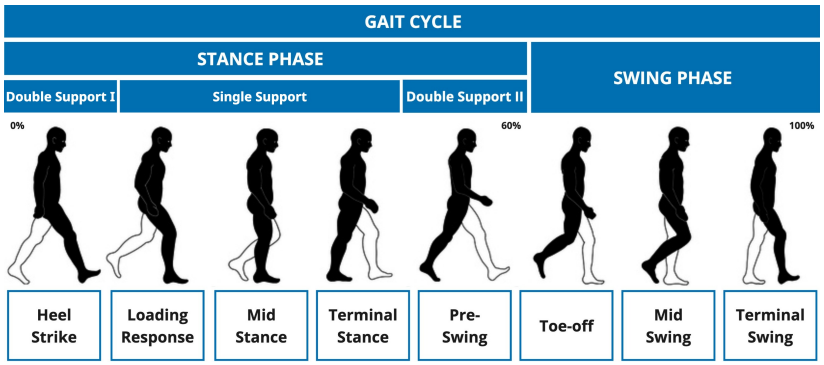

Figure A.4: Gait cycle according to right leg (black) with the various events and phases of gait. Adapted from [22].

Table A.1: Reference frame locations for each rigid body segment in the generic Gait2392 MSK model. It is important to note that this model does not include a patella rigid body segment.

Rigid Body Segment	Reference Frame Location
Pelvis	Midpoint of the line connecting the two anterior superior iliac spines
Femur	Centre of the femoral head
Tibia	Midpoint of the line between the medial and lateral femoral epicondyles
Talus	Midpoint of the line between the apices of the medial and lateral malleoli
Calcaneus	Most interior, lateral point on the posterior surface of the calcaneus
Toe	Base of the second metatarsal

Table A.2: Description and function of the muscle groups studied. Dark grey shading indicates the muscle considered solely for their activation and EMG comparison.

Muscle Groups	OpenSim Description	Action
Gluteus Medius	Three actuators representing the anterior, posterior, and intermediate components of the muscle.	Hip abduction Hip internal rotation (anterior part) Pelvic stabilisation
Gluteus Maximus	Three actuators representing the medial, intermediate, and lateral components of the muscle.	Hip extension Hip external rotation Hip abduction (superior part) Hip adduction (inferior part)
Vasti	Three actuators representing three muscles, *vastus medialis*, *vastus intermedius* and *vastus lateralis*. Together with the *rectus femoris*, forms the *quadriceps femoris*.	Knee extension
Hamstrings	Four actuators representing three muscles, *semimembranosus*, *semitendinosus*, *biceps femoris* long head, and *biceps femoris* short head.	Hip extension Knee flexion Hip and knee stabilisation
Gastrocnemius	Two actuators representing the medial, and lateral components of the muscle.	Knee flexion Ankle plantarflexion
Ankle Dorsiflexors	Three actuators representing the primary ankle dorsiflexor muscles, *tibialis anterior*, *extensor digitorum longus*, and *extensor hallucis longus*.	Ankle dorsiflexion
Iliopsoas	Two actuators representing two muscles, *iliacus*, and *psoas*.	Hip flexion Hip external rotation Torso flexion Lateral torso flexion (*psoas*)
Soleus	Single actuator representing the *soleus* muscle.	Ankle plantarflexion
Rectus Femoris	Single actuator representing the *rectus femoris* muscle. Together with the vasti, forms the *quadriceps femoris*.	Hip flexion Knee extension
Adductor Longus	Single actuator representing the *adductor longus* muscle.	Hip adduction Hip flexion Hip external rotation Pelvic stabilisation

Table A.3: Muscle-tendon actuators of the Gait2392 model, categorised by function: hip flexors and extensors, knee flexors and extensors, and ankle dorsiflexors and plantarflexors, according to OpenSim.

Muscle Functions	OpenSim Muscle Actuators	
Hip Flexors	*Adductor brevis*	*Pectineus*
	Adductor longus	*Psoas major*
	Gluteus medius 1	*Rectus femoris*
	Gluteus minimus 1	*Sartorius*
	Gracilis	*Tensor fasciae latae*
	Iliacus	
Hip Extensors	*Adductor longus*	*Gluteus maximus* 2
	Adductor magnus 1	*Gluteus maximus* 3
	Adductor magnus 2	*Gluteus medius* 3
	Adductor magnus 3	*Gluteus minimus* 3
	Biceps femoris long head	*Semimembranosus*
	Gluteus maximus 1	*Semitendinosus*
Knee Flexors	*Biceps femoris* long head	*Gastrocnemius medialis*
	Biceps femoris short head	*Sartorius*
	Gracilis	*Semimembranosus*
	Gastrocnemius lateralis	*Semitendinosus*
Knee Extensors	*Rectus femoris*	*Vastus lateralis*
	Vastus intermedius	*Vastus medialis*
Ankle Dorsiflexors	*Extensor digitorum longus*	*Peroneus tertius*
	Extensor hallucis longus	*Tibialis anterior*
Ankle Plantarflexors	*Flexor digitorum longus*	*Peroneus longus*
	Flexor hallucis longus	*Soleus*
	Peroneus brevis	*Tibialis posterior*

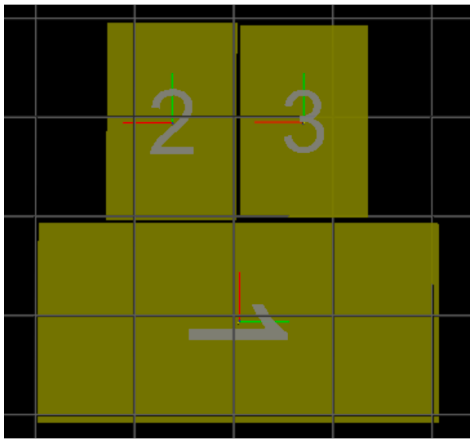

Figure A.5: Placement of the three force platforms used for CGA, shown in Mokka software from a top view perspective [57]. For sessions one and two, force plate one was type AMTI (AMTI, USA), while force plates two and three were type Kistler (Kistler, Switzerland). However, at session one, platform three was not working. In session three, force plates one and three were type Bertec (Bertec, USA), and force plate two was type Kistler (Kistler, Switzerland).

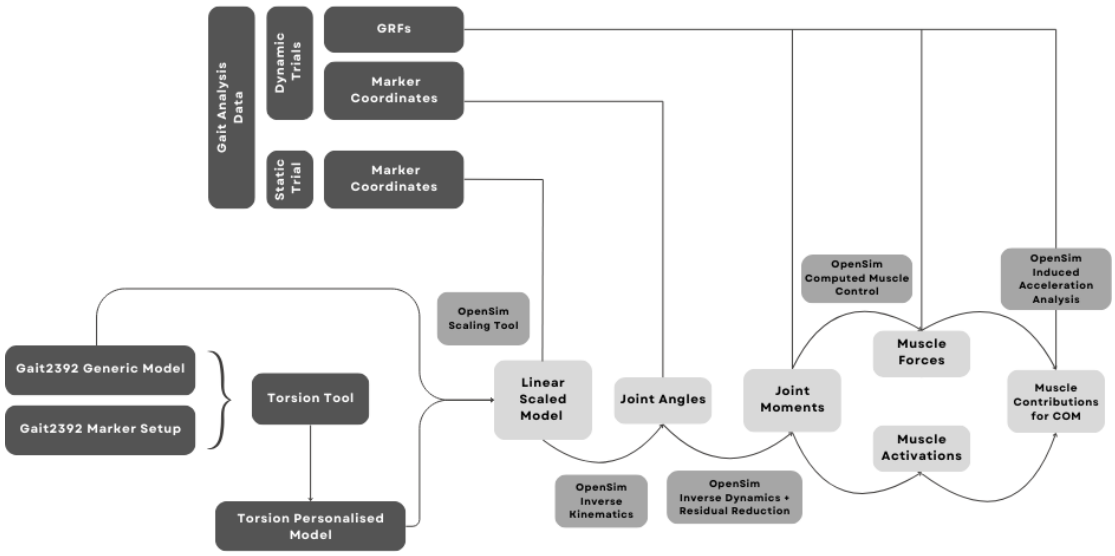

Figure A.6: Flowchart of the creation of each model and OpenSim's pipeline performed in this work.

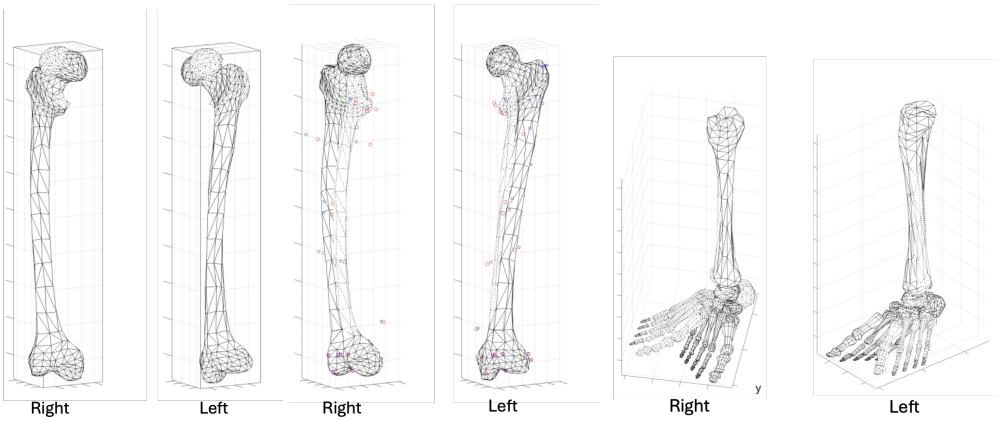

(a) (b) (c)

Figure A.7: Outputs from the Torsion Tool for lower limb rotations for the personalised pre-surgery model using the inputs from Table 4.2, before and after deformation: (a) Femoral AVA rotation, where the femur is rotated along its shaft compared to the unaltered femur, (b) Femoral NSA alteration, exhibiting a change in the inclination of the femoral neck relative to the shaft, and (c) TT, with external rotation of the foot and tibia together [9].

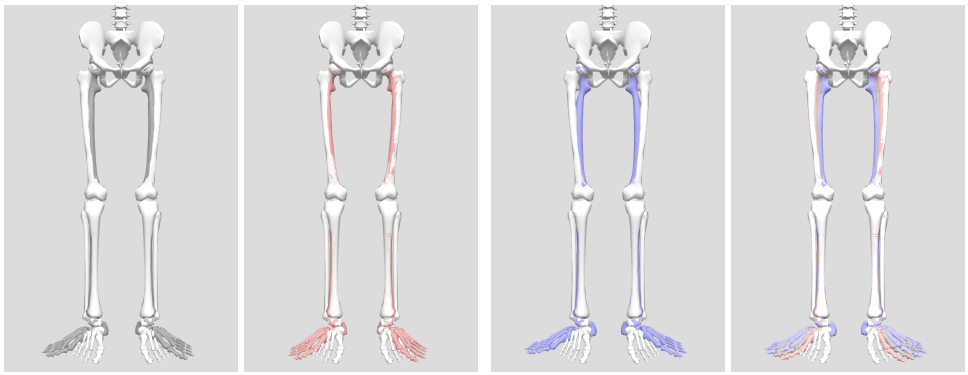

(a) (b) (c) (d)

Figure A.8: Comparison between the generic Gait2392 model (white) and the three pre-surgery Torsion Tool-generated models created with the inputs from Table 4.2: (a) Personalised model (grey), (b) 'Personalised-LoA' model (red), (c) 'Personalised+LoA' model (blue), and (d) All models together [3], [9].

B

Scaling

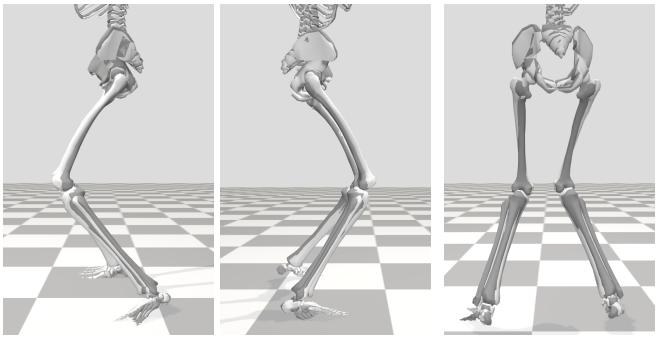

(a) (b) (c)

Figure B.1: Pre-surgery static poses obtained for both the linearly scaled generic and personalised models, computed using the OpenSim's scaling tool: (a) sagittal plane, right lateral view, (b) sagittal plane, left lateral view, and (c) coronal plane, posterior view. The generic scaled model is shown in white, and the personalised scaled model in grey.

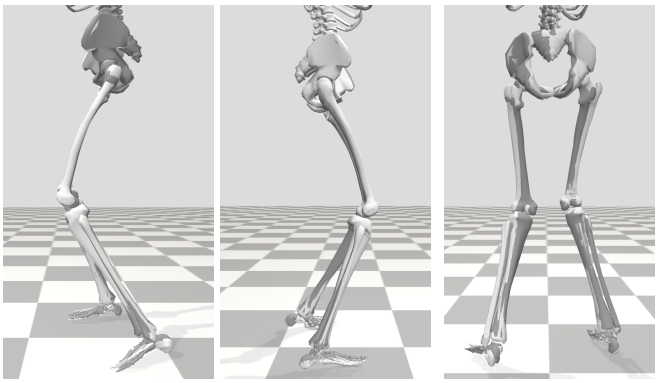

(a) (b) (c)

Figure B.2: One-year post-surgery static poses obtained for both the linearly scaled generic and personalised models, computed using the OpenSim's scaling tool: (a) sagittal plane, right lateral view, (b) sagittal plane, left lateral view, and (c) coronal plane, posterior view. The generic scaled model is shown in white, and the personalised scaled model in grey.

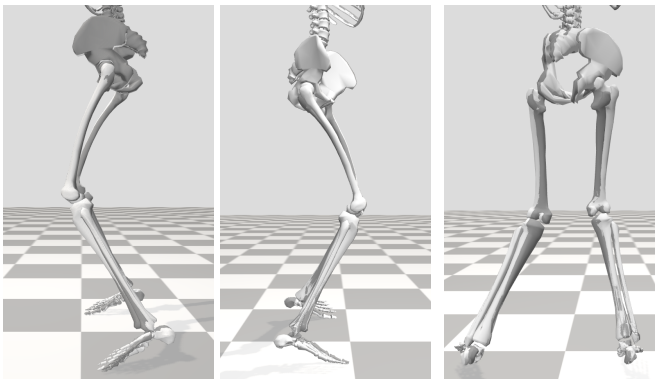

(a) (b) (c)

Figure B.3: Ten-year post-surgery static poses obtained for both the linearly scaled generic and personalised models, computed using the OpenSim's scaling tool: (a) sagittal plane, right lateral view, (b) sagittal plane, left lateral view, and (c) coronal plane, posterior view. The generic scaled model is shown in white, and the personalised scaled model in grey.

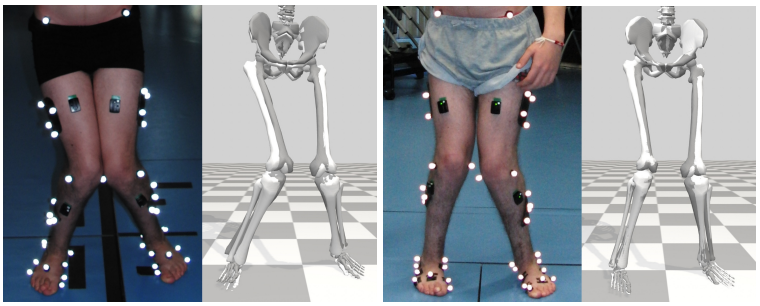

(a) (b)

Figure B.4: Pre- and one-year post-surgery comparison of photos from the CGA's static trials (left) and the static poses computed using the OpenSim's scaling tool from the linearly scaled generic and personalised models (right) in the coronal plane, anterior view: (a) pre-surgery, and (b) one-year post-surgery. The generic model is shown in white, and the personalised model in grey. Images of the static trial were not available for the third CGA session.

C

Joint Kinematics

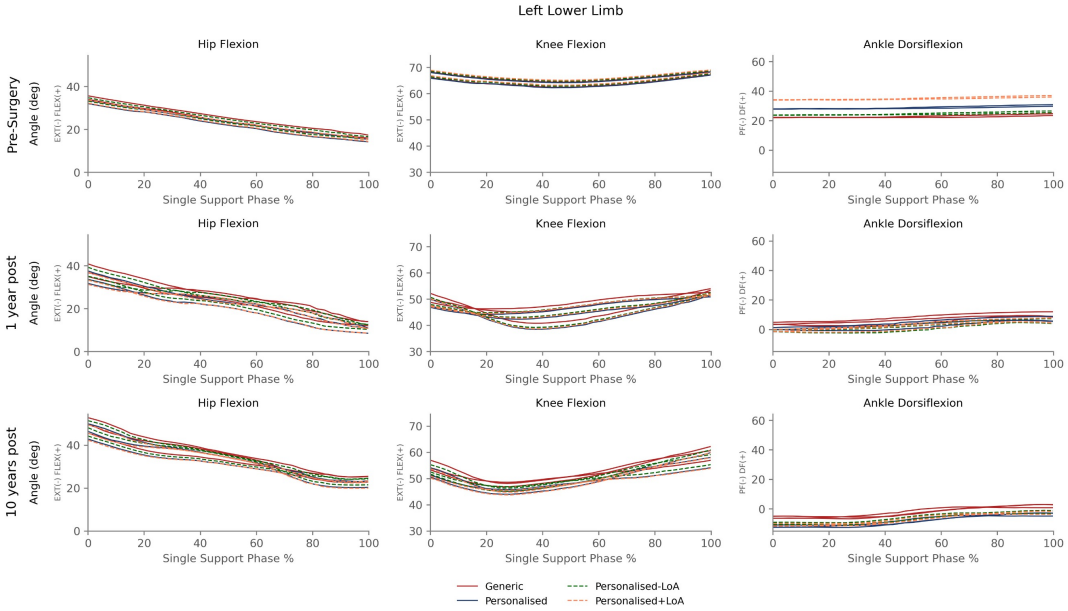

Figure C.1: Left lower limb sagittal joint kinematics of the hip, knee, and ankle during the single support phase, simulated using OpenSim's IK tool. Data are presented for pre-surgery, one-year post-surgery, and ten-year post-surgery, comparing the generic model, personalised model, and personalised models with positive and negative LoA. Each curve represents the average of the trials.

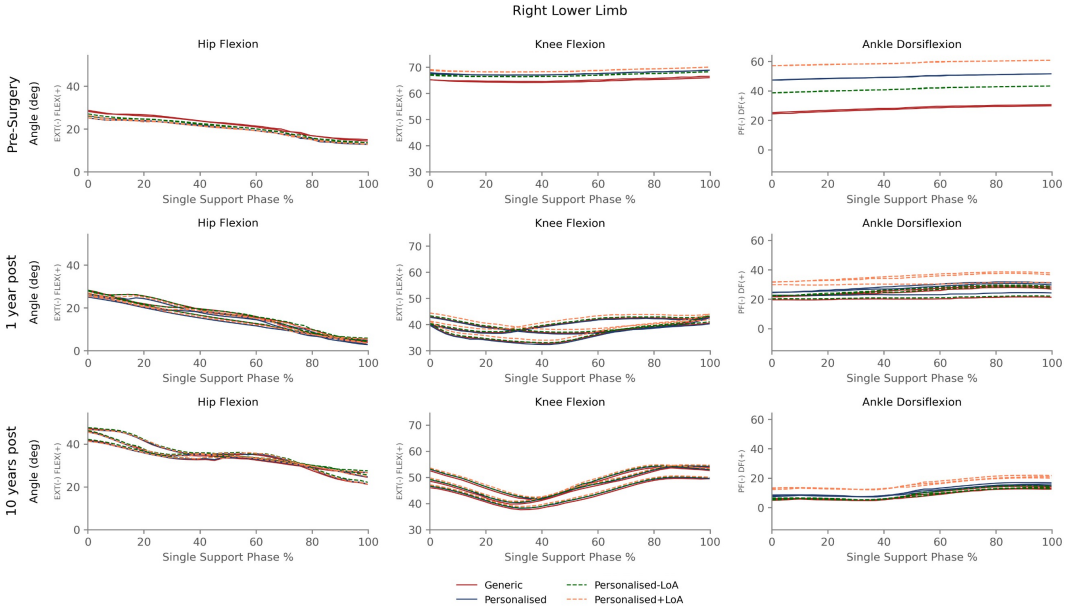

Figure C.2: Right lower limb sagittal joint kinematics of the hip, knee, and ankle during the single support phase, simulated using OpenSim's IK tool. Data are presented for pre-surgery, one-year post-surgery, and ten-year post-surgery, comparing the generic model, personalised model, and personalised models with positive and negative LoA. Each curve represents the average of the trials.

D

Joint Moments

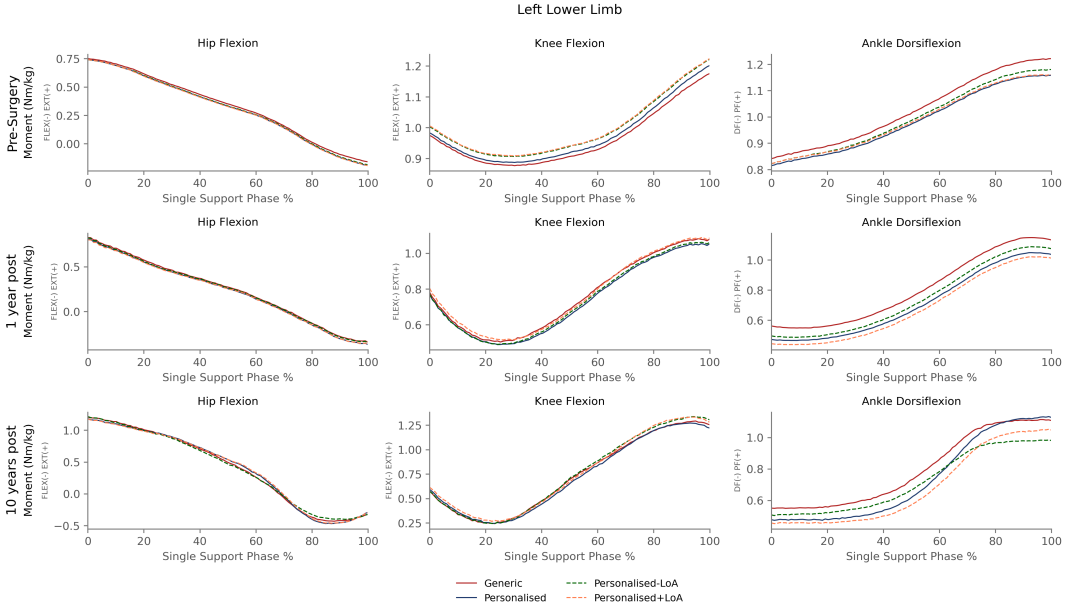

Figure D.1: Left lower limb sagittal joint moments, normalised by subject's mass, of the hip, knee, and ankle during the single support phase, simulated using OpenSim's RRA tool. Data are presented for pre-surgery, one-year post-surgery, and ten-year post-surgery, comparing the generic model, personalised model, and personalised models with positive and negative LoA. Each curve represents the average of the trials.

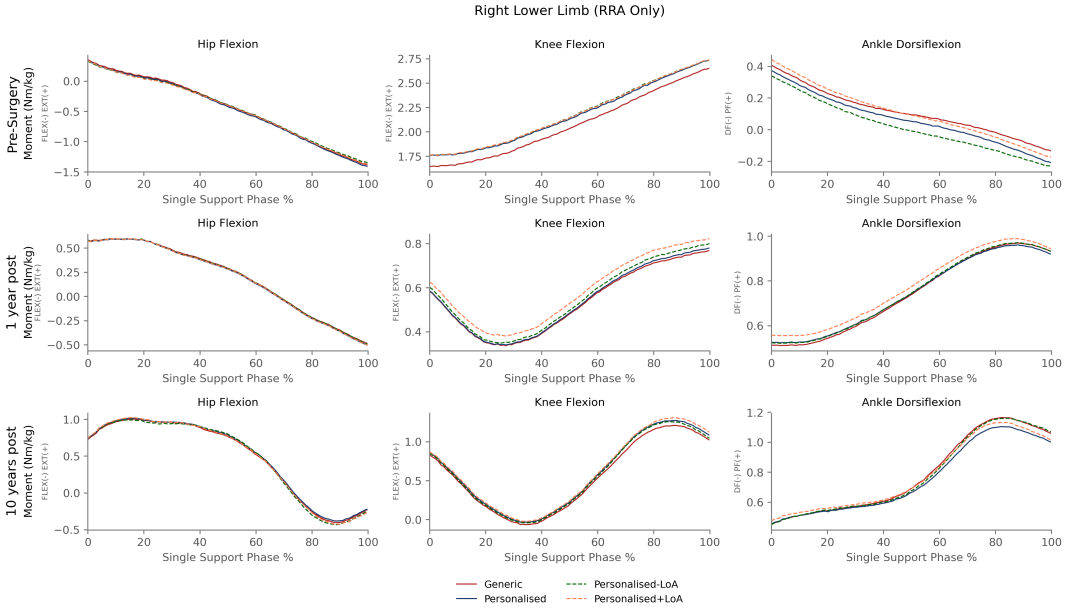

Figure D.2: Right lower limb sagittal joint moments, normalised by subject's mass, of the hip, knee, and ankle during the single support phase, simulated using OpenSim's RRA tool. Data are presented for pre-surgery, one-year post-surgery, and ten-year post-surgery, comparing the generic model, personalised model, and personalised models with positive and negative LoA. Each curve represents the average of the trials.

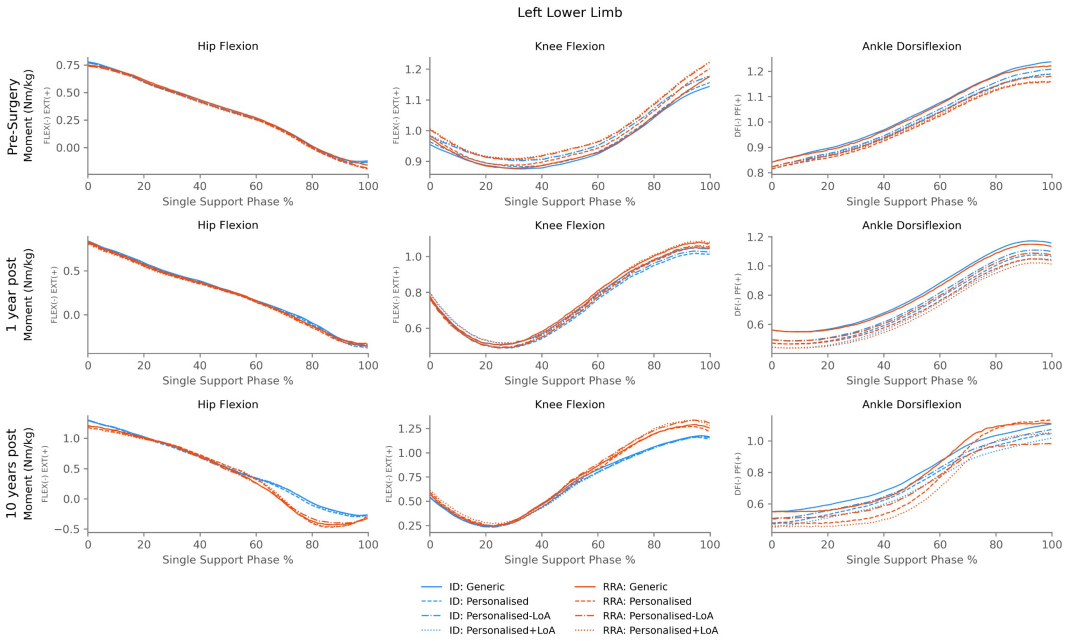

Figure D.3: Left lower limb sagittal joint moments, normalised by subject's mass, of the hip, knee, and ankle during the single support phase, simulated using OpenSim's ID and RRA tools. Data are presented for pre-surgery, one-year post-surgery, and ten-year post-surgery, comparing the generic model, personalised model, and personalised models with positive and negative LoA. Each curve represents the average of the trials. The vertical scale is adjusted for improved visualisation of the results.

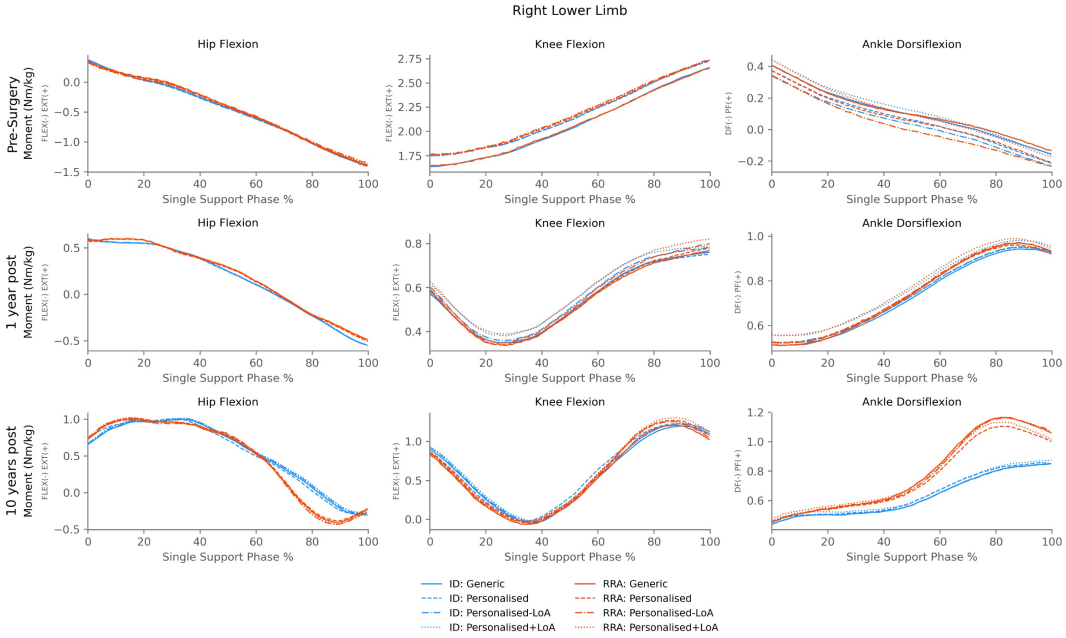

Figure D.4: Right lower limb sagittal joint moments, normalised by subject's mass, of the hip, knee, and ankle during the single support phase, simulated using OpenSim's ID and RRA tools. Data are presented for pre-surgery, one-year post-surgery, and ten-year post-surgery, comparing the generic model, personalised model, and personalised models with positive and negative LoA. Each curve represents the average of the trials. The vertical scale is adjusted for improved visualisation of the results.

E

Residuals Reduction

Table E.1: Pre-surgery range values of the residual forces (F) and moments (M) obtained from ID and RRA, in all models. Their percentage reduction (Reduction (%)), and RMS from RRA are also presented. The X, Y, and Z correspond to the antero-posterior, vertical, and mediolateral directions, respectively. The numbers refer to the trial numbers, while the letters '*l*' and '*r*' specify the lower limb, left and right, respectively, associated with each single support period.

			Residuals					
			FX	FY (N)	FZ	MX	MY (Nm)	MZ
Models		Trials						
Generic	1_l	Range ID	[-152.138;58.201]	[-26.629;163.789]	[-103.570;35.512]	[-47.075;22.998]	[-44.872;2.927]	[-30.880;29.531]
		Range RRA	[-9.133;6.514]	[-12.053;26.455]	[-1.720;3.075]	[-16.713;6.085]	[-7.257;-0.640]	[-8.226;2.799]
		Reduction (%)	92.561	79.777	96.552	67.465	86.156	81.751
		RMS	3.129	8.438	0.991	5.014	4.490	4.028
	1_r	Range ID	[-144.420;45.517]	[-58.529;116.478]	[-25.145;114.622]	[3.001;95.742]	[32.930;102.287]	[-41.942;62.166]
		Range RRA	[-5.078;18.312]	[-21.199;40.083]	[-6.611;8.387]	[-15.244;28.597]	[-31.137;4.917]	[-14.108;21.136]
		Reduction (%)	87.685	64.984	89.269	52.728	48.016	66.147
		RMS	10.924	14.677	5.190	14.219	20.409	11.787
	2_l	Range ID	[-179.164;60.341]	[-33.483;175.904]	[-104.163;38.002]	[-47.711;23.894]	[-37.963;10.547]	[-27.196;29.805]
		Range RRA	[-7.685;5.171]	[-14.873;30.446]	[-1.865;1.042]	[-13.200;4.402]	[-3.865;4.392]	[-4.964;7.929]
		Reduction (%)	94.632	78.356	97.955	75.418	82.978	77.381
		RMS	2.926	10.743	0.929	4.338	2.646	4.809
	2_r	Range ID	[-144.463;47.658]	[-56.806;112.499]	[-23.211;113.300]	[-1.711;95.303]	[36.516;103.430]	[-42.089;65.524]
		Range RRA	[-6.334;18.504]	[-17.113;38.119]	[-6.835;7.235]	[-13.183;29.786]	[-29.931;5.816]	[-14.349;20.735]
		Reduction (%)	87.072	67.377	89.693	55.709	46.578	67.398
		RMS	10.981	11.230	4.407	13.226	19.200	11.723
Personalised	1_l	Range ID	[-149.786;57.946]	[-27.621;163.417]	[-104.968;39.764]	[-45.388;23.249]	[-43.065;3.040]	[-29.355;30.468]
		Range RRA	[-9.243;6.778]	[-13.127;26.161]	[-2.176;3.154]	[-15.477;6.691]	[-7.416;-1.035]	[-7.405;3.332]
		Reduction (%)	92.287	79.434	96.317	67.703	86.160	82.053
		RMS	3.309	8.622	1.161	4.917	4.786	4.074
	1_r	Range ID	[-144.085;47.570]	[-55.821;116.277]	[-27.482;116.201]	[1.652;95.638]	[33.132;101.913]	[-42.804;62.202]
		Range RRA	[-6.305;19.003]	[-23.622;41.977]	[-7.293;8.763]	[-15.683;29.164]	[-31.875;4.509]	[-14.277;21.759]
		Reduction (%)	86.795	61.883	88.825	52.284	47.102	65.682
		RMS	11.532	15.479	5.470	14.185	21.099	11.826
	2_l	Range ID	[-178.020;62.360]	[-34.377;174.819]	[-105.066;40.209]	[-47.311;23.717]	[-36.299;9.544]	[-26.401;30.986]
		Range RRA	[-7.913;5.410]	[-17.093;30.368]	[-1.596;0.990]	[-12.563;4.672]	[-4.199;3.911]	[-3.950;8.512]
		Reduction (%)	94.458	77.312	98.220	75.735	82.308	78.284
		RMS	3.192	11.285	0.946	4.113	2.657	4.656
	2_r	Range ID	[-144.031;49.649]	[-54.035;112.900]	[-24.135;114.190]	[0.186;95.414]	[36.781;102.820]	[-40.848;66.072]
		Range RRA	[-6.611;19.493]	[-15.869;37.805]	[-7.394;7.055]	[-12.278;28.823]	[-28.784;5.856]	[-13.654;21.107]
		Reduction (%)	86.522	67.847	89.554	56.840	47.547	67.489
		RMS	11.203	11.100	4.293	12.102	19.151	11.790
Personalised - LoA	1_l	Range ID	[-150.517;56.824]	[-26.789;163.504]	[-104.486;38.034]	[-45.012;23.665]	[-42.709;2.862]	[-29.244;30.226]
		Range RRA	[-8.835;6.441]	[-13.240;26.144]	[-2.081;2.976]	[-15.811;6.768]	[-7.391;-0.988]	[-7.498;3.093]
		Reduction (%)	92.633	79.304	96.452	67.123	85.951	82.192
		RMS	3.187	8.718	1.082	4.944	4.573	3.986
	1_r	Range ID	[-144.292;46.591]	[-56.526;116.272]	[-25.685;115.415]	[1.907;95.478]	[34.193;102.092]	[-48.089;53.566]
		Range RRA	[-2.126;4.767]	[-5.938;11.796]	[-2.439;2.320]	[-15.977;35.493]	[-32.466;1.055]	[-13.916;21.600]
		Reduction (%)	96.389	89.737	96.627	44.994	50.633	65.062
		RMS	2.551	4.766	1.539	16.152	23.087	11.534
	2_l	Range ID	[-178.870;61.046]	[-31.561;174.601]	[-104.181;38.663]	[-47.053;23.906]	[-36.168;9.674]	[-26.227;30.865]
		Range RRA	[-7.552;5.080]	[-16.974;30.416]	[-1.780;0.890]	[-12.756;4.743]	[-4.083;3.928]	[-4.182;7.976]
		Reduction (%)	94.735	77.013	98.131	75.339	82.525	78.705
		RMS	3.014	11.217	0.950	4.208	2.567	4.549
	2_r	Range ID	[-144.794;49.136]	[-55.145;113.081]	[-23.242;114.415]	[0.599;95.518]	[36.974;103.458]	[-13.929;20.893]
		Range RRA	[-10.297;12.795]	[-22.859;18.364]	[-2.322;2.294]	[-12.890;33.918]	[-31.106;9.655]	[-37.479;36.982]
		Reduction (%)	88.093	75.496	96.646	50.689	38.691	−113.830
		RMS	6.304	12.277	1.390	15.125	21.343	11.657
Personalised + LoA	1_l	Range ID	[-149.714;58.600]	[-27.241;163.677]	[-105.469;39.487]	[-45.889;23.518]	[-42.969;2.637]	[-29.642;30.750]
		Range RRA	[-9.243;6.806]	[-13.448;26.262]	[-2.250;3.067]	[-15.343;6.968]	[-7.429;-1.230]	[-7.533;3.467]
		Reduction (%)	92.296	79.201	96.332	67.854	86.407	81.786
		RMS	3.308	8.729	1.171	4.907	4.538	3.984
	1_r	Range ID	[-143.335;46.884]	[-55.566;115.671]	[-26.543;116.064]	[2.310;95.505]	[32.199;101.441]	[-13.527;22.094]
		Range RRA	[-10.271;12.800]	[-21.578;30.022]	[-4.930;4.778]	[-11.306;18.448]	[-36.261;4.748]	[-36.538;34.656]
		Reduction (%)	87.871	69.866	93.193	68.074	40.774	−99.863
		RMS	5.773	13.006	3.076	9.749	22.663	11.770
	2_l	Range ID	[-177.416;63.593]	[-34.595;175.488]	[-106.541;40.758]	[-47.111;23.542]	[-36.022;9.159]	[-26.236;30.948]
		Range RRA	[-7.825;5.327]	[-17.005;30.243]	[-1.243;0.906]	[-12.283;5.045]	[-4.258;3.573]	[-3.717;8.347]
		Reduction (%)	94.543	77.510	98.541	75.474	82.667	78.902
		RMS	3.191	11.330	0.889	4.078	2.534	4.740
	2_r	Range ID	[-144.091;48.769]	[-54.020;112.708]	[-24.195;114.223]	[-1.650;95.665]	[37.753;102.485]	[-38.371;66.825]
		Range RRA	[-5.607;19.269]	[-16.868;38.270]	[-7.573;6.577]	[-13.556;28.201]	[-27.317;5.506]	[-13.317;21.265]
		Reduction (%)	87.101	66.930	89.777	57.091	49.293	67.126
		RMS	10.948	10.980	4.119	11.373	19.290	11.661

Table E.2: One-year post-surgery range values of the residual forces (F) and moments (M) obtained from ID and RRA, in all models. Their percentage reduction (Reduction (%)), and RMS from RRA are also presented. The X, Y, and Z correspond to the antero-posterior, vertical, and mediolateral directions, respectively. The numbers refer to the trial numbers, while the letters '*l*' and '*r*' specify the lower limb, left and right, respectively, associated with each single support period.

		Residuals					
		FX	FY (N)	FZ	MX	MY (N·m)	MZ
Models	**Trials**						
Generic	1_l	**Range ID** [-21.635;89.370]	[-76.993;92.811]	[-34.695;27.606]	[-60.992;23.230]	[-20.403;13.039]	[-34.728;36.588]
		Range RRA [-8.473;7.637]	[-8.621;23.793]	[-2.472;2.668]	[-20.551;10.544]	[-8.538;5.377]	[-9.671;5.923]
		Reduction (%) 85.487	80.911	91.749	63.080	58.390	78.135
		RMS 3.145	8.553	1.293	6.094	4.301	4.694
	1_r	**Range ID** [-62.242;50.336]	[-47.305;75.175]	[-8.314;62.163]	[-33.770;35.286]	[-17.621;18.229]	[-15.216;34.541]
		Range RRA [-4.222;6.460]	[-25.239;8.336]	[-2.043;3.305]	[-6.882;17.355]	[-1.516;2.748]	[-2.640;11.186]
		Reduction (%) 90.511	72.588	92.412	64.902	88.107	72.213
		RMS 2.026	7.166	1.981	5.792	1.385	3.461
	2_l	**Range ID** [-25.058;96.424]	[-80.637;71.486]	[-62.948;31.009]	[-44.233;16.407]	[-29.216;13.763]	[-27.039;22.939]
		Range RRA [-6.252;5.757]	[-14.552;14.600]	[-4.295;3.919]	[-26.239;13.491]	[-5.209;2.617]	[-6.285;6.866]
		Reduction (%) 90.115	80.837	91.257	34.482	81.790	73.686
		RMS 2.636	7.661	2.001	8.241	1.844	3.914
	2_r	**Range ID** [-51.156;105.238]	[-36.854;130.075]	[-40.737;80.462]	[-44.593;58.655]	[-32.049;32.584]	[-33.616;38.264]
		Range RRA [-7.535;14.171]	[-12.108;9.885]	[-6.474;10.378]	[-35.417;32.054]	[-4.964;1.915]	[-10.176;9.884]
		Reduction (%) 86.121	86.825	86.096	34.651	89.357	72.093
		RMS 4.383	5.996	3.874	15.098	2.929	5.642
	3_l	**Range ID** [-49.972;70.078]	[-85.930;84.911]	[-16.706;20.747]	[-45.250;13.064]	[-43.178;9.611]	[-22.135;25.061]
		Range RRA [-5.169;3.864]	[-16.796;26.972]	[-1.342;6.463]	[-32.450;9.200]	[-2.520;4.471]	[-0.617;7.832]
		Reduction (%) 92.476	74.381	79.161	28.577	86.757	82.099
		RMS 1.772	8.367	1.365	8.121	2.827	5.906
	3_r	**Range ID** [-50.831;75.190]	[-73.922;132.712]	[-18.575;44.143]	[-65.396;41.305]	[-10.587;32.975]	[-42.086;47.120]
		Range RRA [-9.699;8.047]	[-6.322;13.153]	[-2.640;4.675]	[-14.084;19.834]	[-7.045;1.894]	[-8.314;8.081]
		Reduction (%) 85.918	90.575	88.336	68.212	79.478	81.620
		RMS 3.418	5.211	2.072	7.355	4.195	4.728
Personalised	1_l	**Range ID** [-22.023;90.481]	[-77.562;92.773]	[-32.993;27.980]	[-62.044;23.751]	[-19.806;12.494]	[-35.485;37.307]
		Range RRA [-8.995;8.414]	[-9.079;22.816]	[-2.498;2.912]	[-20.274;10.044]	[-8.439;4.906]	[-10.120;5.430]
		Reduction (%) 84.525	81.275	91.128	64.662	58.683	78.639
		RMS 3.394	8.365	1.261	5.950	4.105	4.782
	1_r	**Range ID** [-61.690;47.079]	[-45.222;76.594]	[-6.543;62.732]	[-33.489;34.717]	[-16.226;18.490]	[-14.256;35.925]
		Range RRA [-4.884;6.517]	[-24.429;9.347]	[-2.087;3.307]	[-6.437;14.692]	[-1.722;2.552]	[-2.287;9.342]
		Reduction (%) 89.518	72.272	92.214	69.021	87.689	76.827
		RMS 2.271	7.112	2.052	5.396	1.617	3.183
	2_l	**Range ID** [-23.485;96.734]	[-78.303;72.367]	[-61.416;29.597]	[-44.533;16.503]	[-29.181;14.177]	[-27.964;21.854]
		Range RRA [-6.769;5.828]	[-13.729;13.743]	[-4.602;4.378]	[-27.104;13.458]	[-5.597;2.842]	[-7.327;5.951]
		Reduction (%) 89.522	81.767	90.133	33.545	80.536	73.346
		RMS 2.841	7.387	2.182	8.467	1.959	3.905
	2_r	**Range ID** [-50.291;96.186]	[-36.202;130.747]	[-39.359;85.145]	[-44.492;57.426]	[-30.561;33.057]	[-32.905;40.013]
		Range RRA [-7.721;14.230]	[-11.303;13.415]	[-6.776;10.910]	[-35.323;32.364]	[-5.079;2.826]	[-9.807;10.707]
		Reduction (%) 85.014	85.194	85.795	33.587	87.574	71.867
		RMS 4.272	6.750	4.052	15.119	3.010	5.867
	3_l	**Range ID** [-51.552;70.987]	[-87.012;82.601]	[-16.630;21.830]	[-43.531;12.343]	[-41.232;10.190]	[-22.545;24.848]
		Range RRA [-5.596;4.180]	[-16.387;25.751]	[-1.720;6.577]	[-31.008;9.808]	[-1.834;4.155]	[0.443;7.146]
		Reduction (%) 92.023	75.156	78.427	26.949	88.353	85.857
		RMS 1.841	8.114	1.483	8.001	2.538	5.480
	3_r	**Range ID** [-51.906;75.143]	[-72.213;132.440]	[-17.704;42.966]	[-63.682;39.955]	[-9.326;29.913]	[-40.067;47.618]
		Range RRA [-9.563;8.383]	[-6.781;14.408]	[-2.455;4.388]	[-12.558;18.089]	[-6.334;1.409]	[-7.215;5.394]
		Reduction (%) 85.875	89.646	88.721	70.429	80.266	85.621
		RMS 3.514	5.481	1.982	6.769	3.878	4.466
Personalised - LoA	1_l	**Range ID** [-21.928;89.308]	[-77.505;95.625]	[-33.878;27.453]	[-62.967;22.473]	[-19.582;13.018]	[-35.222;35.394]
		Range RRA [-8.544;7.663]	[-8.609;23.203]	[-2.453;2.614]	[-19.994;10.051]	[-8.727;5.491]	[-10.086;5.840]
		Reduction (%) 85.429	81.625	91.738	64.835	56.386	77.448
		RMS 3.160	8.278	1.253	5.806	4.350	4.884
	1_r	**Range ID** [-62.095;49.309]	[-44.476;75.357]	[-8.431;62.469]	[-33.468;35.779]	[-17.618;18.323]	[-14.638;35.565]
		Range RRA [-4.696;6.404]	[-25.181;9.180]	[-2.032;3.344]	[-6.763;15.920]	[-1.495;2.459]	[-2.322;10.093]
		Reduction (%) 90.036	71.326	92.417	67.243	88.997	75.270
		RMS 2.181	7.093	2.023	5.687	1.357	3.197
	2_l	**Range ID** [-23.538;96.073]	[-79.390;71.833]	[-61.807;29.961]	[-43.535;17.422]	[-28.888;14.062]	[-27.667;21.984]
		Range RRA [-6.403;5.630]	[-14.468;14.343]	[-4.322;3.793]	[-25.609;13.203]	[-5.024;2.837]	[-6.953;6.119]
		Reduction (%) 89.939	80.948	91.158	36.328	81.696	73.673
		RMS 2.696	7.558	1.994	7.995	1.772	3.807
	2_r	**Range ID** [-49.660;97.658]	[-37.829;130.385]	[-39.032;83.421]	[-42.437;58.333]	[-31.973;32.985]	[-32.196;39.043]
		Range RRA [-7.171;13.814]	[-11.300;13.321]	[-6.342;10.689]	[-36.210;31.715]	[-5.147;2.106]	[-9.648;10.258]
		Reduction (%) 85.755	85.363	86.092	32.595	88.833	72.058
		RMS 4.174	6.784	3.972	15.083	2.976	5.591
	3_l	**Range ID** [-49.248;71.437]	[-86.323;84.637]	[-16.459;21.040]	[-48.210;11.975]	[-43.062;10.124]	[-23.372;24.526]
		Range RRA [-5.534;3.846]	[-16.767;26.818]	[-1.632;6.471]	[-32.407;8.746]	[-2.547;4.382]	[-0.139;7.378]
		Reduction (%) 92.227	74.506	78.393	31.622	86.974	84.305
		RMS 1.837	8.302	1.421	8.025	2.712	5.585
	3_r	**Range ID** [-50.012;74.419]	[-73.490;133.640]	[-18.383;42.639]	[-66.366;41.698]	[-9.913;30.688]	[-42.072;47.238]
		Range RRA [-9.618;7.928]	[-7.292;13.573]	[-2.334;4.546]	[-13.746;18.179]	[-6.383;1.357]	[-7.258;5.951]
		Reduction (%) 85.899	89.927	88.726	70.458	80.935	85.209
		RMS 3.501	5.824	2.029	7.201	4.116	4.577
Personalised + LoA	1_l	**Range ID** [-21.757;89.558]	[-74.962;93.406]	[-33.131;26.275]	[-62.713;21.960]	[-19.219;12.796]	[-35.410;35.265]
		Range RRA [-8.421;7.491]	[-8.790;22.409]	[-2.278;2.630]	[-20.502;9.457]	[-8.987;5.209]	[-10.610;5.504]
		Reduction (%) 85.705	81.470	91.737	64.617	55.658	77.201
		RMS 3.153	8.125	1.243	5.773	4.400	5.011
	1_r	**Range ID** [-62.082;48.130]	[-42.173;76.517]	[-5.724;63.216]	[-34.111;35.283]	[-16.682;19.000]	[-14.992;35.535]
		Range RRA [-4.961;5.970]	[-24.409;9.688]	[-2.021;3.405]	[-6.825;15.319]	[-1.997;2.868]	[-2.783;9.361]
		Reduction (%) 90.082	71.272	92.130	68.089	86.365	75.966
		RMS 2.245	7.014	2.087	5.473	1.779	3.176
	2_l	**Range ID** [-23.903;96.532]	[-77.332;72.973]	[-60.874;27.818]	[-43.890;17.839]	[-28.817;14.377]	[-27.704;20.778]
		Range RRA [-6.286;5.369]	[-13.975;13.502]	[-4.510;3.995]	[-27.653;13.513]	[-5.403;2.861]	[-7.900;5.990]
		Reduction (%) 90.323	81.719	90.411	33.311	80.867	71.351
		RMS 2.738	7.352	2.148	8.633	1.912	3.892
	2_r	**Range ID** [-49.421;93.724]	[-36.004;130.970]	[-38.708;84.663]	[-44.259;59.383]	[-39.259;35.453]	[-32.099;40.922]
		Range RRA [-7.013;13.675]	[-12.931;15.362]	[-7.043;12.015]	[-41.935;35.259]	[-5.499;2.447]	[-9.522;11.039]
		Reduction (%) 85.548	83.055	84.552	25.518	89.364	71.842
		RMS 4.140	7.453	4.333	16.970	3.082	5.712
	3_l	**Range ID** [-51.922;71.211]	[-85.811;81.476]	[-16.480;20.237]	[-42.537;11.347]	[-41.926;11.453]	[-22.915;24.050]
		Range RRA [-5.369;3.707]	[-16.603;25.608]	[-1.773;6.165]	[-31.695;9.695]	[-1.746;4.680]	[0.648;6.906]
		Reduction (%) 92.629	74.767	78.383	23.188	87.960	86.676
		RMS 1.807	8.110	1.436	7.867	2.588	5.415
	3_r	**Range ID** [-52.074;74.296]	[-72.024;133.612]	[-17.224;42.524]	[-64.943;41.997]	[-9.808;27.589]	[-40.155;48.412]
		Range RRA [-8.939;7.781]	[-7.172;14.941]	[-2.359;4.207]	[-12.375;16.990]	[-6.126;0.741]	[-7.138;4.905]
		Reduction (%) 86.770	89.247	89.011	72.541	81.639	86.402
		RMS 3.389	5.629	1.929	6.836	4.027	4.700

Table E.3: Ten-year post-surgery range values of the residual forces (F) and moments (M) obtained from ID and RRA, in all models. Their percentage reduction (Reduction (%)), and RMS from RRA are also presented. The X, Y, and Z correspond to the antero-posterior, vertical, and mediolateral directions, respectively. The numbers refer to the trial numbers, while the letters '*l*' and '*r*' specify the lower limb, left and right, respectively, associated with each single support period.

		Residuals					
		FX	FY (N)	FZ	MX	MY (Nm)	MZ
Models	Trials						
Generic	1_l	Range ID	[-137.227;114.471]	[-98.959;135.756]	[-131.014;78.060]	[-134.299;54.128]	[-96.446;64.836]	[-36.732;64.529]
		Range RRA	[-28.632;48.778]	[-22.750;22.971]	[-42.402;-2.129]	[-45.685;11.885]	[-39.581;34.561]	[-10.187;31.646]
		Reduction (%)	69.245	80.521	80.737	69.447	54.030	58.688
		RMS	24.552	13.159	30.575	30.156	24.750	15.735
	1_r	Range ID	[-150.666;156.026]	[-154.958;161.408]	[-113.296;128.764]	[-160.683;95.855]	[-83.410;77.359]	[-8.939;38.851]
		Range RRA	[-2.416;9.731]	[-21.200;26.472]	[-4.961;3.824]	[-12.999;19.033]	[-16.650;36.693]	[-29.622;39.903]
		Reduction (%)	96.039	84.932	96.371	87.514	66.820	−45.477
		RMS	4.687	13.781	3.124	12.210	18.385	18.756
	2_l	Range ID	[-106.647;155.071]	[-118.740;26.668]	[-160.008;138.595]	[-136.964;35.621]	[-74.064;114.529]	[-27.113;33.040]
		Range RRA	[-30.624;24.078]	[-42.454;49.119]	[-24.358;-0.495]	[-30.836;-2.604]	[-27.469;28.370]	[-5.926;33.331]
		Reduction (%)	79.099	37.023	92.009	83.642	70.392	34.738
		RMS	16.814	23.091	14.292	18.280	18.061	13.754
	2_r	Range ID	[-104.510;219.701]	[-184.193;48.950]	[-135.310;131.637]	[-128.200;64.892]	[-48.764;75.154]	[-31.095;50.842]
		Range RRA	-30.636;47.907]	[-38.955;7.382]	[-23.891;33.256]	[-16.520;32.456]	[-14.348;29.009]	[-26.064;45.354]
		Reduction (%)	75.774	80.125	78.592	74.636	65.012	12.839
		RMS	26.274	20.776	17.199	16.901	14.956	23.400
	3_l	Range ID	[-100.771;199.435]	[-161.523;174.647]	[-174.354;183.526]	[-112.616;52.204]	[-91.902;155.214]	[-18.545;37.728]
		Range RRA	[-4.810;8.794]	[-22.995;15.092]	[-0.356;9.815]	[-47.117;0.489]	[-41.870;33.623]	[-16.931;16.376]
		Reduction (%)	95.468	88.670	97.158	71.117	69.450	40.810
		RMS	3.572	12.598	5.279	25.883	24.638	10.453
	3_r	Range ID	[-58.712;215.206]	[-86.083;112.930]	[-116.169;157.986]	[-159.919;60.259]	[-63.968;68.992]	[-33.355;35.886]
		Range RRA	[-4.838;32.258]	[-41.222;15.433]	[-23.981;3.835]	[0.637;26.051]	[-24.011;30.388]	[-4.438;34.036]
		Reduction (%)	86.457	71.532	89.854	88.458	59.086	44.435
		RMS	14.006	18.851	11.232	12.450	20.389	14.755
Personalised	1_l	Range ID	[-146.391;125.618]	[-93.151;137.564]	[-144.494;79.912]	[-141.994;55.810]	[-102.787;60.659]	[-12.239;29.208]
		Range RRA	[-10.611;23.606]	[-41.582;30.562]	[-25.476;-1.001]	[-40.816;-4.579]	[-32.337;27.331]	[-15.638;29.201]
		Reduction (%)	87.420	68.730	89.093	81.681	63.493	−8.183
		RMS	11.253	22.482	16.513	29.453	19.687	14.403
	1_r	Range ID	[-160.058;147.017]	[-162.585;175.822]	[-118.105;139.292]	[-157.733;101.989]	[-89.635;68.286]	[-32.021;38.449]
		Range RRA	[-2.397;10.154]	[-17.786;21.277]	[-7.550;14.187]	[-46.975;32.651]	[-15.446;33.694]	[-8.507;40.359]
		Reduction (%)	95.913	88.457	91.555	69.342	68.883	30.656
		RMS	4.813	11.003	6.376	23.679	17.996	19.240
	2_l	Range ID	[-100.683;168.319]	[-112.101;29.229]	[-157.174;131.318]	[-147.794;34.999]	[-78.935;106.127]	[-30.566;38.055]
		Range RRA	[-33.077;28.085]	[-13.898;14.682]	[-16.030;-1.380]	[-29.782;-2.429]	[-25.987;26.523]	[-7.346;31.375]
		Reduction (%)	77.263	79.778	94.922	85.036	71.626	43.572
		RMS	18.692	7.618	10.684	18.125	17.027	12.104
	2_r	Range ID	[-130.906;233.891]	[-185.338;77.978]	[-155.046;135.530]	[-131.628;78.757]	[-64.301;76.024]	[-36.069;55.554]
		Range RRA	[-33.224;50.680]	[-39.812;7.220]	[-25.978;33.923]	[-17.449;33.319]	[-15.528;28.948]	[-26.056;42.752]
		Reduction (%)	77.000	82.138	79.385	75.869	68.304	24.901
		RMS	28.145	21.150	17.609	18.020	15.382	21.828
	3_l	Range ID	[-95.422;200.278]	[-151.612;174.933]	[-173.923;176.601]	[-115.330;50.865]	[-92.914;145.914]	[-18.092;36.340]
		Range RRA	[-4.434;8.506]	[-24.521;14.746]	[-14.718;-2.124]	[-44.614;0.852]	[-35.949;29.640]	[-19.817;14.317]
		Reduction (%)	95.624	87.975	96.407	72.643	72.537	37.289
		RMS	3.639	13.757	10.054	24.196	21.516	10.413
	3_r	Range ID	[-74.020;216.975]	[-86.765;119.358]	[-122.378;162.668]	[-163.648;69.708]	[-72.208;61.878]	[-32.629;35.403]
		Range RRA	[-6.072;31.773]	[-40.325;15.849]	[-1.866;32.688]	[0.967;26.787]	[-24.730;28.088]	[-5.539;34.359]
		Reduction (%)	86.995	72.748	87.878	88.936	60.609	41.355
		RMS	13.587	18.580	15.672	12.823	19.409	14.660
Personalised - LoA	1_l	Range ID	[-138.151;116.239]	[-94.940;135.370]	[-133.737;76.917]	[-135.392;53.494]	[-94.578;60.565]	[-36.301;60.379]
		Range RRA	[-7.537;12.119]	[-49.896;75.902]	[-56.268;-3.927]	[-35.809;3.182]	[-33.096;32.832]	[-11.482;27.872]
		Reduction (%)	92.273	45.379	75.153	79.357	57.505	59.294
		RMS	6.134	32.897	41.297	22.992	22.254	14.151
	1_r	Range ID	[-148.496;156.572]	[-157.737;169.011]	[-132.421;139.382]	[-156.914;95.910]	[-96.777;74.880]	[-31.068;39.927]
		Range RRA	[-5.708;35.266]	[-15.258;23.634]	[-25.952;26.800]	[-10.240;20.293]	[-8.729;27.339]	[-5.086;39.002]
		Reduction (%)	86.569	88.097	80.592	87.923	78.988	37.899
		RMS	19.940	12.357	16.558	13.133	14.487	18.721
	2_l	Range ID	[-100.892;154.628]	[-116.431;29.040]	[-157.390;132.218]	[-138.852;33.160]	[-73.538;107.036]	[-62.973;48.892]
		Range RRA	[-5.230;2.189]	[-34.789;26.174]	[-58.725;-6.765]	[-62.298;52.582]	[-33.670;37.128]	[-6.853;30.448]
		Reduction (%)	97.097	58.093	82.059	33.214	60.793	66.656
		RMS	2.360	16.628	38.403	35.586	23.719	11.996
	2_r	Range ID	[-115.712;232.222]	[-183.751;46.328]	[-155.972;136.116]	[-129.686;70.206]	[-64.939;72.840]	[-25.917;42.306]
		Range RRA	[-3.048;5.123]	[-15.182;2.578]	[-4.845;2.531]	[-0.275;16.370]	[-13.667;26.447]	[-13.917;21.442]
		Reduction (%)	97.652	92.281	97.475	91.673	70.886	48.172
		RMS	2.661	7.753	2.393	9.739	14.406	11.306
	3_l	Range ID	[-93.391;200.526]	[-156.466;174.993]	[-176.137;172.063]	[-116.066;49.273]	[-94.932;145.282]	[-20.417;43.679]
		Range RRA	[-7.580;8.872]	[-10.754;5.850]	[-41.413;-2.564]	[-29.075;0.473]	[-35.253;29.723]	[-19.809;14.243]
		Reduction (%)	94.403	94.991	88.843	82.129	72.951	46.873
		RMS	5.221	6.257	25.414	16.172	21.395	10.473
	3_r	Range ID	[-74.769;214.335]	[-89.516;117.648]	[-119.163;159.629]	[-159.983;71.745]	[-69.850;61.037]	[-32.781;34.898]
		Range RRA	[-5.335;32.365]	[-41.120;15.245]	[-2.596;32.994]	[0.715;26.883]	[-25.538;28.640]	[-4.781;34.778]
		Reduction (%)	86.960	72.792	87.234	88.707	58.607	41.549
		RMS	13.857	18.598	15.723	12.889	19.812	14.871
Personalised + LoA	1_l	Range ID	[-147.152;124.857]	[-91.692;137.694]	[-150.783;83.115]	[-140.726;55.669]	[-108.486;61.987]	[-12.954;28.208]
		Range RRA	[-10.766;23.749]	[-42.033;30.210]	[-27.301;-1.100]	[-40.720;-4.172]	[-29.501;25.953]	[-16.011;29.340]
		Reduction (%)	87.311	68.506	88.798	81.390	67.470	−10.177
		RMS	11.119	22.696	16.899	29.782	18.419	14.126
	1_r	Range ID	[-177.848;160.816]	[-172.479;185.972]	[-126.647;146.675]	[-164.720;113.201]	[-96.285;67.143]	[-31.817;38.126]
		Range RRA	[-7.207;41.147]	[-21.543;20.252]	[-21.516;9.844]	[-7.502;21.434]	[-12.324;33.194]	[-5.817;42.261]
		Reduction (%)	85.722	88.340	88.526	89.588	72.148	31.261
		RMS	19.765	11.870	12.630	12.923	17.740	20.394
	2_l	Range ID	[-100.996;165.771]	[-108.835;31.525]	[-156.638;128.954]	[-148.753;36.996]	[-83.462;103.028]	[-28.666;41.684]
		Range RRA	[-31.609;30.539]	[-47.512;45.846]	[-21.419;-1.638]	[-52.270;10.866]	[-28.643;30.033]	[-8.513;31.290]
		Reduction (%)	76.703	33.487	93.074	66.010	68.536	43.421
		RMS	19.148	27.512	14.491	28.668	19.788	12.128
	2_r	Range ID	[-118.327;259.463]	[-186.004;44.824]	[-169.550;135.601]	[-136.506;66.581]	[-73.228;76.801]	[-32.452;56.938]
		Range RRA	[-34.184;50.820]	[-38.590;8.849]	[-26.535;34.064]	[-18.070;34.405]	[-15.589;28.622]	[-25.329;42.276]
		Reduction (%)	77.500	79.448	80.141	74.161	70.532	24.370
		RMS	27.110	20.488	17.662	18.804	15.475	22.005
	3_l	Range ID	[-93.724;199.929]	[-147.010;175.756]	[-176.121;171.987]	[-112.602;50.517]	[-97.422;141.353]	[-28.064;23.550]
		Range RRA	[-27.343;24.067]	[-25.987;13.672]	[-34.926;-4.506]	[-45.344;0.510]	[-32.470;31.749]	[-20.422;13.242]
		Reduction (%)	82.493	87.713	91.261	71.889	73.105	34.778
		RMS	14.377	15.982	24.854	24.821	20.029	10.256
	3_r	Range ID	[-72.272;200.781]	[-81.764;117.319]	[-120.828;163.959]	[-155.058;70.488]	[-72.441;61.135]	[-33.229;33.658]
		Range RRA	[-1.544;7.815]	[-37.968;15.382]	[-0.352;9.589]	[1.200;25.428]	[-24.656;29.405]	[-5.575;33.561]
		Reduction (%)	96.572	73.202	96.509	89.258	59.527	41.489
		RMS	3.337	17.833	4.643	12.354	19.624	14.294

F

Muscle Forces

F.1 Reserve Actuators

Table F.1: Pre-surgery range values for the reserve actuator moments, in Nm, of the joints DoF from CMC, in all models. RMS is also presented. The numbers refer to the trial numbers, while the letters *'l'* and *'r'* specify the lower limb, left and right, respectively, associated with each single support period.

		Reserves												
Models	Trials	Left Hip Flexion	Left Hip Adduction	Left Hip Rotation	Left Knee Angle	Left Ankle Angle	Right Hip Flexion	Right Hip Adduction (Nm)	Right Hip Rotation	Right Knee Angle	Right Ankle Angle	Lumbar Extension	Lumbar Bending	Lumbar Rotation
Generic	1_l	Range	[-0.012;-0.000]	[0.000;0.005]	[-0.002;0.018]	[0.006;0.011]	[-0.010;0.005]	[-0.001;0.007]	[-0.003;0.003]	[-0.004;0.017]	[-0.017;0.002]	[-0.000;0.010]	[-0.001;0.007]	[-0.003;0.003]	[-0.004;0.017]
		RMS	0.007	0.003	0.013	0.008	0.008	0.007	0.004	0.006	0.010	0.007	0.002	0.002	0.005
	1_r	Range	[0.002;0.019]	[-0.017;0.001]	[-0.034;-0.001]	[-0.034;-0.007]	[0.004;0.017]	[0.001;0.004]	[0.009;0.019]	[-0.050;0.028]	[0.011;0.017]	[-0.003;0.861]	[-0.013;0.003]	[-0.012;-0.004]	[-0.013;0.010]
		RMS	0.013	0.011	0.020	0.022	0.010	0.003	0.013	0.035	0.013	0.166	0.007	0.007	0.007
	2_l	Range	[-0.013;-0.002]	[-0.003;0.004]	[-0.010;0.008]	[0.006;0.013]	[-0.014;0.013]	[-0.001;0.012]	[-0.002;0.008]	[-0.010;0.011]	[-0.015;0.001]	[0.003;0.013]	[0.000;0.003]	[-0.001;0.002]	[-0.003;0.004]
		RMS	0.007	0.003	0.007	0.008	0.009	0.007	0.003	0.007	0.008	0.008	0.002	0.001	0.003
	2_r	Range	[0.003;0.018]	[-0.017;-0.000]	[-0.030;-0.002]	[-0.033;-0.008]	[0.004;0.017]	[-0.000;0.004]	[0.009;0.018]	[-0.048;0.031]	[0.011;0.016]	[-0.003;0.964]	[-0.007;-0.001]	[-0.009;-0.004]	[-0.009;0.001]
		RMS	0.013	0.011	0.018	0.023	0.010	0.002	0.013	0.036	0.012	0.196	0.005	0.006	0.006
Personalised	1_l	Range	[-0.009;0.001]	[0.001;0.005]	[0.003;0.029]	[0.006;0.012]	[-0.013;0.007]	[0.002;0.016]	[0.005;0.019]	[-0.026;0.032]	[-0.015;-0.001]	[0.004;0.012]	[-0.001;0.003]	[-0.001;0.003]	[-0.003;0.013]
		RMS	0.006	0.003	0.021	0.008	0.010	0.010	0.010	0.021	0.009	0.008	0.002	0.002	0.003
	1_r	Range	[0.002;0.014]	[-0.002;0.007]	[-0.083;0.011]	[-0.023;0.002]	[0.002;0.013]	[-0.003;0.037]	[0.010;0.068]	[-0.068;0.138]	[0.014;0.017]	[-0.009;0.021]	[-0.014;-0.002]	[-0.013;-0.004]	[-0.015;0.001]
		RMS	0.010	0.005	0.054	0.016	0.007	0.009	0.020	0.061	0.015	0.012	0.006	0.007	0.006
	2_l	Range	[-0.013;-0.002]	[-0.012;0.005]	[-0.020;-0.003]	[0.006;0.013]	[-0.020;0.009]	[0.002;0.018]	[0.004;0.021]	[-0.020;0.035]	[-0.016;-0.002]	[0.005;0.013]	[0.000;0.003]	[-0.001;0.003]	[-0.003;0.004]
		RMS	0.008	0.008	0.009	0.008	0.011	0.012	0.010	0.021	0.010	0.010	0.002	0.002	0.002
	2_r	Range	[0.003;0.016]	[-0.003;0.007]	[-0.079;0.013]	[-0.022;0.002]	[0.002;0.013]	[-0.003;0.036]	[0.011;0.065]	[-0.068;0.135]	[0.013;0.016]	[-0.007;0.021]	[-0.008;-0.002]	[-0.009;-0.004]	[-0.009;0.000]
		RMS	0.011	0.004	0.049	0.016	0.008	0.009	0.020	0.062	0.015	0.012	0.005	0.006	0.007
Personalised - LoA	1_l	Range	[-0.011;0.000]	[0.001;0.005]	[0.005;0.019]	[0.006;0.011]	[-0.011;0.004]	[0.000;0.010]	[0.002;0.013]	[-0.005;0.015]	[-0.011;0.000]	[0.001;0.010]	[-0.001;0.003]	[-0.001;0.002]	[-0.003;0.014]
		RMS	0.007	0.003	0.015	0.008	0.007	0.007	0.006	0.008	0.007	0.005	0.001	0.002	0.002
	1_r	Range	[0.001;0.016]	[-0.015;0.002]	[-0.031;0.001]	[-0.028;-0.004]	[0.002;0.013]	[0.001;0.009]	[0.010;0.030]	[-0.049;0.058]	[0.012;0.019]	[-0.003;0.021]	[-0.014;-0.003]	[-0.012;-0.003]	[-0.013;-0.001]
		RMS	0.011	0.007	0.017	0.019	0.007	0.003	0.014	0.038	0.014	0.012	0.007	0.007	0.007
	2_l	Range	[-0.013;-0.001]	[-0.003;0.004]	[-0.010;0.008]	[0.006;0.013]	[-0.013;0.012]	[-0.001;0.011]	[0.002;0.016]	[-0.006;0.018]	[-0.011;0.001]	[0.003;0.010]	[0.000;0.003]	[-0.001;0.002]	[-0.003;0.004]
		RMS	0.008	0.003	0.006	0.008	0.009	0.007	0.008	0.010	0.007	0.006	0.002	0.001	0.002
	2_r	Range	[0.001;0.015]	[-0.013;0.002]	[-0.026;-0.003]	[-0.027;-0.003]	[0.003;0.013]	[-0.000;0.007]	[0.010;0.029]	[-0.046;0.055]	[0.013;0.019]	[-0.005;0.027]	[-0.009;-0.002]	[-0.008;-0.003]	[-0.009;-0.000]
		RMS	0.011	0.007	0.015	0.019	0.008	0.002	0.014	0.039	0.014	0.013	0.006	0.006	0.008
Personalised + LoA	1_l	Range	[-0.010;0.000]	[-0.003;0.006]	[-0.056;0.000]	[0.006;0.013]	[-0.081;0.006]	[0.005;0.013]	[0.006;0.028]	[-0.055;-0.031]	[-0.012;0.001]	[-0.004;0.021]	[-0.001;0.003]	[-0.000;0.002]	[-0.003;0.015]
		RMS	0.005	0.003	0.028	0.008	0.025	0.009	0.013	0.047	0.007	0.013	0.001	0.002	0.003
	1_r	Range	[-0.017;0.019]	[-0.101;0.007]	[-0.143;-0.097]	[-0.027;0.003]	[0.003;0.014]	[-0.005;0.050]	[0.012;0.075]	[-0.104;0.195]	[0.016;0.484]	[-1.460;0.023]	[-0.026;-0.003]	[-0.021;-0.004]	[-0.021;0.002]
		RMS	0.015	0.024	0.122	0.019	0.009	0.013	0.023	0.092	0.124	0.044	0.008	0.008	0.009
	2_l	Range	[-0.014;-0.004]	[-0.017;0.006]	[-0.073;-0.049]	[0.007;0.015]	[-0.105;0.005]	[0.006;0.016]	[0.004;0.029]	[-0.056;-0.006]	[-0.013;-0.001]	[-0.003;0.020]	[0.000;0.003]	[-0.001;0.002]	[-0.003;0.004]
		RMS	0.009	0.009	0.057	0.010	0.033	0.011	0.015	0.040	0.008	0.014	0.002	0.002	0.003
	2_r	Range	[0.005;0.019]	[-0.017;0.005]	[-0.140;-0.104]	[-0.025;0.002]	[0.003;0.012]	[-0.007;0.062]	[0.014;0.084]	[-0.104;0.249]	[0.015;0.025]	[-0.178;0.020]	[-0.008;-0.002]	[-0.008;-0.003]	[-0.009;0.000]
		RMS	0.014	0.006	0.123	0.018	0.009	0.016	0.025	0.101	0.017	0.075	0.005	0.006	0.007

Table F.2: One-year post-surgery range values for the reserve actuator moments, in Nm, of the joints DoF from CMC, in all models. RMS is also presented. The numbers refer to the trial numbers, while the letters '*l*' and '*r*' specify the lower limb, left and right, respectively, associated with each single support period.

		Reserves												
Models	Trials	Left Hip Flexion	Left Hip Adduction	Left Hip Rotation	Left Knee Angle	Left Ankle Angle	Right Hip Flexion	Right Hip Adduction (Nm)	Right Hip Rotation	Right Knee Angle	Right Ankle Angle	Lumbar Extension	Lumbar Bending	Lumbar Rotation
Generic	1_l Range	[-0.011;0.001]	[-0.006;0.003]	[0.002;0.031]	[0.003;0.007]	[-0.008;0.011]	[-0.001;0.009]	[-0.003;0.007]	[-0.015;0.016]	[-0.010;0.001]	[-0.000;0.008]	[-0.002;0.002]	[-0.001;0.002]	[-0.003;0.004]
	RMS	0.005	0.002	0.020	0.004	0.005	0.005	0.004	0.009	0.005	0.005	0.001	0.001	0.002
	1_r Range	[-0.001;0.016]	[-0.011;0.003]	[-0.020;0.002]	[-0.020;0.000]	[-0.000;0.019]	[-0.015;-0.002]	[-0.007;0.005]	[0.022;0.080]	[0.003;0.007]	[-0.008;0.007]	[-0.003;0.002]	[-0.005;0.000]	[-0.003;0.006]
	RMS	0.011	0.007	0.013	0.012	0.007	0.011	0.004	0.044	0.004	0.005	0.001	0.003	0.003
	2_l Range	[-0.013;0.000]	[-0.009;0.004]	[-0.001;0.014]	[0.002;0.012]	[-0.007;0.011]	[-0.003;0.009]	[-0.003;0.006]	[-0.006;0.020]	[-0.007;0.001]	[-0.000;0.008]	[-0.001;0.002]	[-0.000;0.003]	[-0.002;0.005]
	RMS	0.006	0.004	0.008	0.004	0.005	0.005	0.004	0.011	0.003	0.005	0.001	0.002	0.002
	2_r Range	[-0.003;0.019]	[-0.014;0.006]	[-0.027;0.002]	[-0.023;0.002]	[-0.000;0.015]	[-0.013;-0.003]	[-0.015;0.007]	[0.017;0.060]	[0.002;0.009]	[-0.016;0.007]	[-0.004;0.005]	[-0.009;-0.001]	[-0.004;0.024]
	RMS	0.013	0.008	0.013	0.014	0.009	0.010	0.006	0.036	0.004	0.007	0.003	0.006	0.010
	3_l Range	[-0.009;-0.000]	[-0.010;0.007]	[-0.004;0.017]	[0.003;0.006]	[-0.007;0.013]	[-0.001;0.010]	[-0.007;0.006]	[-0.011;0.007]	[-0.011;0.001]	[-0.000;0.009]	[-0.000;0.003]	[-0.000;0.003]	[-0.004;0.006]
	RMS	0.005	0.004	0.010	0.005	0.005	0.005	0.005	0.006	0.004	0.005	0.002	0.002	0.003
	3_r Range	[-0.002;0.018]	[-0.015;0.004]	[-0.035;0.004]	[-0.022;0.001]	[-0.000;0.019]	[-0.013;0.000]	[-0.007;0.006]	[0.010;0.066]	[0.003;0.006]	[-0.010;0.008]	[-0.005;0.002]	[-0.007;-0.001]	[-0.002;0.015]
	RMS	0.012	0.007	0.016	0.014	0.008	0.008	0.003	0.034	0.004	0.006	0.002	0.004	0.006
Personalised	1_l Range	[-0.011;0.009]	[-0.011;0.007]	[-0.001;0.088]	[0.003;0.007]	[-0.006;0.011]	[0.000;0.014]	[0.001;0.013]	[-0.006;0.032]	[-0.011;0.001]	[0.002;0.008]	[-0.002;0.002]	[-0.001;0.002]	[-0.002;0.004]
	RMS	0.007	0.004	0.048	0.004	0.004	0.008	0.006	0.016	0.006	0.005	0.001	0.001	0.002
	1_r Range	[-0.001;0.015]	[-0.001;0.011]	[-0.014;0.013]	[-0.014;0.000]	[-0.000;0.012]	[-0.013;0.010]	[-0.005;0.007]	[0.030;0.166]	[0.003;0.008]	[-0.008;0.007]	[-0.002;0.002]	[-0.004;0.000]	[-0.002;0.007]
	RMS	0.010	0.005	0.011	0.008	0.005	0.010	0.004	0.066	0.004	0.006	0.001	0.003	0.003
	2_l Range	[-0.013;0.002]	[-0.013;0.005]	[-0.002;0.029]	[0.001;0.012]	[-0.006;0.009]	[-0.002;0.015]	[0.003;0.010]	[-0.005;0.027]	[-0.011;0.000]	[0.002;0.006]	[-0.001;0.002]	[-0.001;0.003]	[-0.002;0.005]
	RMS	0.006	0.005	0.016	0.004	0.004	0.008	0.007	0.016	0.005	0.004	0.001	0.002	0.002
	2_r Range	[-0.004;0.020]	[-0.037;0.014]	[-0.043;0.025]	[-0.016;0.002]	[0.001;0.011]	[-0.011;0.005]	[-0.016;0.009]	[0.015;0.073]	[0.002;0.009]	[-0.017;0.006	[-0.005;0.006]	[-0.009;-0.002]	[-0.004;0.023]
	RMS	0.013	0.010	0.018	0.010	0.006	0.008	0.006	0.037	0.003	0.008	0.004	0.006	0.013
	3_l Range	[-0.010;0.002]	[-0.019;0.008]	[-0.011;0.032]	[0.003;0.007]	[-0.005;0.011]	[-0.001;0.015]	[-0.001;0.013]	[-0.007;0.021]	[-0.011;-0.001]	[0.003;0.007]	[-0.001;0.003]	[-0.000;0.004]	[-0.004;0.006]
	RMS	0.005	0.007	0.017	0.004	0.004	0.008	0.009	0.009	0.005	0.005	0.002	0.002	0.003
	3_r Range	[-0.001;0.017]	[-0.011;0.009]	[-0.018;0.022]	[-0.016;0.001]	[-0.001;0.011]	[-0.016;0.011]	[-0.006;0.006]	[0.009;0.120]	[-0.002;0.006]	[-0.010;0.006]	[-0.005;0.003]	[-0.007;-0.001]	[-0.001;0.016]
	RMS	0.010	0.004	0.012	0.009	0.005	0.010	0.003	0.056	0.004	0.006	0.002	0.005	0.007
Personalised - LoA	1_l Range	[-0.014;0.004]	[-0.002;0.006]	[0.016;0.065]	[0.003;0.007]	[-0.006;0.012]	[-0.001;0.009]	[-0.000;0.012]	[-0.007;0.061]	[-0.010;0.001]	[-0.000;0.008]	[-0.003;0.002]	[-0.001;0.002]	[-0.002;0.004]
	RMS	0.008	0.003	0.041	0.004	0.004	0.005	0.006	0.034	0.005	0.005	0.001	0.001	0.002
	1_r Range	[-0.000;0.012]	[-0.006;0.004]	[-0.014;0.003]	[-0.013;0.000]	[-0.000;0.015]	[-0.020;-0.015]	[-0.007;0.006]	[0.039;0.198]	[0.003;0.008]	[-0.009;0.007]	[-0.001;0.002]	[-0.005;-0.002]	[-0.002;0.007]
	RMS	0.008	0.002	0.008	0.005	0.005	0.018	0.005	0.095	0.005	0.006	0.001	0.003	0.003
	2_l Range	[-0.016;-0.001]	[-0.005;0.008]	[0.015;0.036]	[0.002;0.013]	[-0.006;0.009]	[-0.003;0.009]	[-0.001;0.008]	[-0.007;0.061]	[-0.008;0.001]	[-0.000;0.008]	[-0.001;0.002]	[-0.001;0.002]	[-0.002;0.004]
	RMS	0.008	0.004	0.023	0.005	0.004	0.005	0.005	0.025	0.003	0.005	0.001	0.001	0.003
	2_r Range	[-0.002;0.014]	[-0.011;0.009]	[-0.020;0.010]	[-0.014;0.001]	[-0.000;0.011]	[-0.020;-0.013]	[-0.017;0.007]	[0.030;0.135]	[0.002;0.010]	[-0.017;0.007]	[-0.005;0.006]	[-0.009;-0.001]	[-0.003;0.023]
	RMS	0.009	0.005	0.008	0.008	0.006	0.017	0.007	0.075	0.004	0.008	0.003	0.006	0.009
	3_l Range	[-0.012;0.001]	[-0.009;0.008]	[0.001;0.032]	[0.003;0.007]	[-0.005;0.012]	[-0.002;0.009]	[-0.001;0.010]	[-0.019;0.029]	[-0.010;0.001]	[-0.001;0.010]	[-0.001;0.003]	[-0.001;0.004]	[-0.003;0.005]
	RMS	0.007	0.005	0.020	0.005	0.003	0.005	0.005	0.013	0.003	0.006	0.002	0.002	0.002
	3_r Range	[-0.002;0.013]	[-0.005;0.004]	[-0.037;0.014]	[-0.015;0.001]	[-0.000;0.014]	[-0.016;0.000]	[-0.008;0.005]	[0.020;0.109]	[0.003;0.007]	[-0.010;0.008]	[-0.004;0.002]	[-0.007;-0.001]	[-0.002;0.009]
	RMS	0.009	0.003	0.015	0.008	0.006	0.012	0.004	0.065	0.005	0.006	0.002	0.004	0.004
Personalised + LoA	1_l Range	[-0.013;0.021]	[-0.035;-0.001]	[-0.031;0.270]	[0.002;0.007]	[-0.007;0.011]	[0.002;0.018]	[0.000;0.014]	[-0.029;0.036]	[-0.013;0.001]	[0.000;0.009]	[-0.002;0.002]	[-0.001;0.003]	[-0.002;0.005]
	RMS	0.011	0.020	0.125	0.003	0.004	0.010	0.007	0.024	0.008	0.006	0.001	0.001	0.002
	1_r Range	[0.004;0.020]	[0.002;0.018]	[-0.083;0.035]	[-0.017;0.003]	[-0.001;0.012]	[-0.012;0.014]	[-0.021;0.003]	[0.005;0.159]	[0.003;0.008]	[-0.011;0.008]	[-0.001;0.003]	[-0.005;-0.002]	[-0.001;0.007]
	RMS	0.011	0.007	0.061	0.009	0.005	0.009	0.010	0.067	0.004	0.008	0.001	0.003	0.002
	2_l Range	[-0.016;0.005]	[-0.030;0.002]	[-0.023;0.070]	[0.000;0.012]	[-0.006;0.010]	[0.001;0.018]	[0.002;0.011]	[-0.021;0.029]	[-0.012;-0.000]	[0.003;0.008]	[-0.001;0.002]	[-0.001;0.003]	[-0.002;0.004]
	RMS	0.007	0.015	0.026	0.004	0.004	0.010	0.008	0.018	0.007	0.006	0.001	0.002	0.003
	2_r Range	[-0.031;0.030]	[-0.773;0.016]	[-0.657;0.075]	[-0.023;0.004]	[-0.000;0.017]	[-0.013;0.009]	[-0.032;0.007]	[-0.016;0.088]	[0.002;0.007]	[-0.034;0.004]	[-0.005;0.006]	[-0.010;-0.003]	[-0.002;0.025]
	RMS	0.018	0.134	0.126	0.014	0.007	0.006	0.008	0.033	0.003	0.013	0.004	0.006	0.013
	3_l Range	[-0.015;0.004]	[-0.037;0.007]	[-0.024;0.056]	[0.003;0.007]	[-0.005;0.012]	[0.001;0.019]	[0.004;0.016]	[-0.025;0.022]	[-0.012;0.001]	[0.003;0.010]	[-0.001;0.003]	[-0.000;0.003]	[-0.003;0.006]
	RMS	0.007	0.018	0.028	0.004	0.004	0.010	0.010	0.019	0.007	0.005	0.002	0.002	0.003
	3_r Range	[0.001;0.024]	[-0.000;0.015]	[-0.077;0.052]	[-0.018;0.002]	[-0.001;0.013]	[-0.012;0.018]	[-0.023;0.001]	[-0.019;0.141]	[0.002;0.006]	[-0.014;0.005]	[-0.004;0.002]	[-0.007;-0.000]	[-0.003;0.008]
	RMS	0.012	0.007	0.053	0.010	0.005	0.008	0.009	0.070	0.004	0.009	0.002	0.004	0.004

Table F.3: Ten-year post-surgery range values for the reserve actuator moments, in Nm, of the joints DoF from CMC, in all models. RMS is also presented. The numbers refer to the trial numbers, while the letters '*l*' and '*r*' specify the lower limb, left and right, respectively, associated with each single support period.

		Reserves												
Models	Trials	Left Hip Flexion	Left Hip Adduction	Left Hip Rotation	Left Knee Angle	Left Ankle Angle	Right Hip Flexion	Right Hip Adduction (Nm)	Right Hip Rotation	Right Knee Angle	Right Ankle Angle	Lumbar Extension	Lumbar Bending	Lumbar Rotation
Generic	1_l Range	[-0.017;0.005]	[0.001;0.016]	[-0.075;0.007]	[0.004;0.010]	[-0.010;0.009]	[-0.001;0.015]	[-0.012;0.008]	[-0.018;0.014]	[-0.013;0.001]	[-0.001;0.028]	[-0.002;0.004]	[-0.002;0.006]	[-0.017;0.016]
	RMS	0.009	0.007	0.016	0.006	0.005	0.009	0.006	0.009	0.007	0.009	0.003	0.003	0.011
	1_r Range	[0.000;0.036]	[-0.024;0.002]	[-0.035;-0.004]	[-0.036;-0.002]	[-0.000;0.017]	[-0.024;0.000]	[-0.025;0.015]	[0.007;0.061]	[-0.002;0.015]	[-0.024;0.009]	[-0.002;0.004]	[-0.003;0.002]	[-0.014;0.014]
	RMS	0.018	0.013	0.018	0.022	0.008	0.015	0.014	0.030	0.008	0.008	0.002	0.002	0.009
	2_l Range	[-0.019;0.003]	[-0.003;0.015]	[-0.042;0.008]	[0.003;0.015]	[-0.009;0.009]	[-0.000;0.013]	[0.001;0.014]	[-0.023;0.013]	[-0.014;0.002]	[-0.001;0.028]	[-0.002;0.004]	[-0.001;0.006]	[-0.023;0.012]
	RMS	0.009	0.007	0.019	0.006	0.004	0.009	0.008	0.010	0.007	0.008	0.003	0.003	0.012
	2_r Range	[-0.001;12.489]	[-1.139;0.008]	[-0.037;0.898]	[-0.033;-0.005]	[-0.000;0.018]	[-0.021;0.001]	[-0.019;0.018]	[0.008;0.042]	[-0.001;0.013]	[-0.006;0.010]	[0.001;0.004]	[-0.003;0.002]	[-0.019;0.009]
	RMS	2.645	0.242	0.192	0.019	0.010	0.011	0.011	0.025	0.006	0.004	0.002	0.002	0.011
	3_l Range	[-0.015;0.008]	[-0.006;0.022]	[-0.080;0.021]	[0.002;0.011]	[-0.006;0.008]	[-0.007;0.016]	[-0.005;0.017]	[-0.039;0.017]	[-0.014;0.002]	[-0.001;0.043]	[-0.000;0.004]	[-0.002;0.008]	[-0.031;0.013]
	RMS	0.008	0.009	0.032	0.004	0.004	0.011	0.008	0.015	0.007	0.011	0.003	0.004	0.014
	3_r Range	[-0.001;0.039]	[-0.024;0.004]	[-0.034;0.008]	[-0.026;-0.002]	[0.000;0.019]	[-0.014;0.001]	[-0.012;0.012]	[0.009;0.042]	[-0.002;0.010]	[-0.014;0.008]	[0.001;0.003]	[-0.004;0.002]	[-0.016;0.013]
	RMS	0.018	0.015	0.020	0.019	0.009	0.010	0.008	0.028	0.005	0.004	0.002	0.002	0.010
Personalised	1_l Range	[-0.015;0.005]	[-0.008;0.021]	[-0.071;0.009]	[0.005;0.012]	[-0.007;0.005]	[-0.000;0.028]	[-0.044;0.019]	[-0.051;0.032]	[-0.021;0.002]	[-0.000;0.016]	[-0.001;0.003]	[-0.001;0.006]	[-0.021;0.013]
	RMS	0.009	0.009	0.016	0.006	0.003	0.018	0.015	0.021	0.013	0.008	0.003	0.003	0.011
	1_r Range	[-0.003;0.025]	[-0.033;0.005]	[-0.037;0.016]	[-0.024;0.001]	[-0.001;0.008]	[-0.035;0.009]	[-0.087;0.025]	[-0.009;0.158]	[-0.001;0.014]	[-0.017;0.008]	[-0.003;0.004]	[-0.004;0.002]	[-0.014;0.014]
	RMS	0.012	0.012	0.019	0.011	0.004	0.014	0.021	0.060	0.007	0.006	0.002	0.002	0.009
	2_l Range	[-0.019;0.002]	[-0.019;0.016]	[-0.088;0.009]	[0.003;0.015]	[-0.010;0.006]	[0.001;13.991]	[-0.035;16.584]	[-5.591;9.603]	[-0.021;0.003]	[-0.001;0.019]	[-0.003;0.004]	[-0.001;0.007]	[-0.027;0.013]
	RMS	0.009	0.010	0.020	0.006	0.004	2.459	3.595	2.280	0.013	0.007	0.003	0.004	0.013
	2_r Range	[-0.005;0.034]	[-0.001;0.005]	[-0.049;0.016]	[-0.020;0.002]	[-0.001;0.010]	[-0.019;0.004]	[-0.040;0.022]	[0.002;0.053]	[-0.002;0.013]	[-0.007;0.008]	[0.001;0.004]	[-0.003;0.002]	[-0.018;0.009]
	RMS	0.017	0.003	0.024	0.010	0.005	0.010	0.018	0.027	0.005	0.003	0.003	0.002	0.012
	3_l Range	[-0.014;0.002]	[-0.016;0.016]	[-0.042;0.022]	[0.002;0.011]	[-0.006;0.005]	[-0.005;0.033]	[-0.036;0.025]	[-0.052;0.051]	[-0.022;0.002]	[-0.000;0.013]	[-0.001;0.004]	[-0.002;0.008]	[-0.030;0.013]
	RMS	0.007	0.010	0.015	0.004	0.003	0.020	0.016	0.029	0.013	0.007	0.003	0.004	0.017
	3_r Range	[-0.003;0.025]	[-0.026;0.008]	[-0.038;0.018]	[-0.015;0.003]	[-0.001;0.011]	[-0.015;0.004]	[-0.031;0.015]	[0.006;0.053]	[-0.003;0.010]	[-0.011;0.008]	[0.000;0.003]	[-0.005;0.002]	[-0.017;0.012]
	RMS	0.013	0.010	0.020	0.010	0.004	0.009	0.013	0.029	0.005	0.004	0.002	0.002	0.011
Personalised - LoA	1_l Range	[-0.017;0.003]	[-0.002;0.014]	[-0.074;0.015]	[0.004;0.010]	[-0.009;0.007]	[-0.001;0.016]	[-0.011;0.013]	[-0.019;0.022]	[-0.015;0.001]	[-0.001;0.122]	[-0.003;0.004]	[-0.002;0.005]	[-0.015;0.016]
	RMS	0.009	0.007	0.020	0.006	0.004	0.010	0.008	0.013	0.007	0.019	0.003	0.002	0.010
	1_r Range	[-0.002;0.021]	[-0.016;0.004]	[-0.032;0.003]	[-0.020;0.001]	[-0.000;0.011]	[-0.025;0.006]	[-0.030;0.024]	[0.009;0.065]	[0.000;0.016]	[-0.017;0.009]	[-0.003;0.004]	[-0.003;0.002]	[-0.013;0.012]
	RMS	0.011	0.006	0.015	0.012	0.005	0.015	0.015	0.031	0.008	0.007	0.002	0.002	0.008
	2_l Range	[-0.020;0.001]	[-0.002;0.014]	[-0.019;0.011]	[0.003;0.014]	[-0.006;0.007]	-0.001;0.016]	[-0.009;0.013]	[-0.031;0.024]	[-0.014;0.001]	[-0.001;1.052]	[-0.004;0.004]	[-0.002;0.007]	[-0.021;0.017]
	RMS	0.009	0.007	0.009	0.006	0.003	0.010	0.009	0.016	0.007	0.168	0.003	0.003	0.012
	2_r Range	[-0.003;0.026]	[-0.013;0.004]	[-0.051;0.003]	[-0.018;0.000]	[-0.001;0.013]	[-0.021;0.002]	[-0.020;0.019]	[0.015;0.042]	[-0.001;0.013]	[-0.007;0.009]	[0.001;0.003]	[-0.003;0.001]	[-0.015;0.009]
	RMS	0.013	0.006	0.024	0.011	0.007	0.011	0.011	0.027	0.005	0.003	0.002	0.002	0.009
	3_l Range	[-0.016;0.003]	[-0.005;0.016]	[-0.042;0.027]	[0.003;0.011]	[-0.005;0.006]	[-0.007;0.020]	[-0.010;0.018]	[-0.046;0.027]	[-0.019;0.002]	[-0.001;0.023]	[-0.000;0.004]	[-0.001;0.009]	[-0.028;0.011]
	RMS	0.008	0.008	0.021	0.005	0.003	0.012	0.010	0.021	0.008	0.008	0.003	0.004	0.014
	3_r Range	[-0.001;0.024]	[-0.009;0.005]	[-0.052;0.006]	[-0.015;0.001]	[-0.001;0.011]	[-0.014;0.002]	[-0.012;0.014]	[0.013;0.046]	[-0.001;0.011]	[-0.012;0.008]	[0.000;0.003]	[-0.004;0.002]	[-0.018;0.012]
	RMS	0.012	0.005	0.025	0.009	0.005	0.010	0.008	0.031	0.005	0.004	0.002	0.002	0.010
Personalised + LoA	1_l Range	[-0.021;0.004]	[-0.036;0.025]	[-0.093;-0.014]	[0.005;0.014]	[-0.007;0.006]	[-0.000;0.023]	[-0.060;0.015]	[-0.063;0.039]	[-0.020;0.001]	[-0.000;0.012]	[-0.001;0.003]	[-0.001;0.006]	[-0.018;0.012]
	RMS	0.012	0.020	0.048	0.007	0.003	0.013	0.013	0.041	0.010	0.006	0.003	0.003	0.012
	1_r Range	[-0.012;0.027]	[-0.105;0.007]	[-0.191;0.047]	[-0.020;0.005]	[-0.001;0.010]	[-0.056;0.018]	[-0.193;0.021]	[-0.008;0.237]	[-0.005;0.013]	[-4.725;0.007]	[-0.003;0.004]	[-0.004;0.002]	[-0.013;0.015]
	RMS	0.014	0.023	0.098	0.011	0.004	0.024	0.062	0.099	0.007	0.480	0.002	0.002	0.009
	2_l Range	[-0.035;0.002]	[-0.065;0.024]	[-0.182;-0.014]	[0.002;0.018]	[-0.009;0.006]	[-0.004;0.928]	[-1.041;0.015]	[-0.725;0.058]	[-0.019;0.002]	[-0.001;0.016]	[-0.001;0.004]	[-0.001;0.006]	[-0.026;0.015]
	RMS	0.013	0.023	0.050	0.007	0.004	0.175	0.196	0.143	0.008	0.006	0.003	0.003	0.012
	2_r Range	[-0.010;5.639]	[-2.350;0.004]	[-3.153;0.064]	[-0.025;0.005]	[-0.002;0.008]	[-0.023;0.005]	[-0.074;0.020]	[-0.042;0.084]	[-0.003;0.013]	[-0.008;0.007]	[0.001;0.004]	[-0.003;0.002]	[-0.018;0.010]
	RMS	1.254	0.523	0.706	0.012	0.004	0.013	0.036	0.036	0.006	0.004	0.002	0.002	0.011
	3_l Range	[-0.019;0.001]	[-0.058;0.014]	[-0.081;0.026]	[0.001;0.013]	[-0.006;0.004]	[-0.009;0.029]	[-0.034;0.026]	[-0.068;0.085]	[-0.014;0.001]	[-0.001;0.011]	[-0.001;0.004]	[-0.001;0.007]	[-0.022;0.013]
	RMS	0.012	0.033	0.039	0.005	0.003	0.016	0.015	0.058	0.009	0.006	0.003	0.003	0.012
	3_r Range	[-0.008;0.036]	[-0.058;0.009]	[-0.111;0.061]	[-0.014;0.006]	[-0.001;0.009]	[-0.020;0.004]	[-0.064;0.014]	[-0.002;0.076]	[-0.003;0.010]	[-0.022;0.007]	[-0.000;0.004]	[-0.005;0.002]	[-0.018;0.012
	RMS	0.018	0.017	0.071	0.009	0.004	0.011	0.030	0.037	0.005	0.006	0.002	0.002	0.011

F.2 Generic vs. Personalised Muscle Force Patterns

F.2.1 Pre-Surgery: Generic vs. Personalised

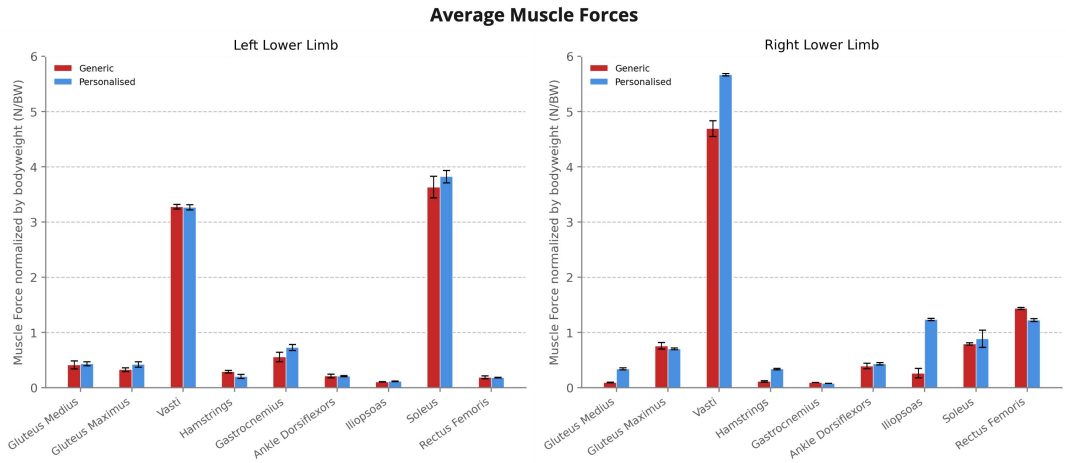

Figure F.1: Pre-surgery average muscle forces for generic and torsion personalised models, categorised by muscle group (see Table A.2). The data presented is the same as in Figure 5.2. Error bars are ±1 standard error.

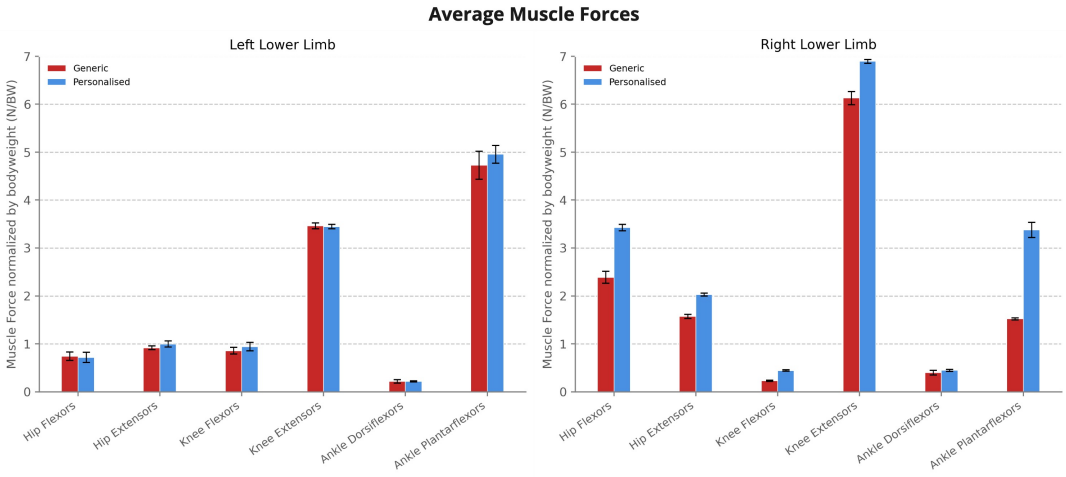

Figure F.2: Pre-surgery average muscle forces for generic and torsion personalised models, grouped by muscle function (see Table A.3). The data presented is the same as in Figure 5.2. Error bars are ±1 standard error.

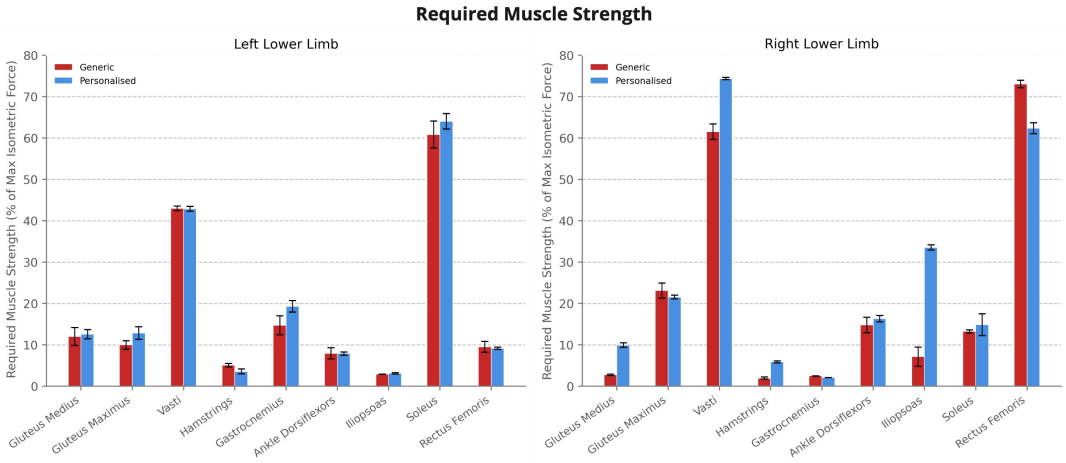

Figure F.3: Pre-surgery required muscle strength, expressed as a percentage of the maximum isometric force, for the generic and torsion personalised models. The data presented is the same as in Figure 5.2. Error bars are ±1 standard error.

F.2.2 Post-Surgery: Generic vs. Personalised

F.2.2.1 One-Year Post-Surgery: Generic vs. Personalised

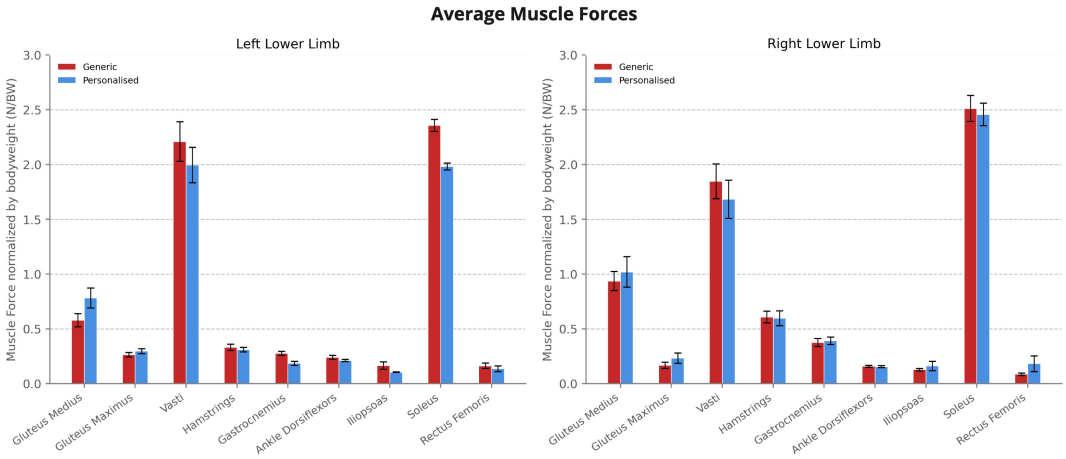

Figure F.4: One-year post-surgery average muscle forces for generic and torsion personalised models, categorised by muscle group (see Table A.2). The data presented is the same as in Figure 5.3. Error bars are ±1 standard error.

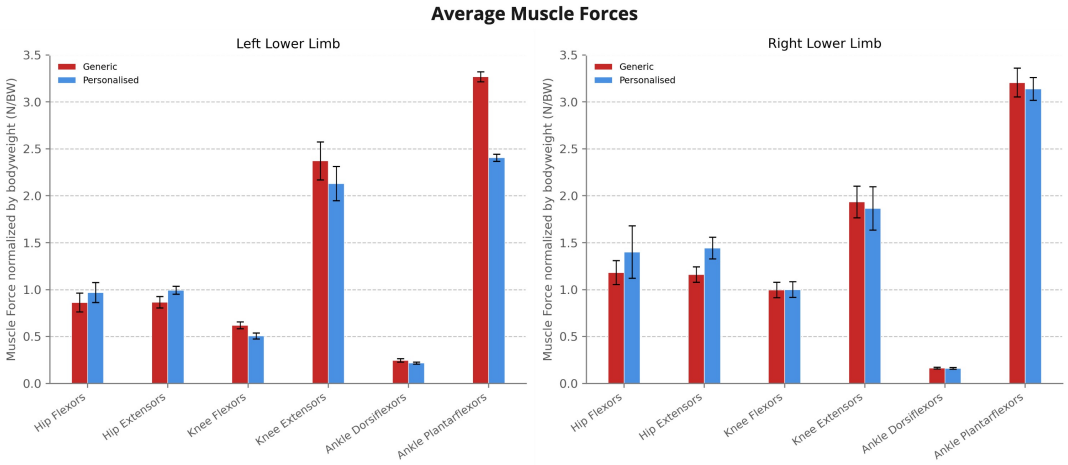

Figure F.5: One-year post-surgery average muscle forces for generic and torsion personalised models, grouped by muscle function (see Table A.3). The data presented is the same as in Figure 5.3. Error bars are ±1 standard error.

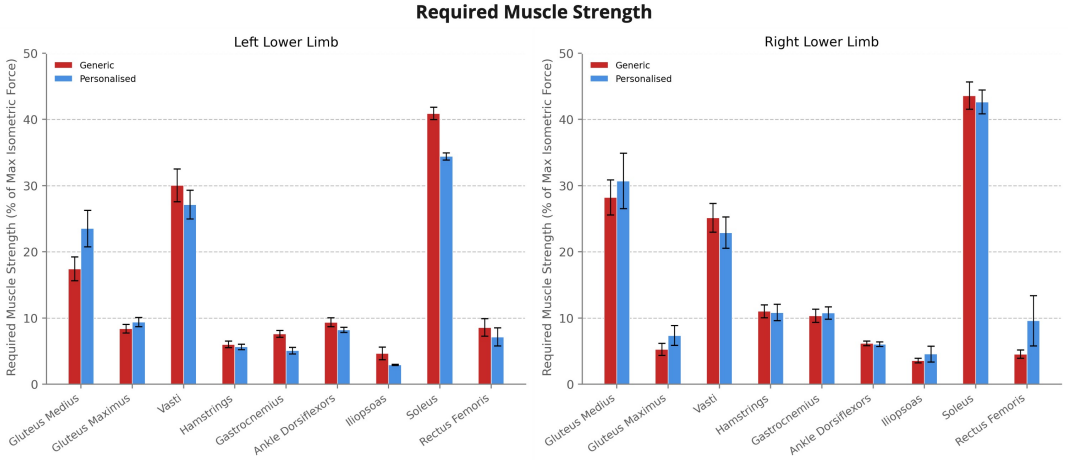

Figure F.6: One-year post-surgery required muscle strength, expressed as a percentage of the maximum isometric force, for the generic and torsion personalised models. The data presented is the same as in Figure 5.3. Error bars are ±1 standard error.

F.2.2.2 Ten-Year Post-Surgery: Generic vs. Personalised

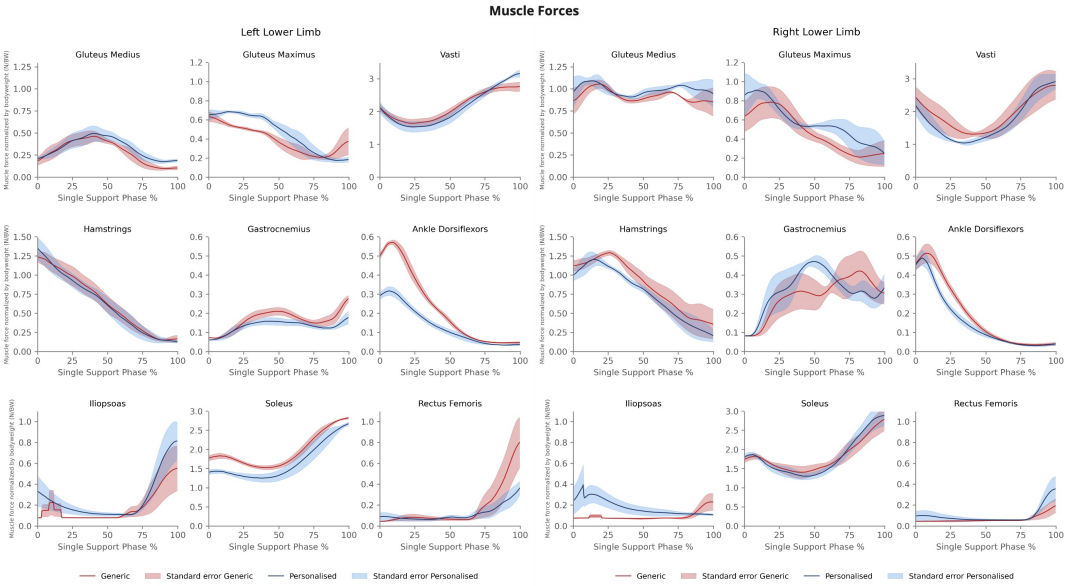

Figure F.7: Ten-year post-surgery muscle forces during the single support phase of walking in a child with CP who underwent SEMLS. Data are presented as mean (lines) and standard errors (shaded) for generic (red) and torsion personalised (blue) models. Muscle forces are normalised to the child's BW.

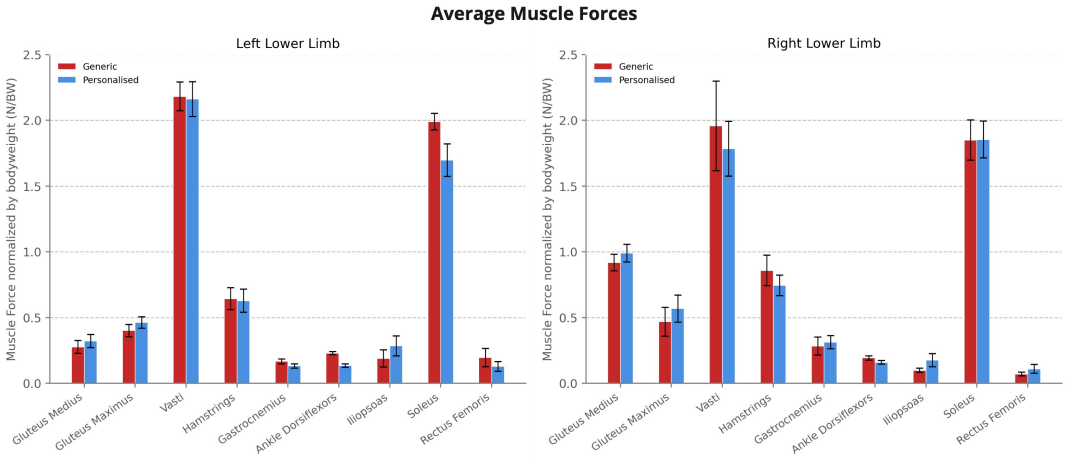

Figure F.8: Ten-year post-surgery average muscle forces for generic and torsion personalised models, categorised by muscle group (see Table A.2). The data presented is the same as in Figure F.7. Error bars are ±1 standard error.

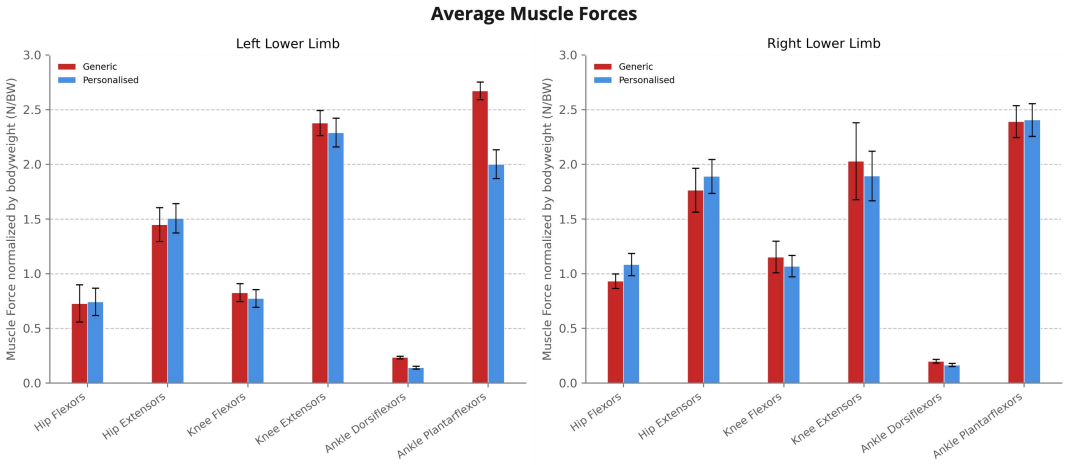

Figure F.9: Ten-year post-surgery average muscle forces for generic and torsion personalised models, grouped by muscle function (see Table A.3). The data presented is the same as in Figure F.7. Error bars are ±1 standard error.

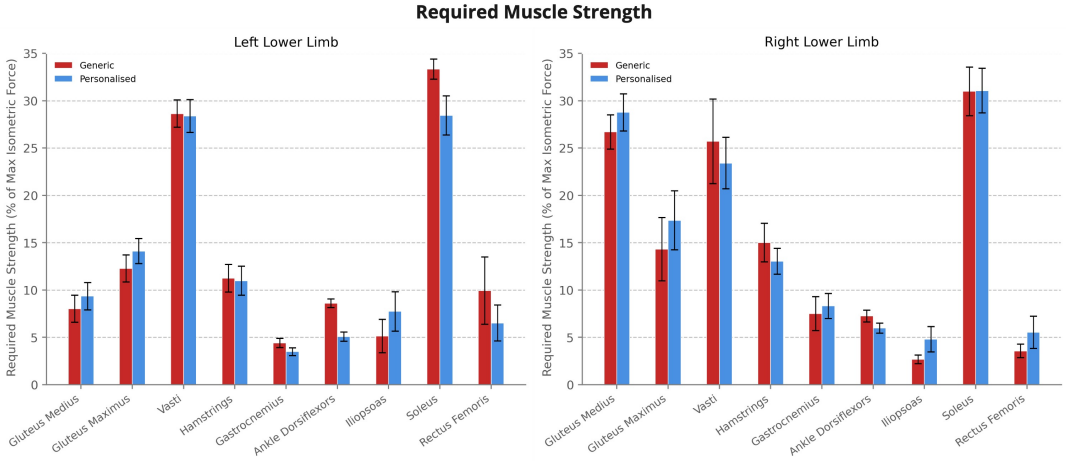

Figure F.10: Ten-year post-surgery required muscle strength, expressed as a percentage of the maximum isometric force, for the generic and torsion personalised models. The data presented is the same as in Figure F.7. Error bars are ±1 standard error.

F.3 Pre vs. Post-Surgery: Muscle Force Patterns

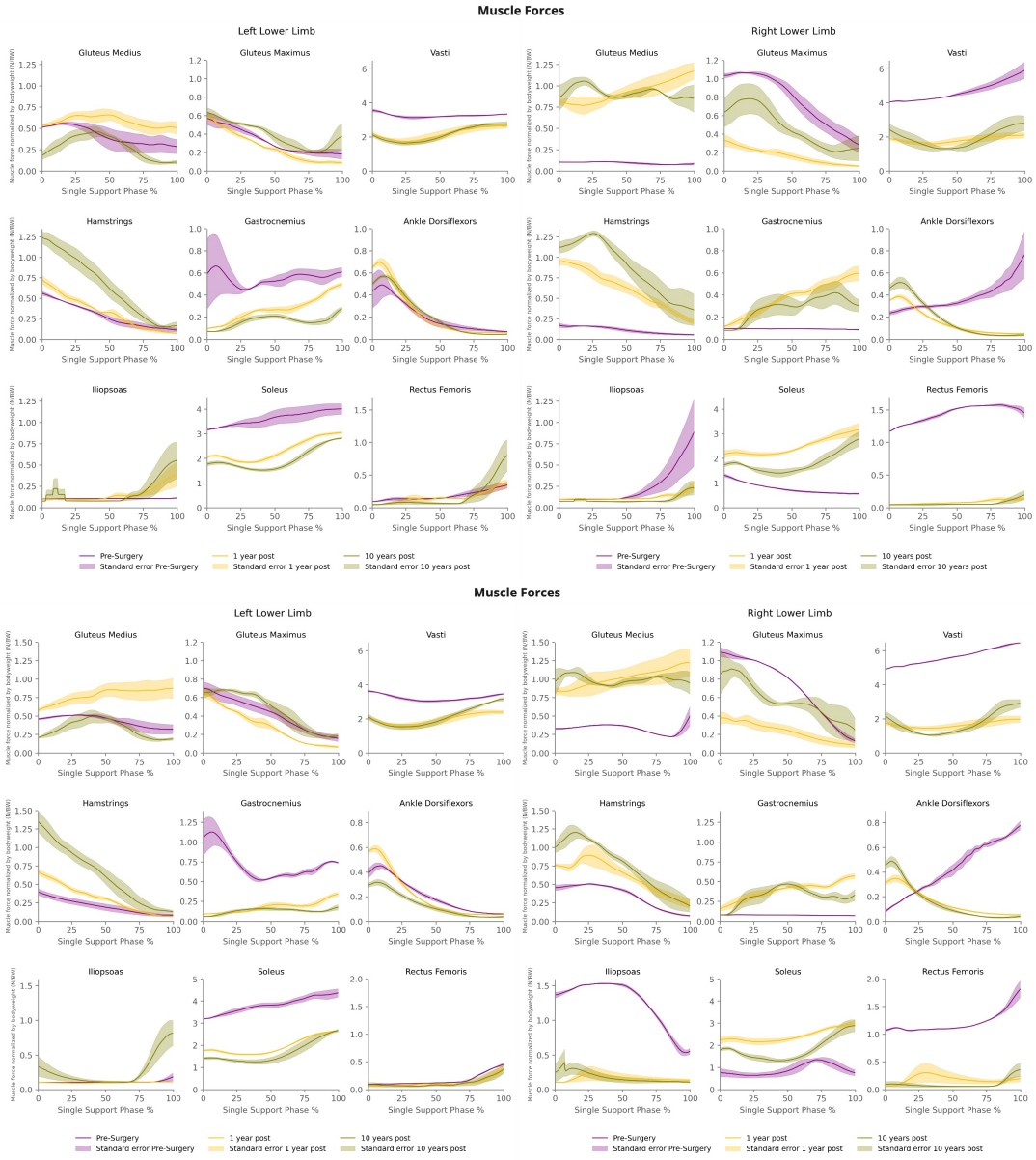

Figure F.11: Pre- vs. post-surgery muscle forces during the single support phase of walking in a child with CP who underwent SEMLS. Data are presented as mean (lines) and standard errors (shaded) for generic (top), and torsion personalised (bottom) models. Muscle forces are normalised to the child's BW.

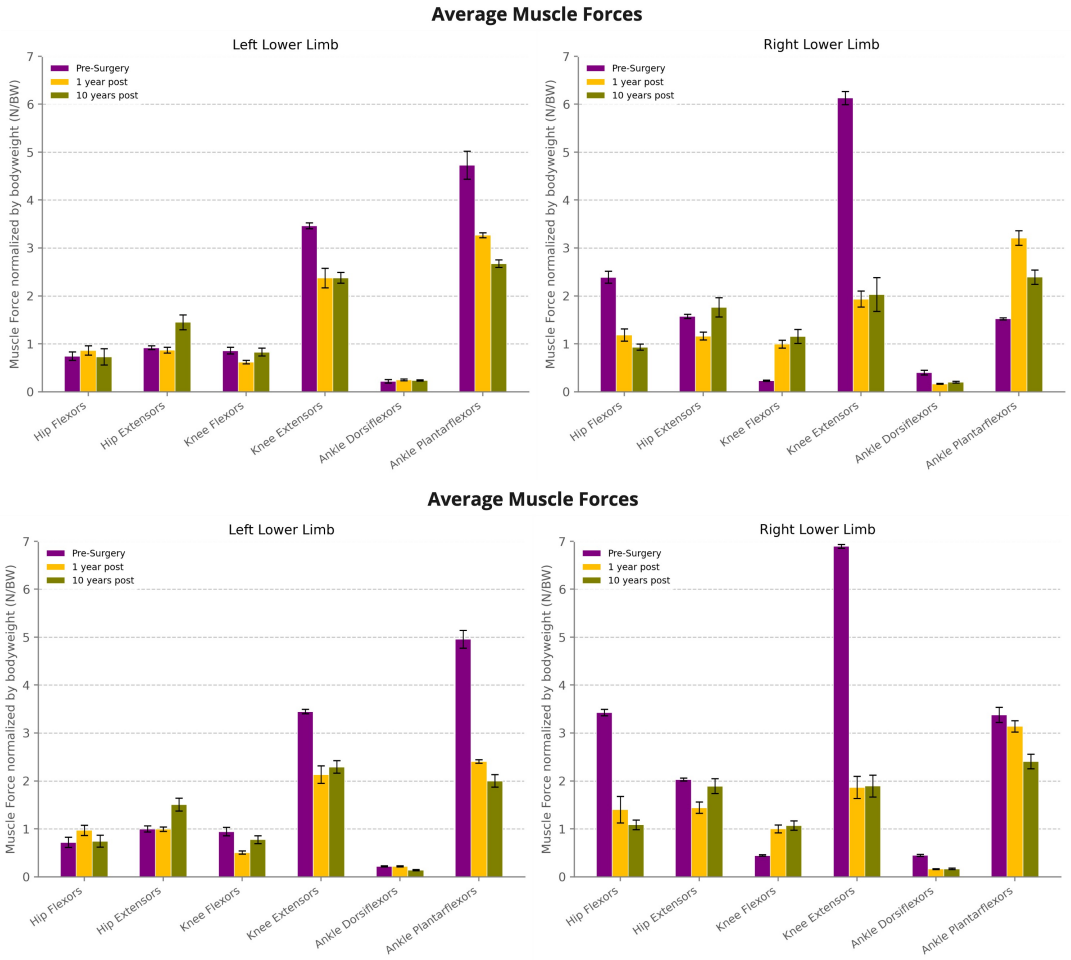

Figure F.12: Pre- vs. post-surgery average muscle forces for generic (top), and torsion personalised (bottom) models, grouped by muscle function (see Table A.3). Muscle forces are normalised to the child's BW. Error bars represent ±1 standard error.

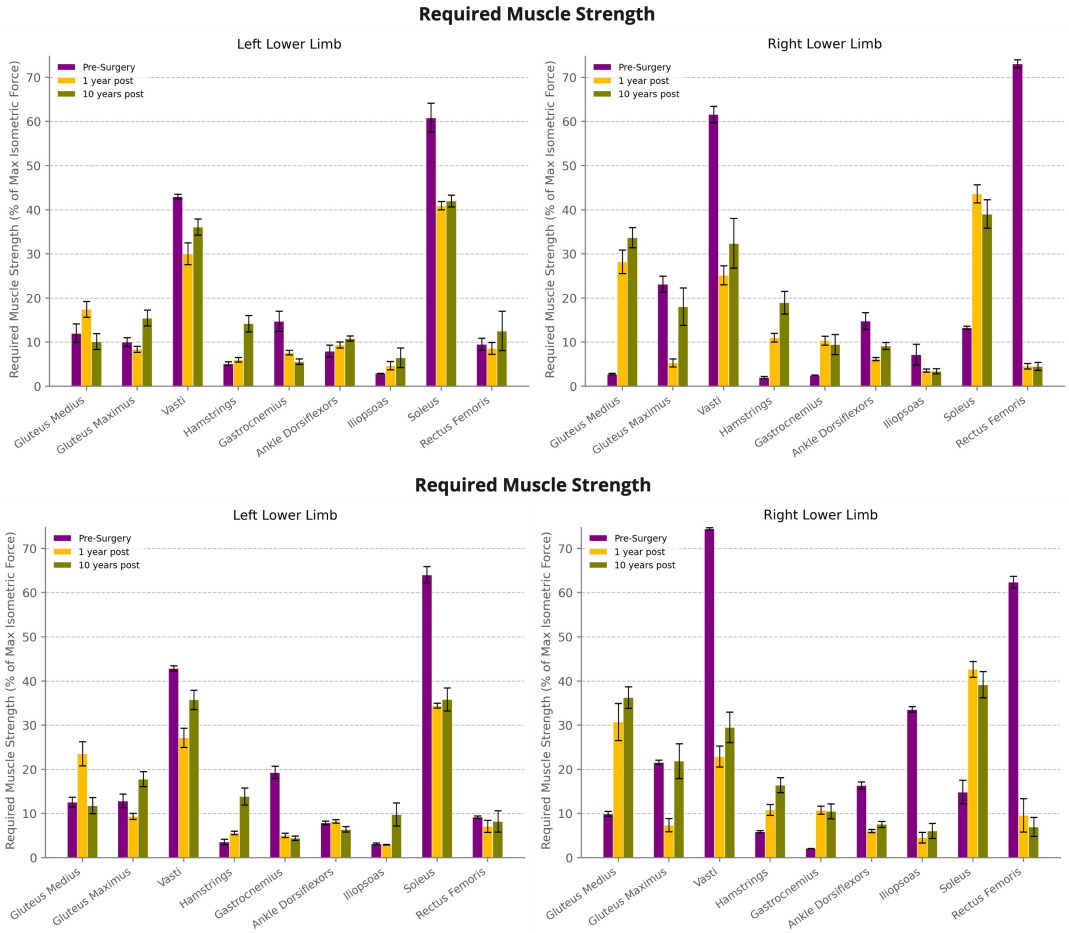

Figure F.13: Pre- vs. post-surgery required muscle strength, expressed as a percentage of the maximum isometric force, for generic (top), and torsion personalised (bottom) models. Error bars are ±1 standard error.

F.4 Impact of Measurement Variability

F.4.1 Pre-Surgery Muscle Force Variability

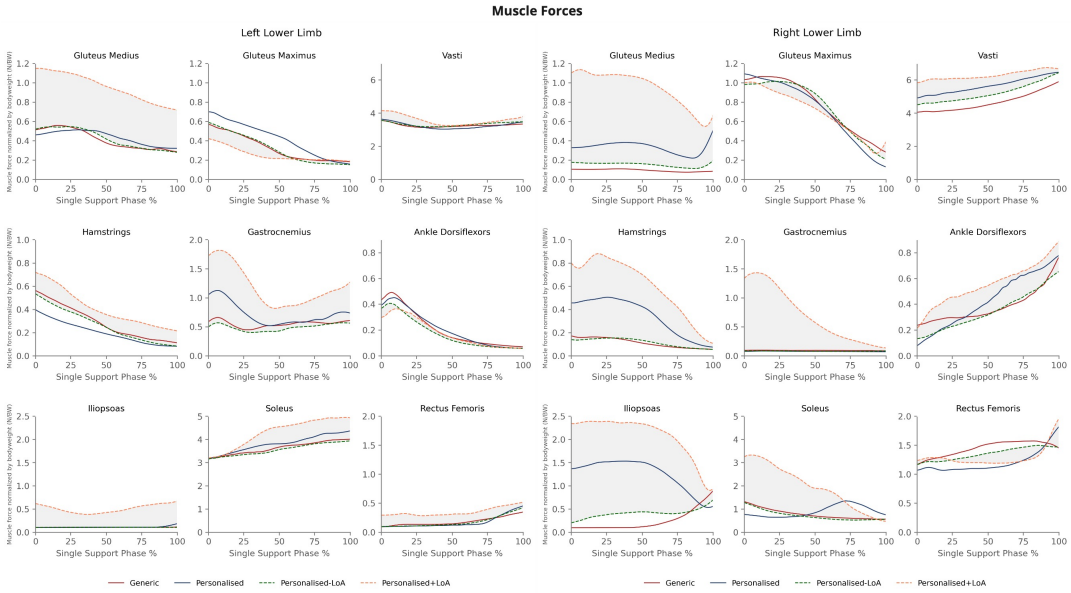

Figure F.14: Pre-surgery muscle forces during the single support phase of walking in a child with CP scheduled for SEMLS. Data are presented as mean (lines) and the interval between the LoA models (shaded) for generic (red), torsion personalised (blue), and LoA models (dashed). Muscle forces are normalised to the child's BW.

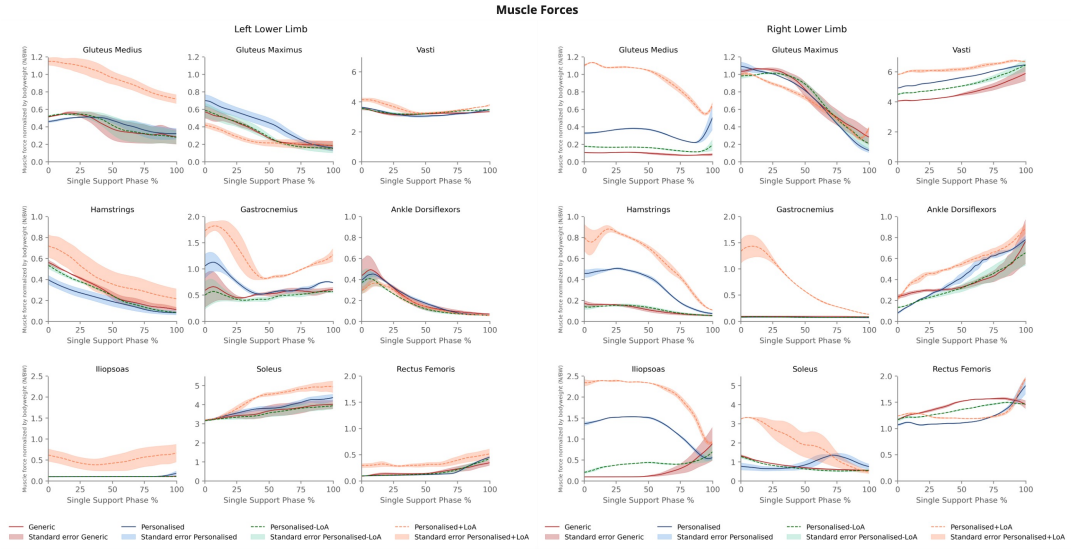

Figure F.15: Pre-surgery muscle forces during the single support phase of walking in a child with CP scheduled for SEMLS. Data are presented as mean (lines) and standard errors (shaded) for generic (red), torsion personalised (blue), and LoA models (dashed). Muscle forces are normalised to the child's BW.

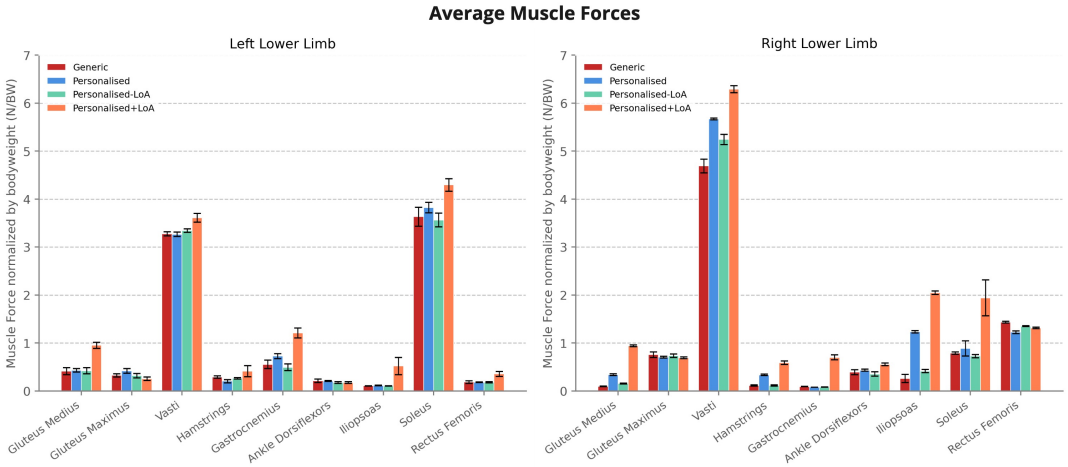

Figure F.16: Pre-surgery average muscle forces for all models, categorised by muscle group (see Table A.2). Muscle forces are normalised to the child's BW. Error bars are ±1 standard error.

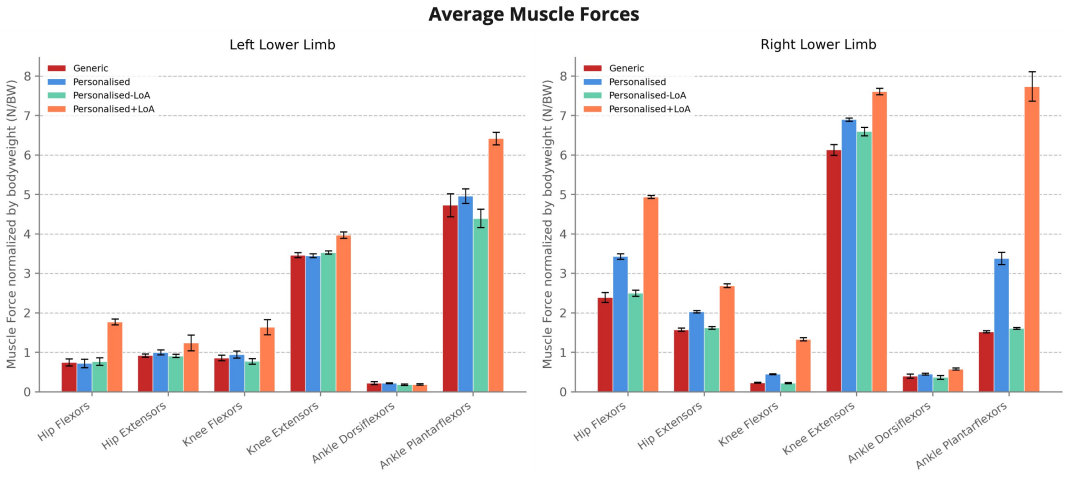

Figure F.17: Pre-surgery average muscle forces for all models, grouped by muscle function (see Table A.3). Muscle forces are normalised to the child's BW. Error bars are ±1 standard error.

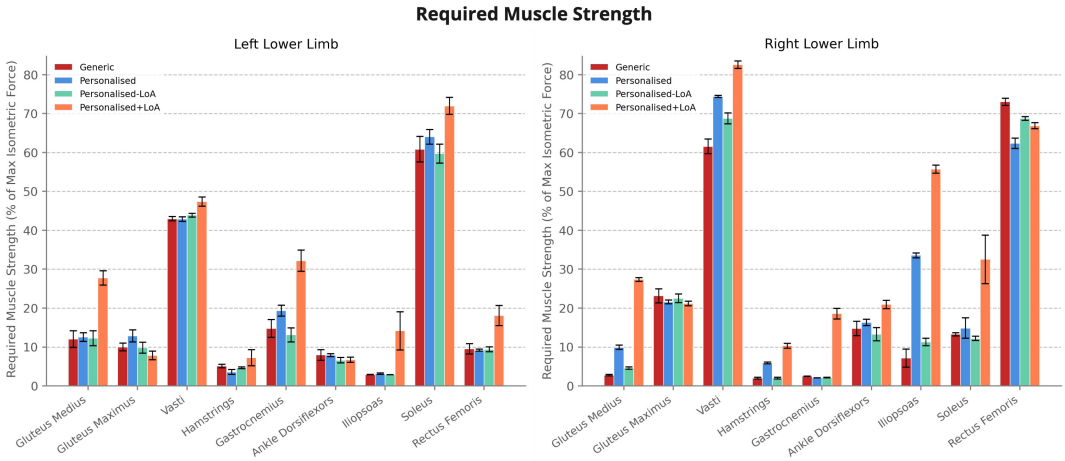

Figure F.18: Pre-surgery required muscle strength, expressed as a percentage of the maximum isometric force, for all models. Error bars are ±1 standard error.

F.4.2 Post-Surgery Muscle Force Variability

F.4.2.1 One-Year Post-Surgery Muscle Force Variability

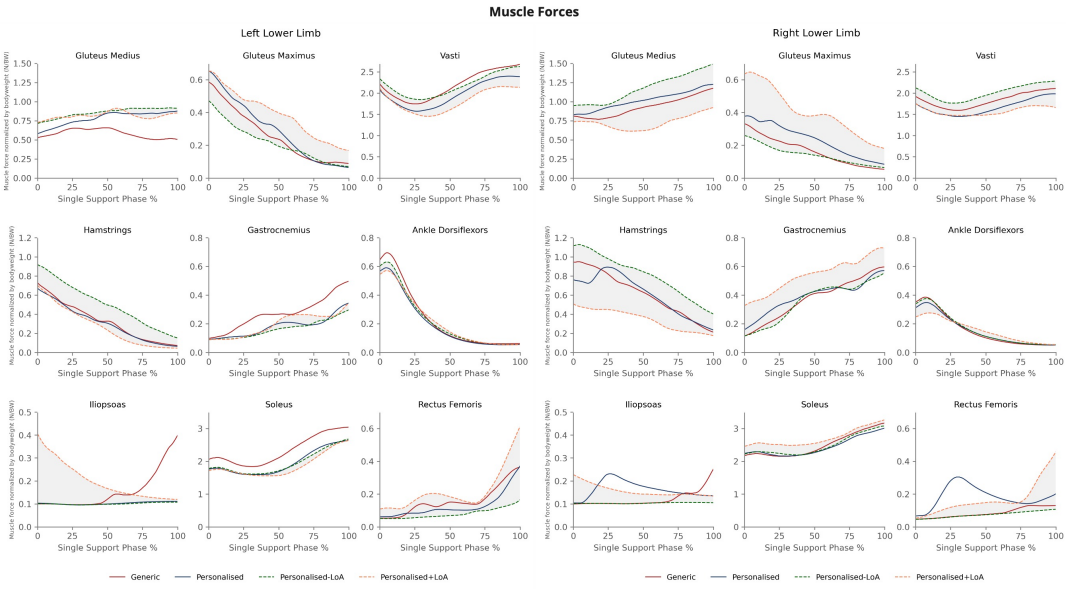

Figure F.19: One-year post-surgery muscle forces during the single support phase of walking in a child with CP who underwent SEMLS. Data are presented as mean (lines) and the interval between the LoA models (shaded) for generic (red), torsion personalised (blue), and LoA models (dashed). Muscle forces are normalised to the child's BW.

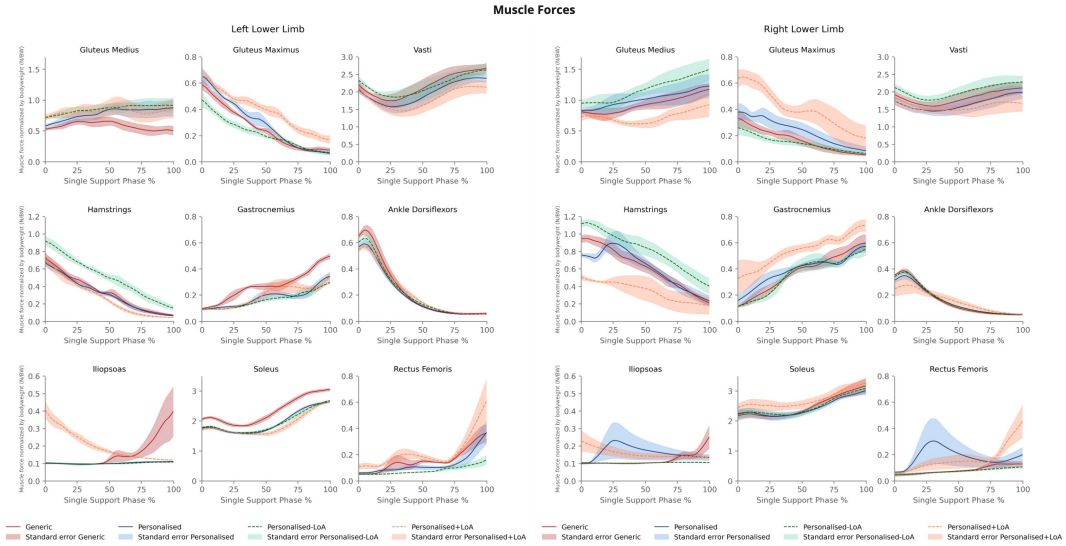

Figure F.20: One-year post-surgery muscle forces during the single support phase of walking in a child with CP who underwent SEMLS. Data are presented as mean (lines) and standard errors (shaded) for generic (red), torsion personalised (blue), and LoA models (dashed). Muscle forces are normalised to the child's BW.

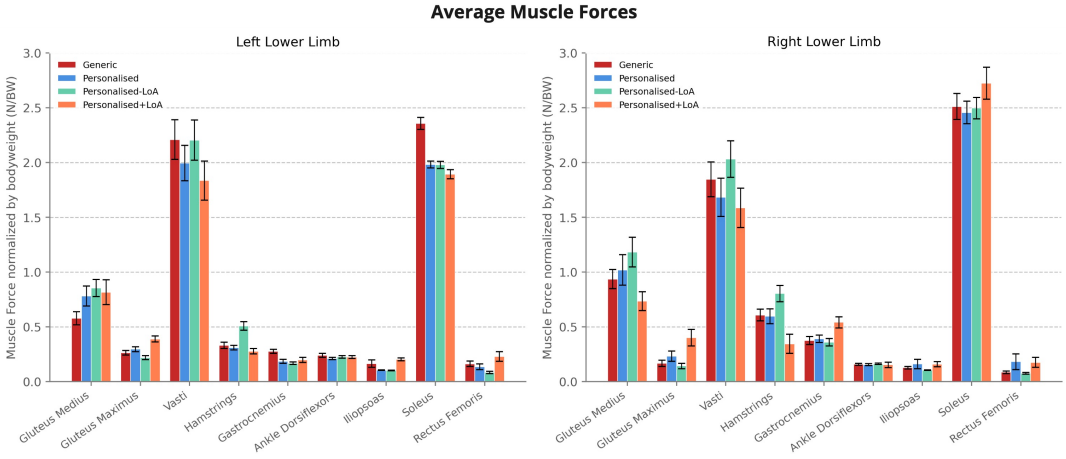

Figure F.21: One-year post-surgery average muscle forces for all models, categorised by muscle group (see Table A.2). Muscle forces are normalised to the child's BW. Error bars are ±1 standard error.

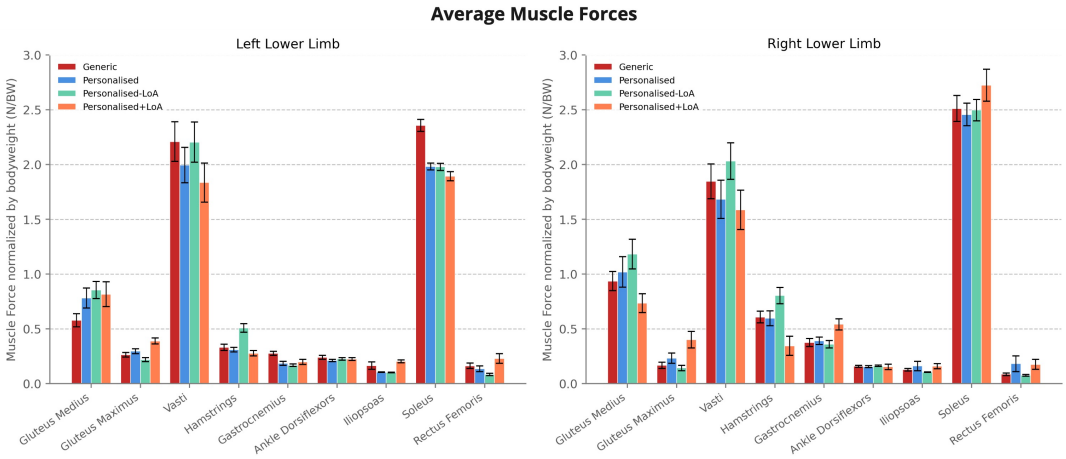

Figure F.22: One-year post-surgery average muscle forces for all models, grouped by muscle function (see Table A.3). Error bars are ±1 standard error.

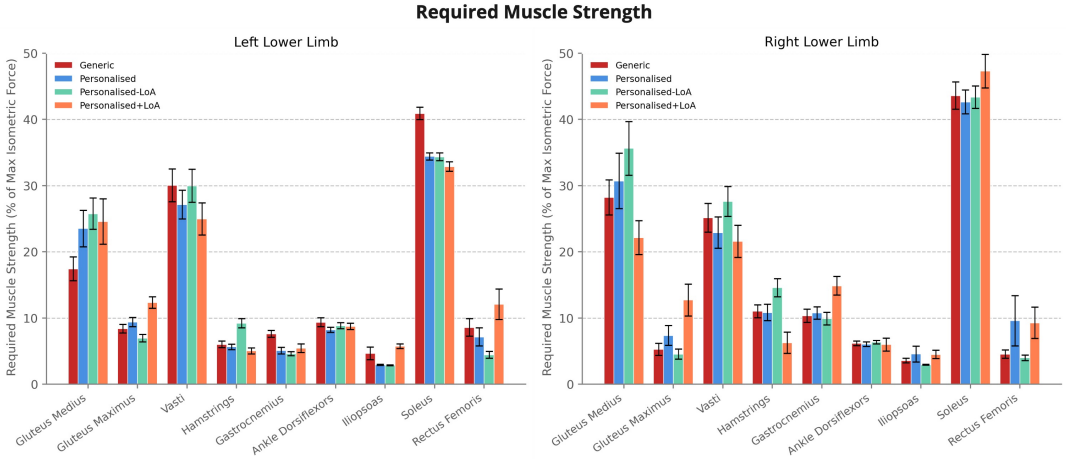

Figure F.23: One-year post-surgery required muscle strength, expressed as a percentage of the maximum isometric force, for all models. Error bars are ±1 standard error.

F.4.2.2 Ten-Year Post-Surgery Muscle Force Variability

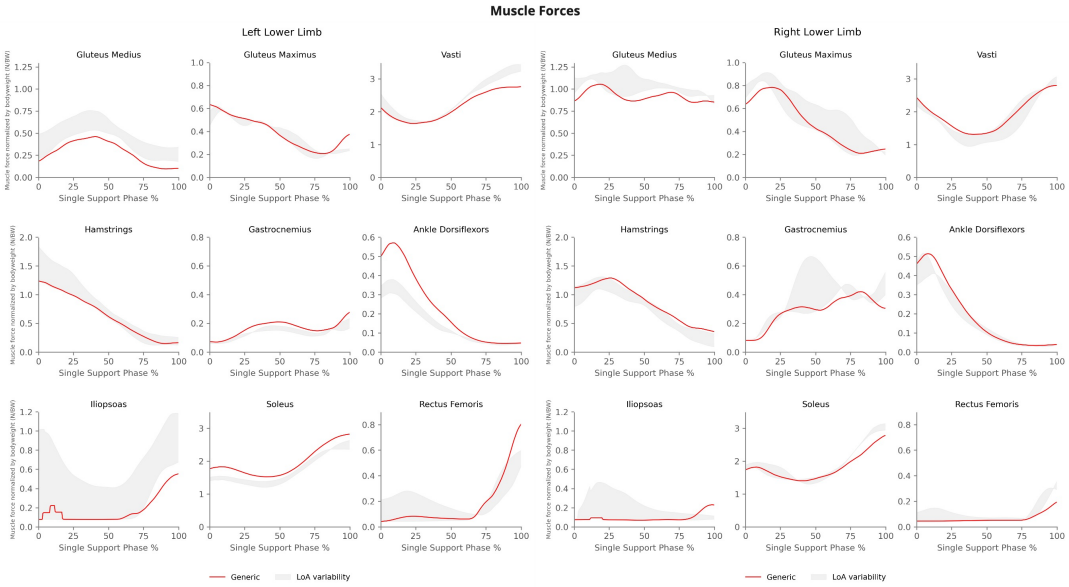

Figure F.24: Ten-year post-surgery muscle forces during the single support phase of walking in a child with CP who underwent SEMLS. Data are presented as mean (lines) for the generic model (red) and the shaded region represents the variability interval between the two LoA models. Muscle forces are normalised to the child's BW.

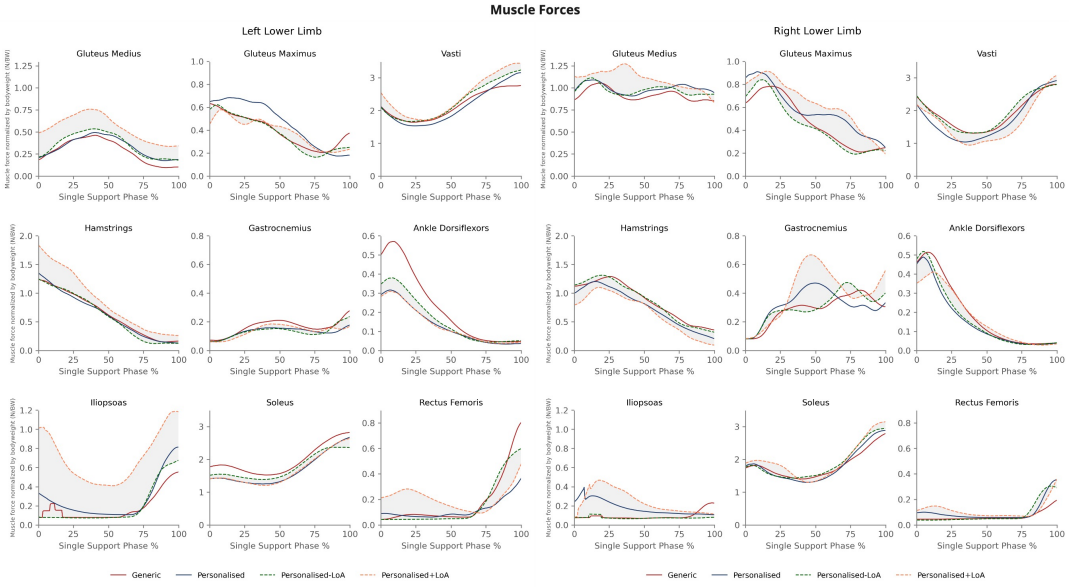

Figure F.25: Ten-year post-surgery muscle forces during the single support phase of walking in a child with CP who underwent SEMLS. Data are presented as mean (lines) and the interval between the LoA models (shaded) for generic (red), torsion personalised (blue), and LoA models (dashed). Muscle forces are normalised to the child's BW.

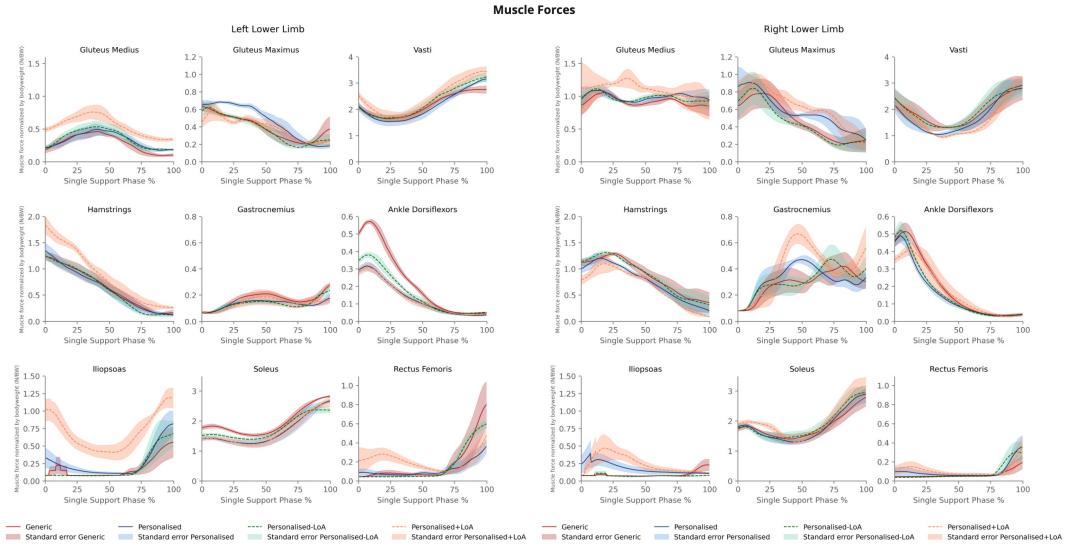

Figure F.26: Ten-year post-surgery muscle forces during the single support phase of walking in a child with CP who underwent SEMLS. Data are presented as mean (lines) and standard errors (shaded) for generic (red), torsion personalised (blue), and LoA models (dashed). Muscle forces are normalised to the child's BW.

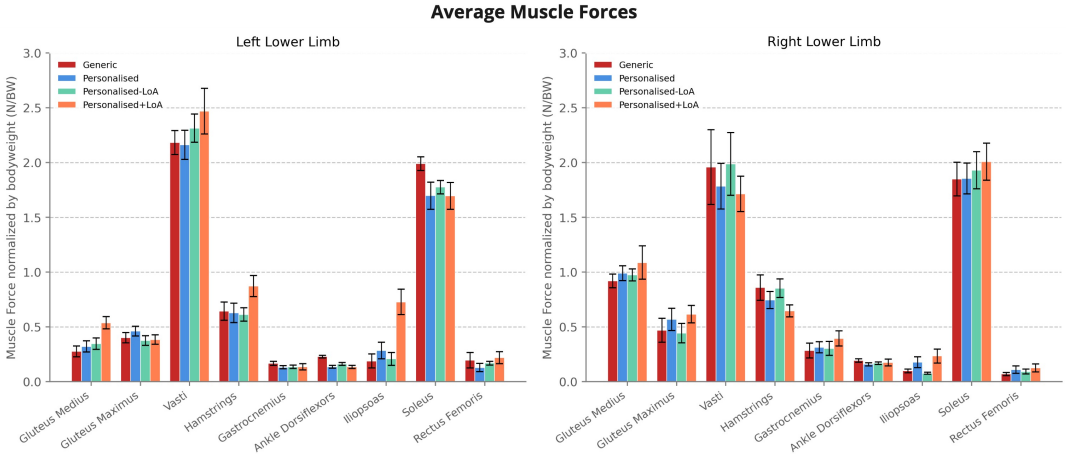

Figure F.27: Ten-year post-surgery average muscle forces for all models, categorised by muscle group (see Table A.2). Muscle forces are normalised to the child's BW. Error bars are ±1 standard error.

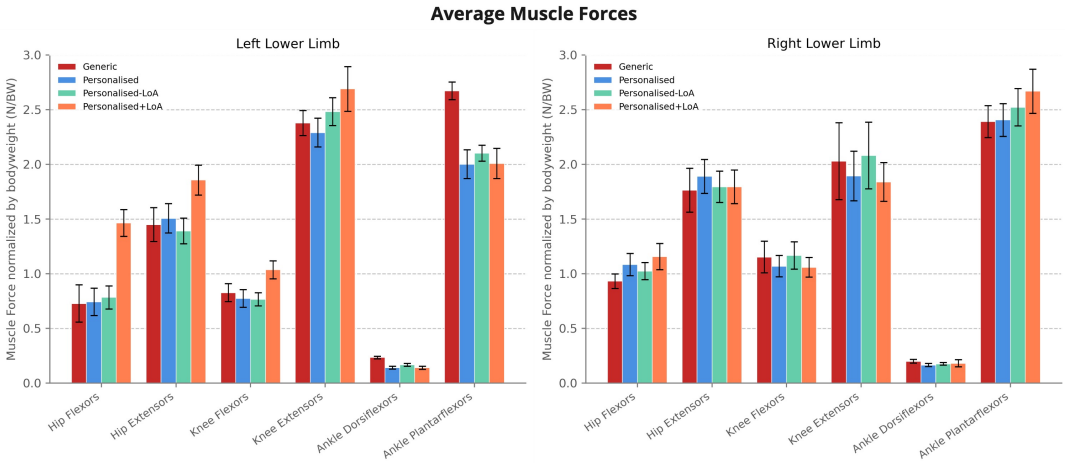

Figure F.28: Ten-year post-surgery average muscle forces for all models, grouped by muscle function (see Table A.3). Muscle forces are normalised to the child's BW. Error bars are ±1 standard error.

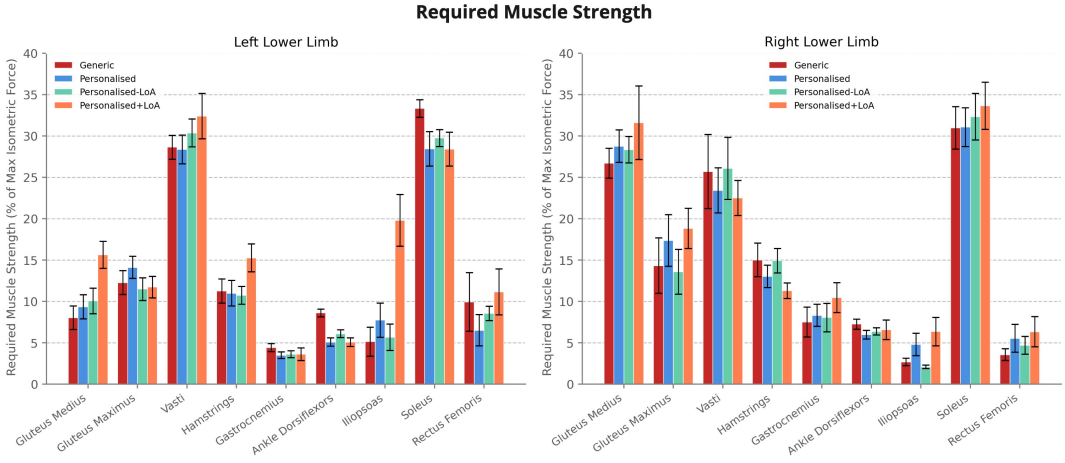

Figure F.29: Ten-year post-surgery required muscle strength, expressed as a percentage of the maximum isometric force, for all models. Error bars are ±1 standard error.

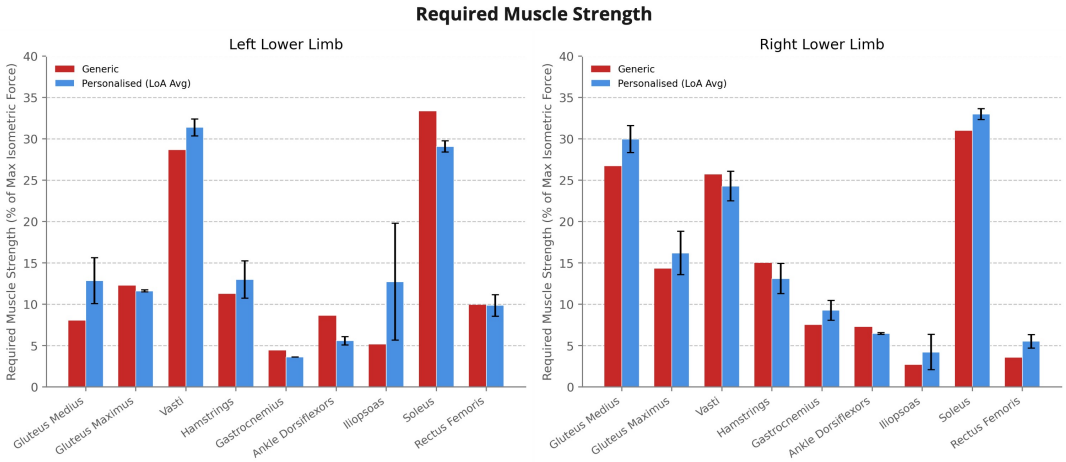

Figure F.30: Ten-year post-surgery comparison of required muscle strength as a percentage of maximum isometric force between generic and personalised models (average of 'Personalised-LoA' and 'Personalised+LoA'). Error bars represent the variability across both LoA models.

F.5 Muscle Activation

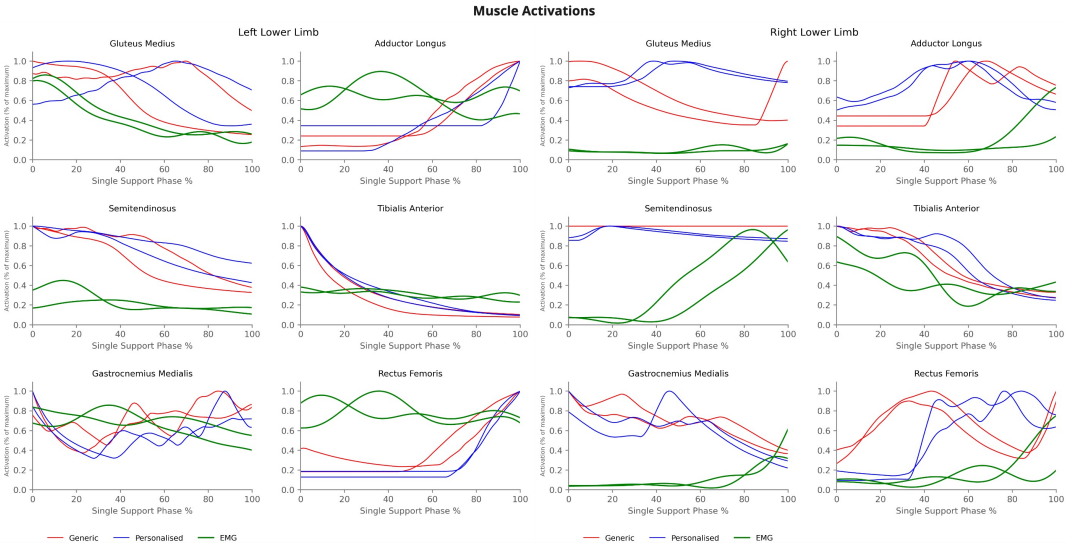

Figure F.31: Comparison between CMC activation results for the generic and personalised models with the EMG activation data pre-surgery. The EMG data was acquired in the CGA, processed as detailed in 4.3.2, and normalised to the maximum value in each trial. In the CMC results, each trial's data are normalised by its own maximum value. Each curve represents one trial.

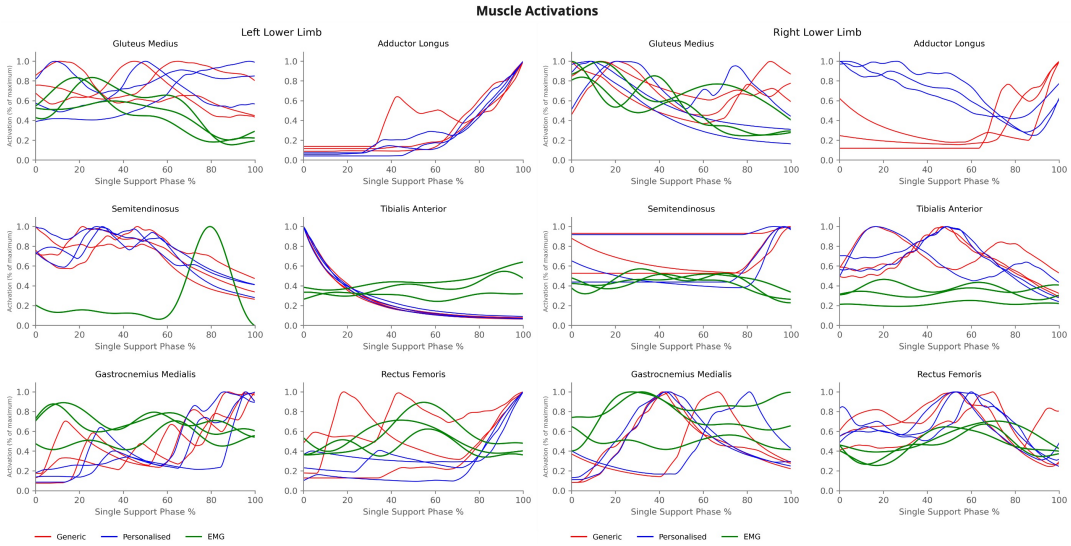

Figure F.32: Comparison between CMC activation results for the generic and personalised models with the EMG activation data one-year post-surgery. The EMG data was acquired in the CGA, processed as detailed in 4.3.2, and normalised to the maximum value in each trial. In the CMC results, each trial's data are normalised by its own maximum value. Each curve represents one trial. The adductor longus EMG data was excluded due to poor quality, as was the semitendinosus left, where only one trial had good EMG data.

G

Muscle Contributions

G.1 Induced Acceleration Analysis Validation

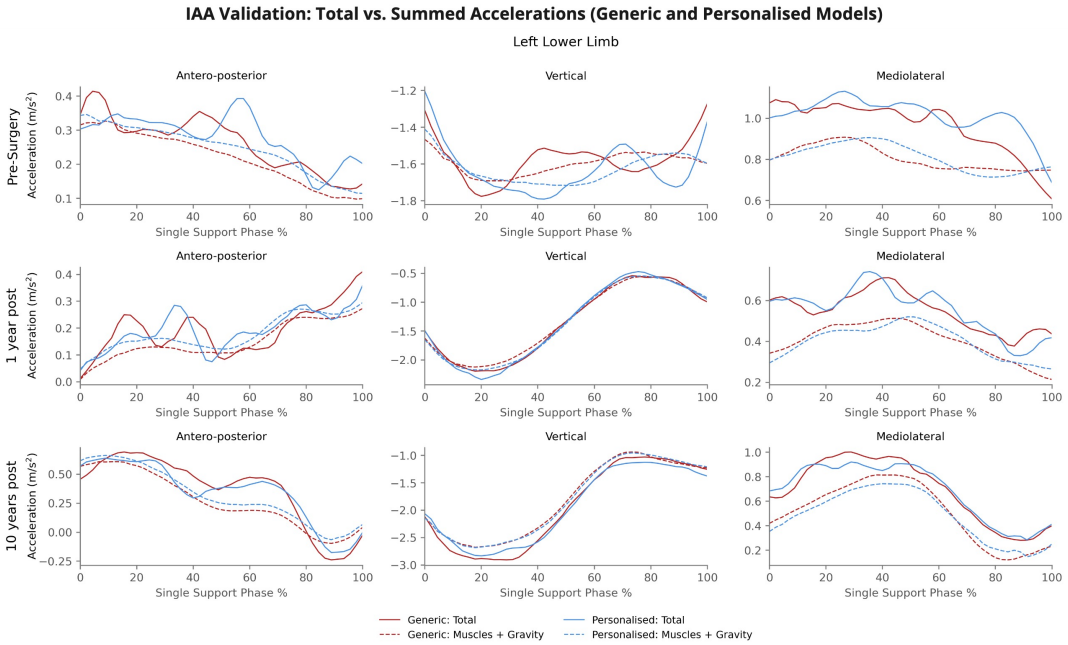

Figure G.1: Validation of the IAA results for the left lower limb by comparing the total acceleration to the sum of the accelerations induced by each muscle and by gravity. Results for the generic and personalised models are presented across all three sessions. Each curve represents the average of the trials. The vertical scale is adjusted for improved visualisation of the results.

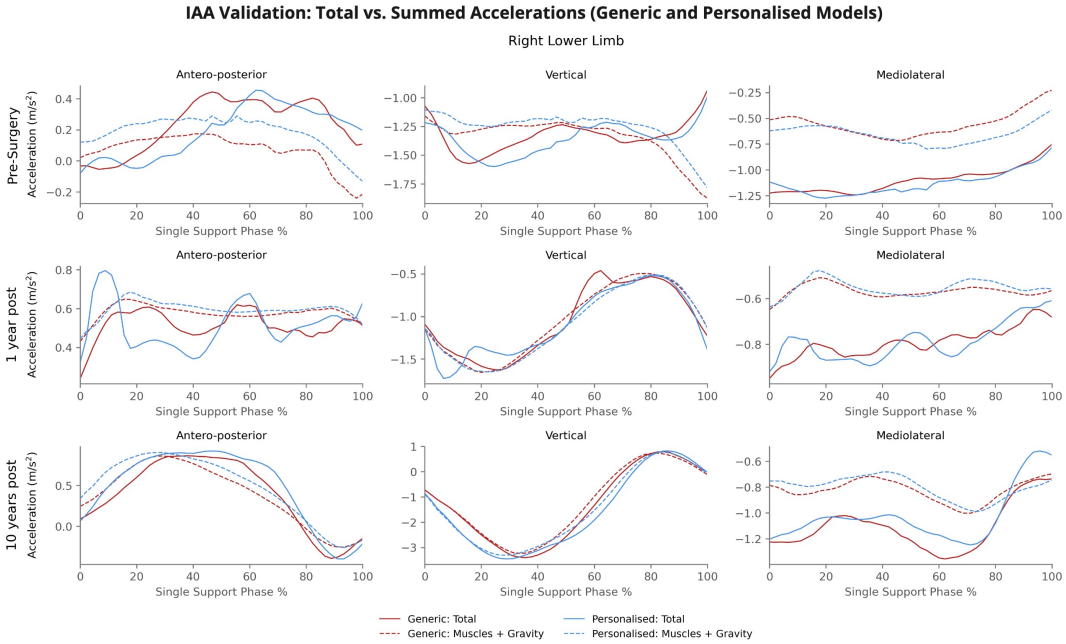

Figure G.2: Validation of the IAA results for the right lower limb by comparing the total acceleration to the sum of the accelerations induced by each muscle and by gravity. Results for the generic and personalised models are presented across all three sessions. Each curve represents the average of the trials. The vertical scale is adjusted for improved visualisation of the results.

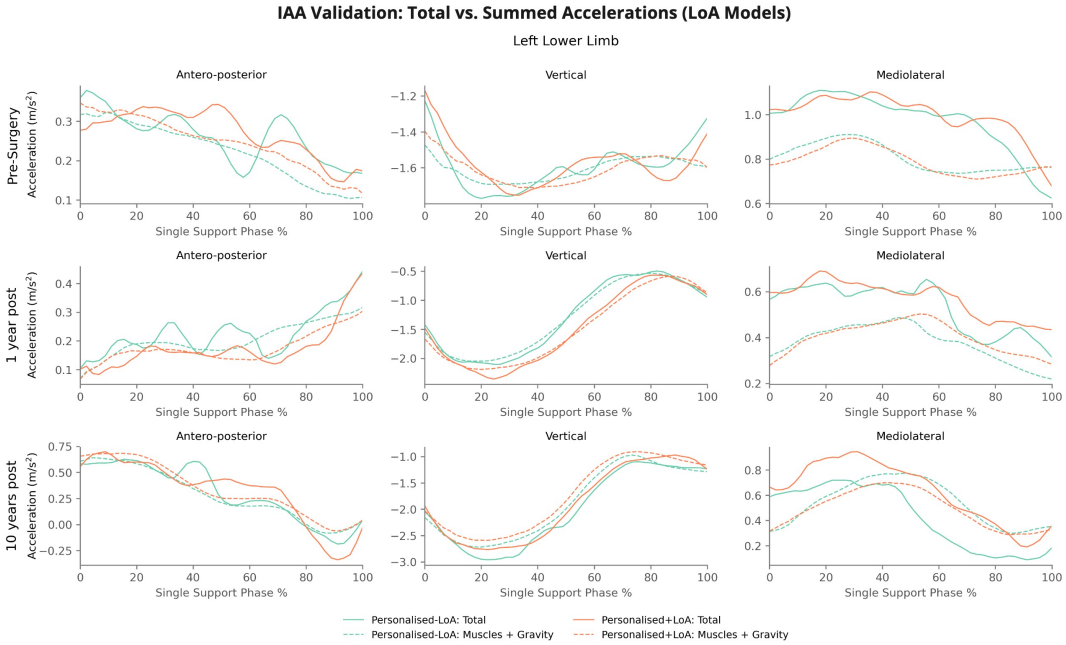

Figure G.3: Validation of the IAA results for the left lower limb by comparing the total acceleration to the sum of the accelerations induced by each muscle and by gravity. Results for the LoA models are presented across all three sessions. Each curve represents the average of the trials. The vertical scale is adjusted for improved visualisation of the results.

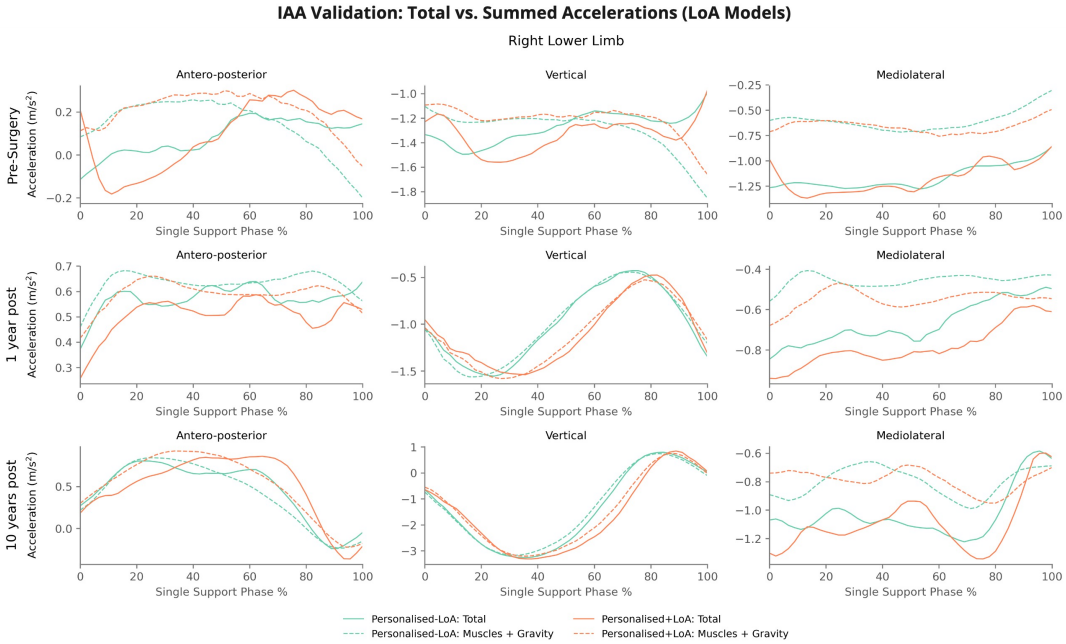

Figure G.4: Validation of the IAA results for the right lower limb by comparing the total acceleration to the sum of the accelerations induced by each muscle and by gravity. Results for the LoA models are presented across all three sessions. Each curve represents the average of the trials. The vertical scale is adjusted for improved visualisation of the results.

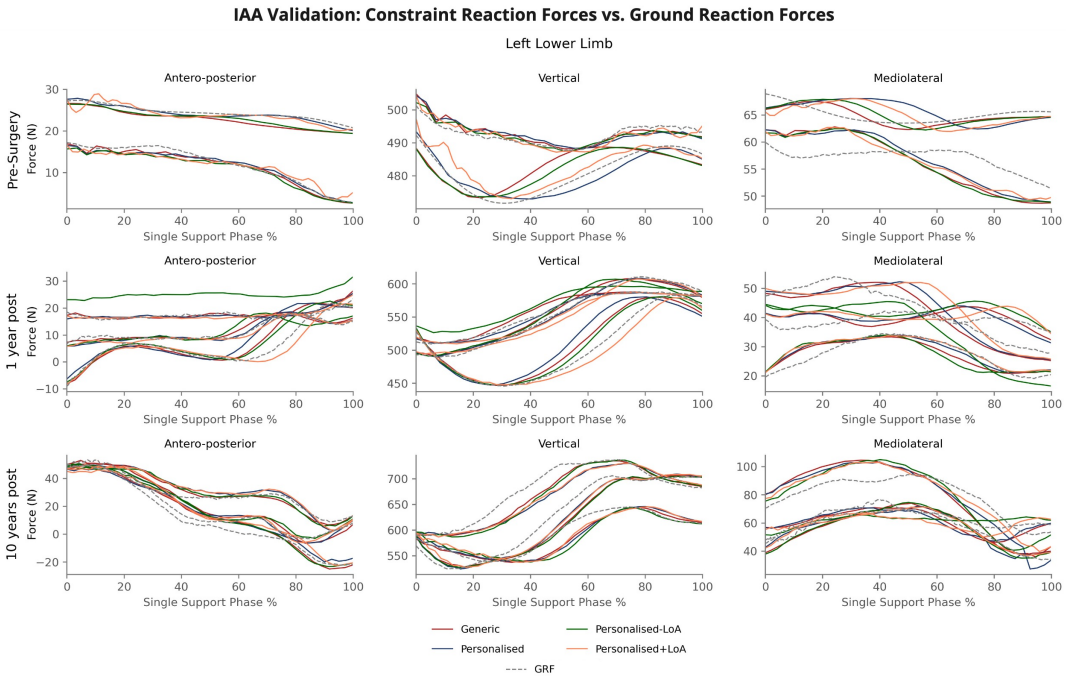

Figure G.5: Validation of the IAA constraint for the left lower limb by comparing computed constraint reaction forces with measured GRF. Results for all four models are presented across all three sessions. Each curve represents one trial. The vertical scale is adjusted for improved visualisation of the results.

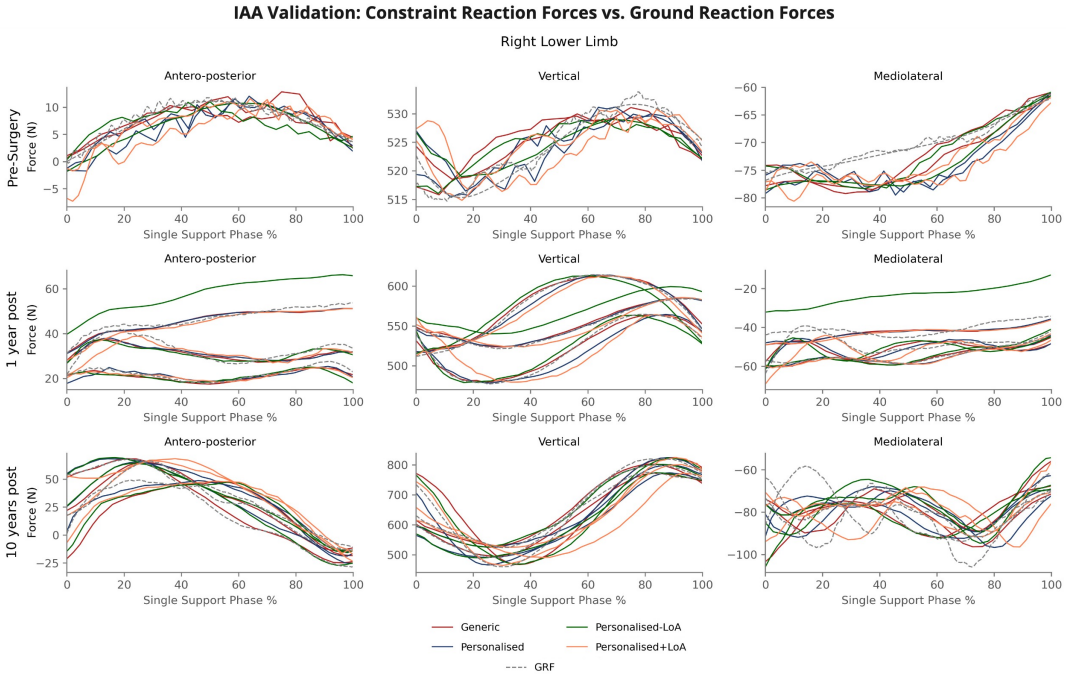

Figure G.6: Validation of the IAA constraint for the right lower limb by comparing computed constraint reaction forces with measured GRF. Results for all four models are presented across all three sessions. Each curve represents one trial. The vertical scale is adjusted for improved visualisation of the results.

G.2 Generic vs. Torsion Tool Muscle Contributions

G.2.1 Antero-Posterior Muscle Contributions

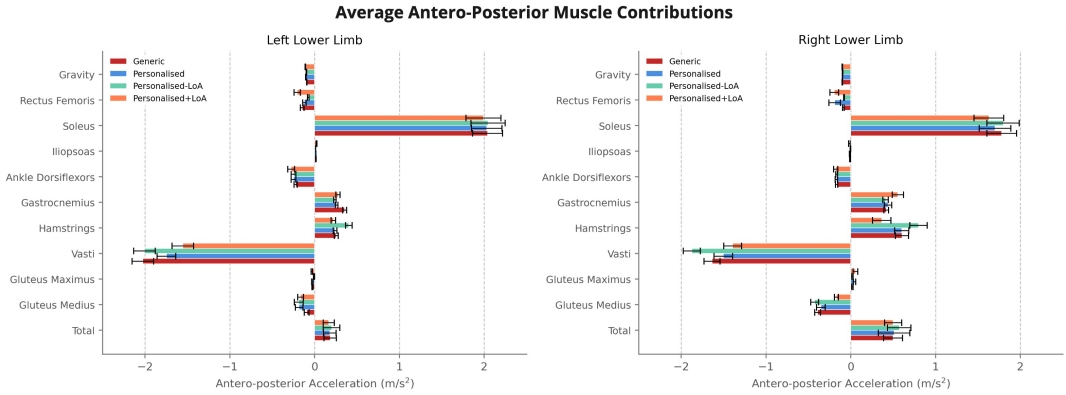

Figure G.7: One-year post-surgery average muscle contributions to antero-posterior COM acceleration for all four models during the single support phase. The total acceleration and contributions from gravity are also shown. Error bars are ±1 standard error. Positive values indicate anterior acceleration, while negative values indicate posterior acceleration.

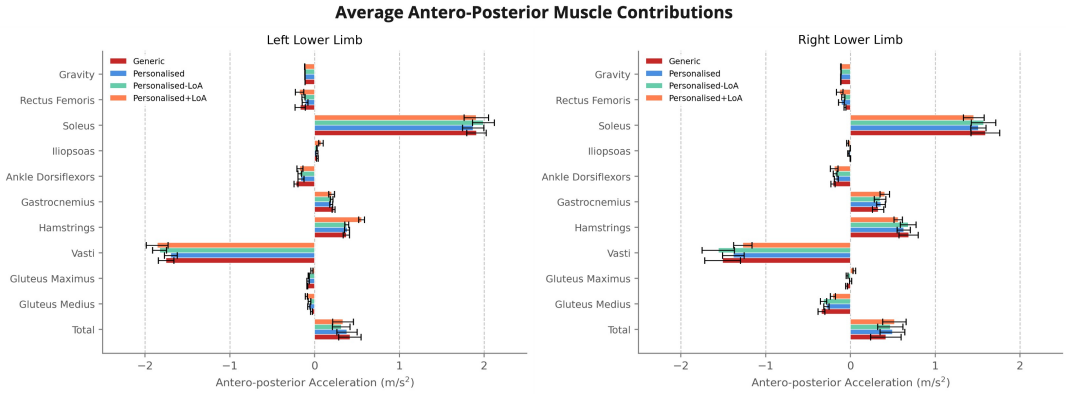

Figure G.8: Ten-year post-surgery average muscle contributions to antero-posterior COM acceleration for all four models during the single support phase. The total acceleration and contributions from gravity are also shown. Error bars are ±1 standard error. Positive values indicate anterior acceleration, while negative values indicate posterior acceleration.

G.2.2 Vertical Muscle Contributions

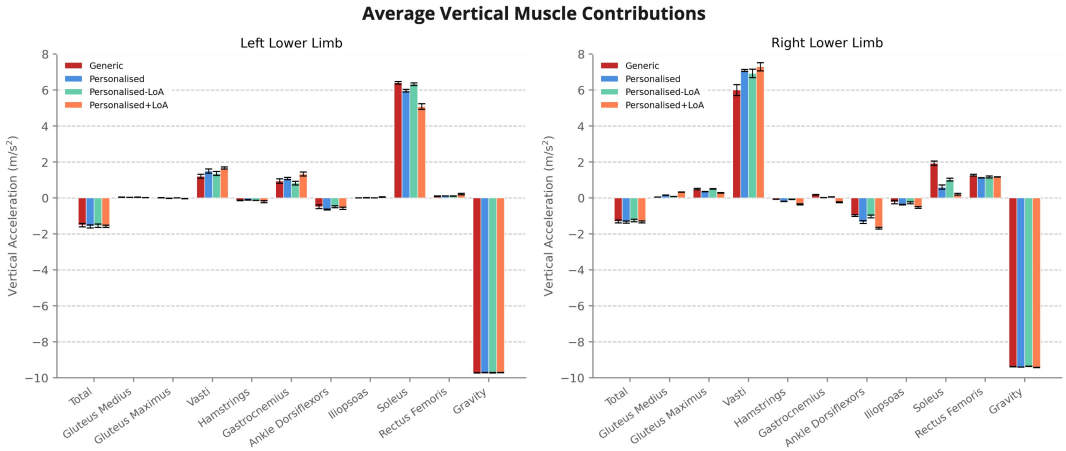

Figure G.9: Pre-surgery average muscle contributions to vertical COM acceleration for all four models during the single support phase. The total acceleration and contributions from gravity are also shown. Error bars are ±1 standard error. Positive values indicate upward acceleration, while negative values indicate downward acceleration.

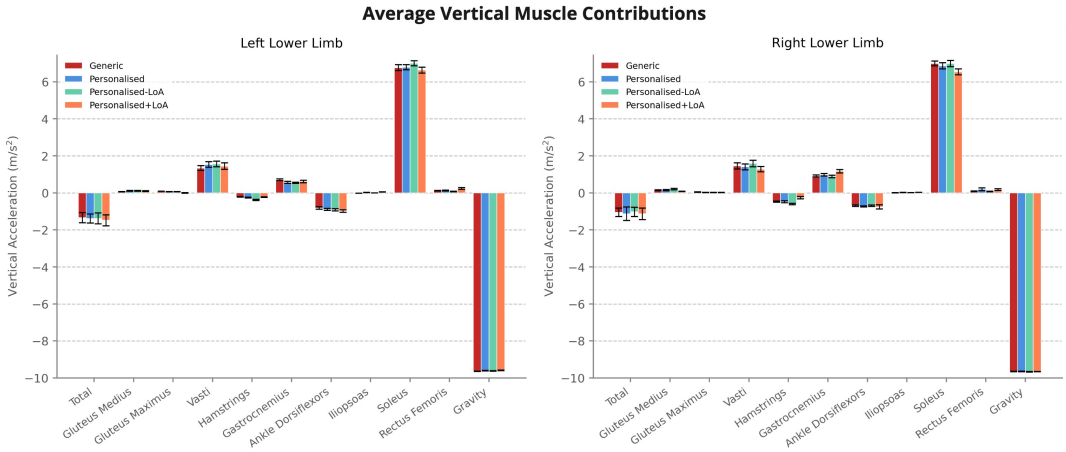

Figure G.10: One-year post-surgery average muscle contributions to vertical COM acceleration for all four models during the single support phase. The total acceleration and contributions from gravity are also shown. Error bars are ±1 standard error. Positive values indicate upward acceleration, while negative values indicate downward acceleration.

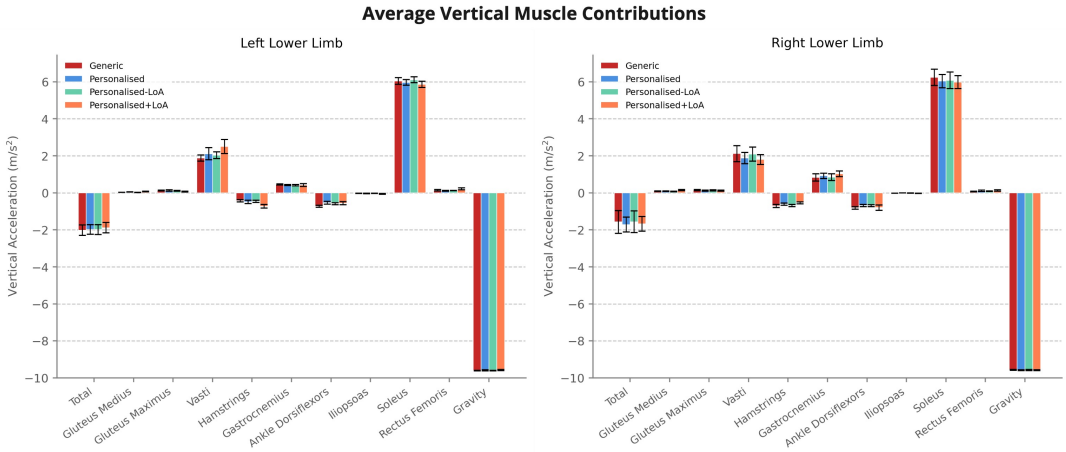

Figure G.11: Ten-year post-surgery average muscle contributions to vertical COM acceleration for all four models during the single support phase. The total acceleration and contributions from gravity are also shown. Error bars are ±1 standard error. Positive values indicate upward acceleration, while negative values indicate downward acceleration.

G.2.3 Mediolateral Muscle Contributions

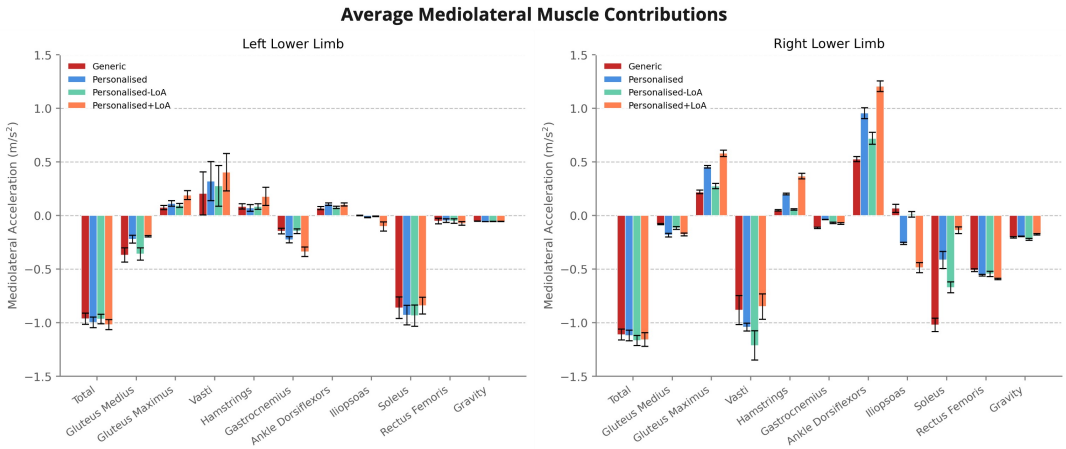

Figure G.12: Pre-surgery average muscle contributions to mediolateral COM acceleration for all four models during the single support phase. The total acceleration and contributions from gravity are also shown. Error bars are ±1 standard error. Positive values correspond to acceleration in the cutting direction, and negative values to the opposite direction..

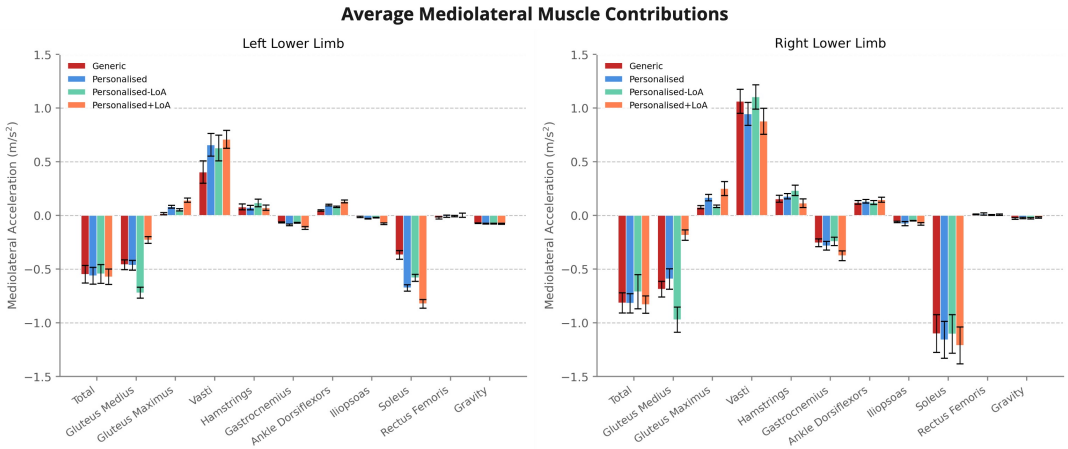

Figure G.13: One-year post-surgery average muscle contributions to mediolateral COM acceleration for all four models during the single support phase. The total acceleration and contributions from gravity are also shown. Error bars are ±1 standard error. Positive values correspond to acceleration in the cutting direction, and negative values to the opposite direction.

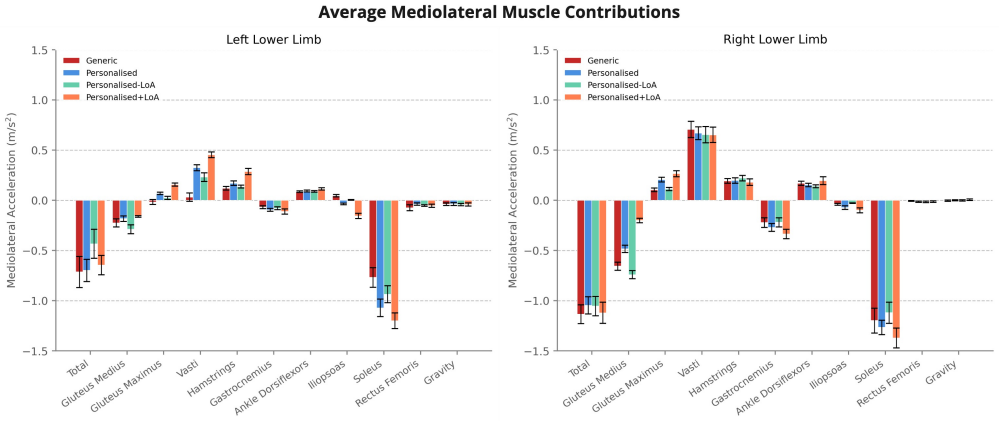

Figure G.14: Ten-year post-surgery average muscle contributions to mediolateral COM acceleration for all four models during the single support phase. The total acceleration and contributions from gravity are also shown. Error bars are ±1 standard error. Positive values correspond to acceleration in the cutting direction, and negative values to the opposite direction.

G.3 Pre- vs. Post-Surgery Muscle Contributions

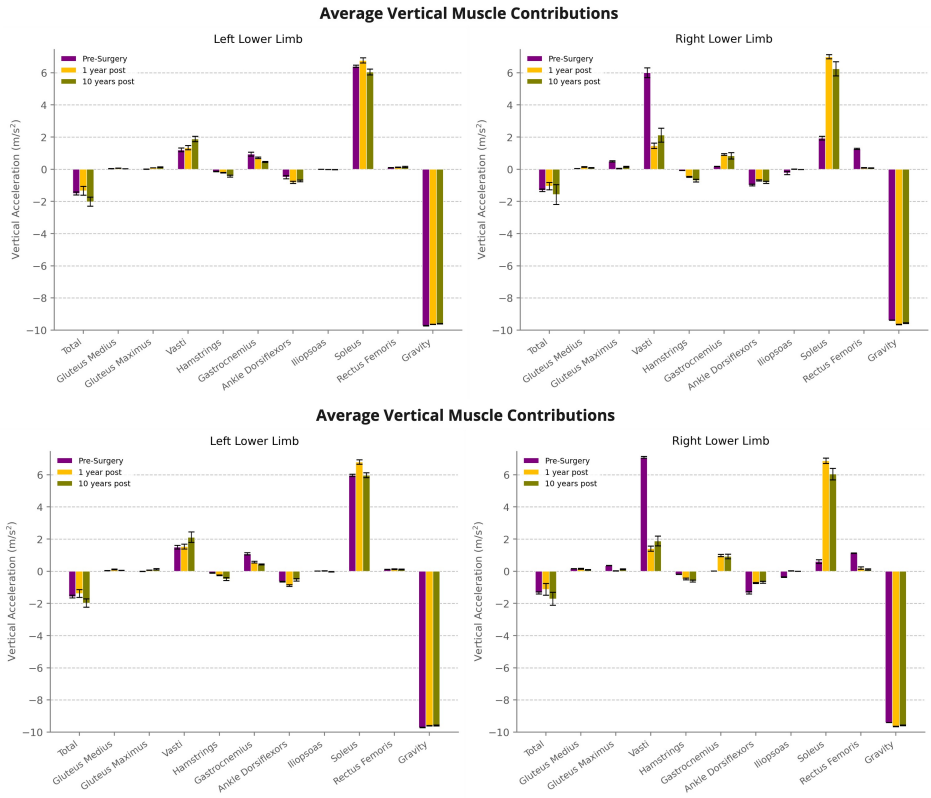

Figure G.15: Pre- vs. post-surgery average muscle contributions to vertical COM acceleration for generic (top), and torsion personalised (bottom) models, during the single support phase. The total acceleration and contributions from gravity are also shown. Error bars are ±1 standard error. Positive values indicate upward acceleration, while negative values indicate downward acceleration.

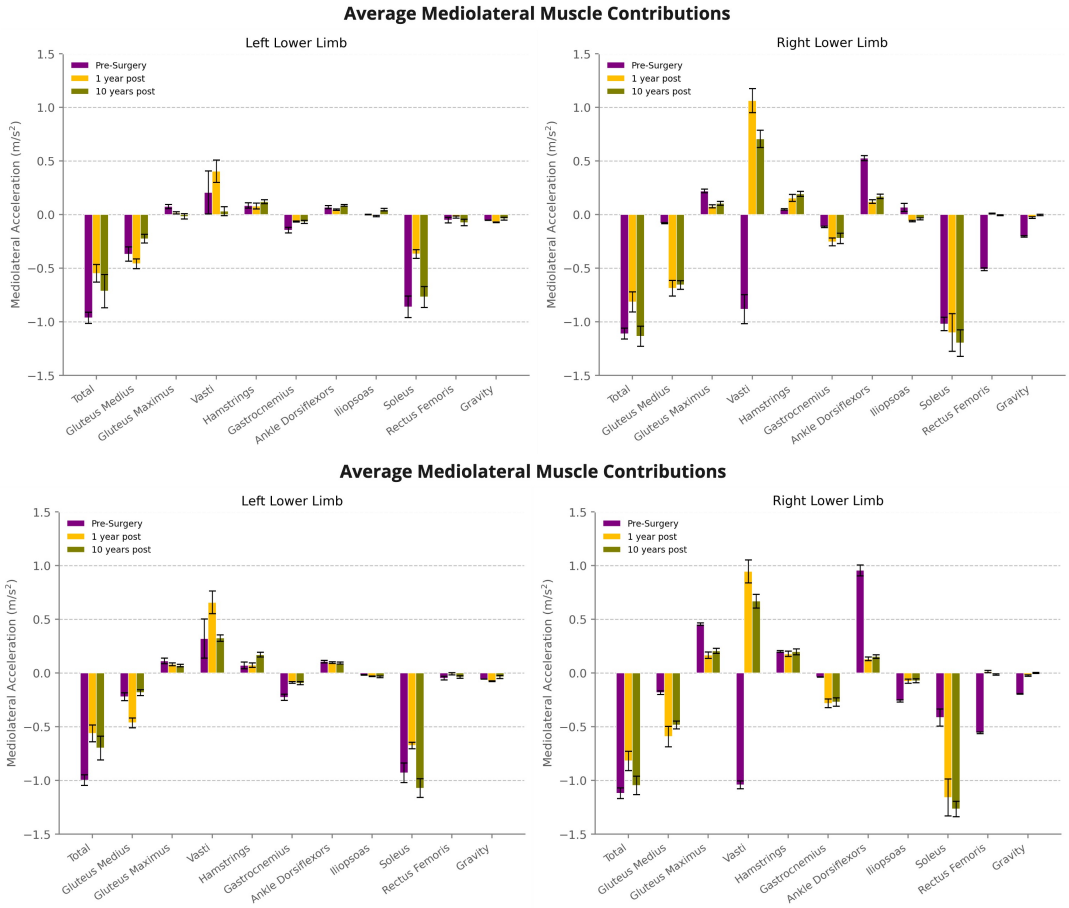

Figure G.16: Pre- vs. post-surgery average muscle contributions to mediolateral COM acceleration for generic (top), and torsion personalised (bottom) models, during the single support phase. The total acceleration and contributions from gravity are also shown. Error bars are ±1 standard error. Positive values correspond to acceleration in the cutting direction, and negative values to the opposite direction.

I

Complementary Work

This annex contains the abstract titled "Effects of model personalisation on the study of crouch gait biomechanics", which shares the same name as this dissertation. The abstract presents the pre-surgery generic vs. personalised model comparison developed in this work, focusing on the results for required muscle strength across all models. It was submitted to the XI *Congresso Nacional de Biomecânica*, in the category of *Biomecânica do Movimento*, where it was reviewed, accepted, and presented in February. The corresponding certificate is also included in this annex.

11º CONGRESSO NACIONAL DE BIOMECÂNICA
A. P. G. Castro, C. Pina, P. R. Fernandes, C. Santos, J. Folgado & A. Amaro (Eds)
Sesimbra, Portugal, 21-22 de Fevereiro, 2025

EFFECTS OF MODEL PERSONALISATION ON THE STUDY OF CROUCH GAIT BIOMECHANICS

Carolina Silva [1,3], Basílio Gonçalves[2], Filipa João[3], Rodrigo Mateus[3], e António Veloso[3]

[1] Faculdade de Ciências e Tecnologia, Universidade Nova de Lisboa, Portugal

[2] University of Vienna

[3] Universidade de Lisboa, Faculdade de Motricidade Humana, CIPER, LBMF, Portugal

crm.silva@campus.fct.unl.pt; basilio.goncalves@univie.ac.at; filipajoao@fmh.ulisboa.pt; rodrigoabmateus@gmail.com; apveloso@fmh.ulisboa.pt;

KEYWORDS: Cerebral palsy, Gait analysis, Musculoskeletal modelling, Subject-specific, Torsion tool.

1 INTRODUCTION

Children with cerebral palsy (CP) often exhibit crouch gait (CG), a severe pathological gait pattern [1]. Musculoskeletal (MSK) modelling is used to study CG, typically relying on generic models based on healthy adults, overlooking individual bone deformities caused by CP [2].
Subject-specific MSK models have been developed to address this limitation, with varying levels of detail [3]. OpenSim's torsion tool offers a time-efficient and straightforward method for model personalisation by incorporating solely femoral and tibial torsional angles [2]. This study aims to investigate the impact of this tool on CG biomechanics in children with CP.

2 METHODS

This study focuses on a child with spastic diplegic CP, Gross Motor Function Classification System level III, CG, who underwent Single-Event Multilevel Surgery. Clinical examination to measure anthropometric features and ranges of motion, followed by gait analysis were performed one month pre-surgery (age: 13 years; height: 169.7 cm; mass: 60.6 Kg). Clinical gait analysis used marker-based motion capture with 14 Qualysis cameras at 100 Hz and CAST marker set [4]. The participant performed a static trial and walked along a 10 m corridor for dynamic trials. Ground reaction forces were recorded by two force plates at 1000 Hz.
Two models were studied: the generic Gait2392 and a model created with the torsion tool, considering femoral and tibial deformities. Since bone deformities were evaluated using clinical analysis and radiography, both subject to errors, two additional models were developed to incorporate the maximum estimated measurement error. Input values for each model are shown in Table 1. Muscle forces were attained for all models during the single support phase, and muscle strength requirements calculated to compare the percentage of maximum force across models.

Table 1 – Bone deformity angles used as inputs in the torsion tool to generate each model. Personalised values were measured in clinical examination and radiography, with limits of agreement (LoA) lower (- LoA) and upper (+ LoA) bounds sourced from literature. LoA values for femoral anteversion and tibial torsion are between computed tomography (CT) and clinical examination, and between CT and radiography for femoral neck-shaft angle.

		Femoral Anteversion Angle (º)		Femoral Neck-Shaft Angle (º)		Tibial Torsion Angle (º)	
		Left	Right	Left	Right	Left	Right
Model Inputs	Personalised	44	50	140	140	31	44
	Personalised - LoA	18.56	24.56	129.34	129.34	21.65	34.65
	Personalised + LoA	73.44	79.44	142.66	142.66	39.45	52.45

3 RESULTS

The left side of Figure 1 shows that the generic and personalised models require very similar muscle forces, with slight increases in required strength for the *gluteus maximus*, *gastrocnemius*, and *soleus*, for the personalised model during single support. On the right limb, the torsion model shows noticeable lower demand for the *rectus femoris* and higher for the *gluteus medius*, *vasti*, and *iliopsoas*.

Considering the LoA models, the one with the highest torsional angles overall shows the greatest muscle demand, while the lower bound LoA model closely resembles the generic model.

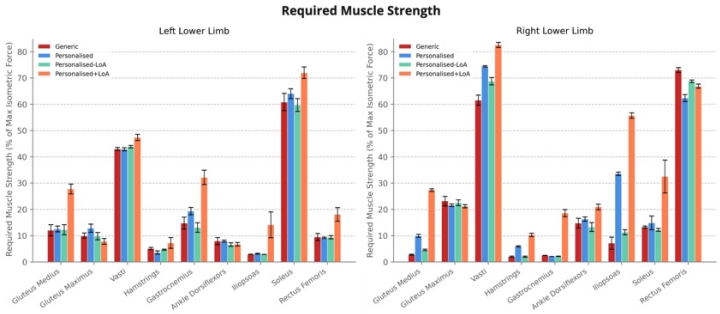

Figure 1 – Pre-surgery required strength for each muscle group in both limbs during the single support period, expressed as a percentage of the maximum isometric force. Error bars represent ±1 standard error.

4 DISCUSSION

This study evaluated the impact of torsional variations on muscle force-generating capacity. On the right lower limb, pronounced differences were observed between the generic and personalised models, particularly in the knee extensors and *iliopsoas*, suggesting that anatomical variations influence biomechanical outcomes. In contrast, muscle force predictions for the left limb were consistent across models, except for the one with a greater torsion angle. The generic model's results fall outside the interval defined by the two LoA models, reflecting actual biomechanical differences between the generic and personalised models rather than measurement errors.

Previous research determined that required knee extensor and ankle plantarflexor strength increased with crouch severity, whereas hip abductor strength decreased [1]. When examining the three torsion-based models, our results align with those for the *vasti* and ankle plantarflexors but differ for the *rectus femoris* and *gluteus medius*.

Given the relevance of MSK modelling in clinical applications such as surgical planning and prosthetic design, adopting an approach that improves accuracy could lead to more customized clinical strategies. The observed impact of torsion tool-based models on muscle force estimates highlights their potential and underlines the need for future research involving more participants to compare model accuracy, strengthen reliability, and support broader conclusions.

ACKNOWLEDGEMENTS

This study is supported by the project referenced as PTDC/EMD-EMD/5804/2020 (https://doi.org/10.54499/PTDC/EMD-EMD/5804/2020).

REFERENCES

[1] K. M. Steele, van der Krogt MM, M. H. Schwartz, and S. L. Delp. "How much muscle strength is required to walk in a crouch gait?", Journal of Biomechanics, vol. 45(15), pp. 2564-9, Oct 2012.

[2] K. Veerkamp, H. Kainz, B. A. Killen, H. Jónasdóttir, and M. M. van der Krogt, "Torsion tool: An automated tool for personalising femoral and tibial geometries in opensim musculoskeletal models", J Biomech, vol. 125, Aug 2021.

[3] R. Akhundov, D. J. Saxby, L. E. Diamond, et al., "Is subject-specific musculoskeletal modelling worth the extra effort or is generic modelling worth the shortcut?", PLoS ONE, vol. 17(1), Jan 2022.

[4] A. Cappozzo, U. della Croce, A. Leardini, and L. Chiari, "Human movement analysis using stereophotogrammetry. Part 1: Theoretical background", Gait and Posture, vol. 21(2), pp. 186–196, Feb 2005.

CNB'25

XI CONGRESSO NACIONAL DE BIOMECÂNICA

CERTIFICADO DE PARTICIPAÇÃO

Carolina Silva

Participou no

XI Congresso Nacional de Biomecânica

que teve lugar em Sesimbra, Portugal,

nos dias 21 e 22 de Fevereiro de 2025

O titulo do trabalho apresentado pelo participante foi:

EFFECTS OF MODEL PERSONALISATION ON THE STUDY OF CROUCH GAIT BIOMECHANICS

Carolina Silva | Basílio Gonçalves | Filipa João | Rodrigo Mateus | António Veloso

André Castro

PRESIDENTE CNB2025

idmec IST engenharia mecânica · TÉCNICO LISBOA · POLITECNICO SETUBAL

II

Informed Consent

Presented in this annex is the Portuguese informed consent form provided to the participant involved in this study.

FACULDADE DE MOTRICIDADE HUMANA

LISBOA
UNIVERSIDADE DE LISBOA

CONSELHO DE ÉTICA DA FACULDADE DE MOTRICIDADE HUMANA

CONSENTIMENTO INFORMADO LIVRE E ESCLARECIDO PARA INVESTIGAÇÃO CIENTÍFICA COM SERES HUMANOS

PC 013

Título do projeto ou estudo:

Avaliação biomecânica da marcha em crianças com Paralisia Cerebral

Pessoa responsável pelo projeto:

Professor Doutor António Prieto Veloso

Instituição de acolhimento:

Faculdade de Motricidade Humana/Universidade de Lisboa.

Este documento, designado **Consentimento, Informado, Livre e Esclarecido**, contém informação importante em relação ao estudo para o qual foi abordado/a, bem como o que esperar se decidir participar no mesmo. Leia atentamente toda a informação aqui contida. Deve sentir-se inteiramente livre para colocar qualquer questão, assim como para discutir com terceiros (amigos, familiares) a decisão da sua participação neste estudo.

Informação geral
Paralisia Cerebral é um termo abrangente para designar um grupo de situações clinicas; é permanente, mas não inalterável, origina uma perturbação do movimento e/ou postura e da função motora; é devida a uma alteração/ lesão/ anomalia não progressiva do cérebro imaturo e em desenvolvimento. As alterações neuromusculares resultantes demonstram um caráter evolutivo, contribuindo não só para um padrão de marcha progressivamente disfuncional, mas também para uma menor interação da criança com o meio que a rodeia limitando o seu processo de aprendizagem cognitiva. Por esta razão, a análise de marcha, utilizando parâmetros biomecânicos quantitativos, é um método complementar e importante ao atual processo de avaliação clínica da marcha. Este estudo tem como objetivo descrever o padrão da marcha de crianças com paralisia cerebral, permitindo deste modo avaliar de forma objetiva o grau de funcionalidade destas crianças e assim contribuir para a tomada de decisão clínica.

Qual a duração esperada da minha participação do meu educando?

Aproximadamente 90 minutos.

Quais os procedimentos do estudo em que o meu educando vai participar?

Este estudo irá incluir quatro tipos de testes:

(1) Avaliação antropométrica: esta avaliação incluirá massa e altura.

(2) Avaliação postural: serão recolhidos vídeos e fotografias para auxiliar a construção do modelo biomecânico.

(3) Goniometria e força muscular: esta avaliação incluirá amplitudes articulares máximas do membro inferior e testes manuais de força para os principais grupos musculares do membro inferior.

(4) Avaliação da marcha: a marcha será avaliada através de um sistema composto por dois tipos de câmaras - umas que captarão a posição de marcadores refletores colocados em proeminências ósseas específicas e outras que recolhem vídeo. Durante esta avaliação serão também utilizadas plataformas de força para medir a força produzida durante o apoio do pé no solo. Serão igualmente recolhidos dados de pressão plantar através de um tapete de pressões ou de palmilhas de pressão e dados de eletromiografia através de sensores de eletromiografia para medir a atividade elétrica de músculos do membro inferior. O participante terá de caminhar à sua velocidade natural. Esta tarefa será repetida algumas vezes na condição descalça e calçado com ortóteses (caso se aplique)

Para a realização destas sessões o participante deve trazer roupa confortável (sendo aconselhável o uso de calções e top/t-shirt).

A participação do meu educando é voluntária?

A participação do seu educando é voluntária, podendo desistir a qualquer momento. No caso de decidir abandonar o estudo, a sua relação com a Faculdade de Motricidade Humana (FMH) não será afetada, tendo apenas que devolver qualquer equipamento/material que lhe tiver sido cedido durante a realização do estudo. Se for o caso, o seu estatuto enquanto estudante ou funcionário da FMH será mantido e não sofrerá nenhuma consequência da sua não-participação ou desistência.

Quais os possíveis benefícios da participação do meu educando?

Ao participar no estudo o seu educando terá direito a um relatório personalizado e detalhado desta avaliação contendo a descrição do seu padrão de marcha, que poderá requerer, junto do médico ou profissional clínico que acompanha o seu educando.

Quais os possíveis riscos da participação do meu educando?

Uma vez que as tarefas a desempenhar nas diversas sessões não envolvem atividade física de risco, a probabilidade de sofrer qualquer dano é mínima.

Quem assume a responsabilidade, no caso de um evento negativo?

A probabilidade de qualquer ocorrência é mínima, mas caso se verifique o contrário, a Faculdade de Motricidade Humana assumirá as despesas consideradas razoáveis e inerentes a qualquer dano sofrido como resultado direto da participação do seu educando neste estudo.
Há cobertura por uma companhia de seguros?
Não existe cobertura por parte de uma companhia de seguros.
Quem deve ser contactado em caso de urgência?
Nome da pessoa a contactar: Grau de parentesco relativamente ao participante em estudo: Contacto telefónico:
Como é assegurada a confidencialidade dos dados?
Para garantir a privacidade do participante, todos os estudos serão realizados à porta fechada estando presente as pessoas da equipa de investigação, os encarregados de educação e o médico ou profissional clínico que acompanha o participante. A confidencialidade dos dados será garantida substituindo o nome do participante por um código conhecido exclusivamente pelos investigadores, que consta no canto superior direito da primeira página deste documento. Após a recolha, os dados serão armazenados, devidamente codificados, apenas no servidor do Laboratório de Biomecânica e Morfologia Funcional.
O que acontecerá aos dados quando a investigação terminar?
Os dados recolhidos passarão a fazer parte da base de dados da Laboratório de Biomecânica e Morfologia Funcional e serão posteriormente usados para fins de investigação, sempre com garantia do anonimato do participante.
Como irão os resultados do estudo ser divulgados e com que finalidades?
Os resultados do estudo serão divulgados à comunidade científica através da publicação de artigos e apresentações em congressos de referência na área. Serão também divulgados ao participante através do relatório produzido e entregue ao clínico que o acompanha.
Em caso de dúvidas quem devo contactar?
Para qualquer questão relacionada com a sua participação neste estudo, por favor, contactar: Professora Doutora Filipa João Faculdade de Motricidade Humana da Universidade de Lisboa Estrada da Costa, 1499-002 Cruz-Quebrada — Dafundo Tel.: 214 149 129 / 918116054 filipajoao@fmh.ulisboa.pt http://lbmf.fmh.ulisboa.pt/

Assinatura do Consentimento Informado, Livre e Esclarecido

Li (ou alguém leu para mim) o presente documento e estou consciente do que esperar quanto à minha participação no estudo "Avaliação biomecânica da marcha em crianças com Paralisia Cerebral". Tive a oportunidade de colocar todas as questões e as respostas esclareceram todas as minhas dúvidas. Assim, aceito voluntariamente participar neste estudo. Foi-me dada uma cópia deste documento.

Nome do participante **Assinatura do participante**

Data

Nome do representante legal do participante
(se aplicável)

Grau de relação com o participante

Investigador/Equipa de Investigação

Os aspetos mais importantes deste estudo foram explicados ao participante ou ao seu representante, antes de solicitar a sua assinatura. Uma cópia deste documento ser-lhe-á fornecida.

Nome da pessoa que obtém o consentimento **Assinatura da pessoa que obtém o consentimento**

Data